UNIVERSIDAD DE CHILE

FACULTAD DE CIENCIAS QUÍMICAS Y FARMACÉUTICAS

The therapeutic potential of dibenzoylmethane (DBM) in a C9ORF72-mediated FTD/ALS mouse model

Tesis presentada a la Universidad de Chile para optar al grado de Doctor en Ciencias Farmacéuticas:

Paulina Mackarena Torres Corales

Director de Tesis: Dr. Claudio Hetz

Santiago-CHILE

Enero/2022

UNIVERSIDAD DE CHILE

FACULTAD DE CIENCIAS QUÍMICAS Y FARMACÉUTICAS

INFORME DE APROBACIÓN DE TESIS DE DOCTORADO

Se informa a la Dirección de la Escuela de Postgrado de la Facultad de Ciencias Químicas y Farmacéuticas que la Tesis de Doctorado presentada por la candidata

Paulina Mackarena Torres Corales

Ha sido aprobada por la Comisión de Evaluadora de Tesis como requisito para optar al grado de Doctor en Ciencias Farmacéuticas, en el examen público rendido el día _____.

Director de tesis:

Dr. Claudio Hetz _____

Comisión evaluadora de tesis:

Dr. Guillermo Díaz _____

Dr. Sergio Lavandero _____

Dr. Mario Chiong _____

Dr. Federico Batiz _____

AGRADECIMIENTOS

En primer lugar, a mi familia por ser mi pilar en todo momento, por creer en mí y por estar siempre que los necesité.

A Felipe, por ser mi apoyo y contención desde el comienzo, por ayudarme tanto en lo emocional como intelectual y por inspirarme día a día ser una mejor científica.

Al team ALS: Jose, Vicho, Dani, Guillermo, Pepe, Danilo, por todo el apoyo tanto experimental como de discusión de resultados.

A todo el Hetzlab, por estar siempre tanto en la amistad como en el trabajo. Todos fueron un tremendo grupo humano e importante a lo largo de estos cinco años.

Y finalmente a Claudio por darme la oportunidad de ser parte de un laboratorio de alto nivel y por guiarme en este difícil camino. También por brindarme apoyo económico cuando lo necesité y por los contactos tanto en Chile como en el extranjero que me permitieron realizar diferentes colaboraciones y una pasantía en Estados Unidos.

FINANCIAMIENTO

This thesis was performed in the laboratory of Proteostasis Control and Biomedicine in the Biomedical Neuroscience Institute, University of Chile. The project was funding by FONDECYT 1180186 (2018-2022), Millennium Institute P09-15-F (2011-2021), FONDAP 15150012 (2015-2020) and CONICYT doctoral fellowship 21161332 (2016-2020).

INDEX

INDEX OF FIGURES

INDEX OF TABLES

ABBREVIATIONS

AAV : Adeno-associated virus
AD : Alzheimer's disease
ALS : Amyotrophic lateral sclerosis
ATF4 : Activating transcription factor 4
ATF6 : Activating transcription factor 6
ATF6f : Fragment of ATF6 that acts as a transcriptional factor
BiP : Binding immunoglobulin protein
BSA : Bovine serum albumin
C57BL/6 : Mouse strain used in scientific research
C9FTD/ALS : FTD and ALS cases associated with the C9ORF72 mutation
C9ORF72 : Chromosome 9 open reading frame 72
C9ORF72-L : C9ORF72 protein long form
C9ORF72-S : C9ORF72 protein short form
CHOP : CCAAT/-enhancer-binding protein homologous protein
CNS : Central Nervous System
CO_2 : Carbon dioxide
CRISPR : Clustered regularly interspaced short palindromic repeats
Ddit3 : DNA-damage inducible transcript 3
DNA : Deoxyribonucleic acid
DPR : Dipeptide repeats
EDTA : Ethylenediaminetetraacetic acid
eIF2B : Eukaryotic translation initiation factor 2B
eIF2α : Eukaryotic initiation factor 2α
ER : Endoplasmic reticulum
FTD : Frontotemporal dementia
GCN2 : General control nonderepressible 2 kinase
GFAP : Glial fibrillary acidic protein
GRN : Granulin
GTP : Guanosine triphosphate
HRI : Heme-regulated eIF2α kinase

Iba1 : Ionized calcium binding adaptor molecule 1
ICV : Intracerebroventricular
IHQ : Immunohistochemistry
iPSC : Induced pluripotent stem cell
IRE1α : Inositol requiring kinase 1 alpha
ISR : Integrated stress response
ISRIB : Integrated stress response inhibitor
MAPT : Microtubule-associated protein tau
mRNA : Messenger ribonucleic acid
NeuN : Neuronal nuclei
NINDS : National Institute of Neurological Disorders and Stroke
NOL : Novel object location
NOR : Novel object recognition
NP40 : Nonidet P-40
NT : Non-treated
PBS : Phosphate buffer saline
PCR : Polymerase chain reaction
PERK : Protein kinase RNA-like endoplasmic reticulum kinase
PFA : Paraformaldehyde
PKR : Protein kinase R
PrD : Prion disease
qPCR : Quantitative PCR
RAN : Repeat associated non-AUG translation
RNA : Ribonucleic acid
RT-qPCR : Reverse transcription followed by quantitative PCR
SOD1 : Superoxide dismutase-1
TDP-43 : TAR-DNA binding protein 43 kDa
uORF : Upstream open reading frame
UPR : Unfolded protein response
WT : Wild type
XBP1 : X-Box Binding Protein 1
XBP1s : X-Box Binding Protein 1 spliced

ABSTRACT

The most frequent genetic cause of C9FTD/ALS is a hexanucleotide repeat expansion in the C9ORF72 gene. This mutation produces dipeptide repeats (DPR) that are neurotoxic and form inclusion bodies. Recent studies suggest that DPR production led to the phosphorylation of the translation initiation factor eIF2α and hence blocking protein synthesis. This molecular event is a convergent point of several stress signals, a pathway known as integrated stress response (ISR). Studies in fly and cellular models indicated that inhibition of the ISR protects against C9ORF72 pathogenesis. Recently, a compound with promising translational potential known as dibenzoylmethane (DBM) has been identified, which reverses the translational attenuation mediated by eIF2α phosphorylation. This molecule provided neuroprotection to prion-infected mice and Tau transgenic animals. Therefore, the aim of this project was to investigate the role of oral delivery of DBM in the neurodegeneration associated to the accumulation of DPR in C9ORF72-mediated FTD/ALS in a mouse model. To this purpose, newborn pups were injected with AAV encoding AAV-2R or the expanded AAV-66R by intracerebroventricular injection. At two months of age, mice were orally treated with 0.5% of DBM mixture in powdered food *ad libitum* until the end of the experiment (eighth months later). At the third and sixth month of age, several behavioral tests were performed to investigate the impact of DBM treatment in the progression of C9ORF72-mediated FTD/ALS. Then, to determine the consequences of DBM treatment in the C9ORF72-mediated FTD/ALS mice model, different histopathological and biochemical analysis were performed. Finally, to assess the molecular changes generated by the AAV injection and define

the possibly mechanisms explaining the protective effects of DBM, we performed unbiased quantitative proteomics of brain tissue of C9ORF72-FTD/ALS mice.

We found that AAV-66R mice showed memory impairment at 6 months compared to controls, as revealed by the novel object recognition (NOR) and novel object location (NOL) tests. DBM administration was sufficient to prevent such impairment in our C9FTD/ALS mouse model. Additionally, AAV-66R mice developed inclusions of poly(GA) and poly(GR) in the hippocampus and brain cortex, but rarely in cerebellum. Moreover, an increase in the expression of GFAP and Iba1, markers of astrogliosis and microgliosis respectively, were found in AAV-66R mice. However, DBM did not significatively decrease the expression of these markers. Regarding to the expression of downstream targets of eIF2α phosphorylation, DBM administration did not reduce markers of stress including *Chop, Atf3, Trb3*, in addition to *Bip* and *Xbp1s*, by real time PCR. Finally, by proteomics analysis indicate that the main pathways altered by DBM in C9ORF72-mediated FTD/ALS mice were related to cytoskeleton organization and metabolic processes.

Overall, the results obtained in this PhD thesis suggest a protector effect of DBM in the pathogenesis of C9ORF72 highlighting a possible novel therapeutic strategy to treat C9FTD/ALS.

RESUMEN

La causa genética más frecuente de C9FTD/ALS es la expansión repetida de hexanucleótidos en el gen C9ORF72. Esta mutación produce repeticiones de dipéptidos (DPR) que son neurotóxicas y forman cuerpos de inclusión. Estudios recientes sugieren que la producción de DPR condujo a la fosforilación del factor de iniciación de la traducción eIF2α y, por tanto, a la inhibición de la síntesis de proteínas. Este evento molecular es un punto convergente de varias señales de estrés, una vía conocida como respuesta integrada al estrés (ISR). Estudios en modelos celulares y de moscas indicaron que la inhibición del ISR protege contra la patogénesis de C9ORF72. Recientemente, se ha identificado un compuesto con un potencial prometedor conocido como dibenzoilmetano (DBM), que muestra el potencial de atenuación de la traducción inversa mediada por la fosforilación de eIF2α. Esta molécula proporcionó neuroprotección a ratones infectados por priones y animales transgénicos Tau. Por lo tanto, el objetivo de este proyecto fue investigar el impacto de la administración oral de DBM en la toxicidad asociada a la acumulación de DPR en FTD/ALS mediada por C9ORF72. Con este fin, se inyectó a los ratones recién nacidos con AAV que codifica AAV-2R o el AAV-66R expandido mediante inyección intracerebroventricular. A los dos meses de edad, los ratones se trataron por vía oral con 0,5% de mezcla de DBM en alimento en polvo *ad libitum* hasta el final del experimento (ocho meses). Al tercer y sexto mes de edad, se realizaron varias pruebas de comportamiento para investigar el impacto del tratamiento con DBM en la progresión de FTD/ALS mediada por C9ORF72. Luego, para determinar las consecuencias del tratamiento con DBM en el modelo de

ratones FTD/ALS mediado por C9ORF72, se realizaron diferentes análisis histopatológicos y bioquímicos. Finalmente, con el fin de determinar los cambios moleculares generados por la inyección de AAV y definir los posibles mecanismos que explican los efectos protectores de DBM, realizamos proteómica cuantitativa del tejido cerebral de ratones C9ORF72-FTD/ALS.

Encontramos que los ratones AAV-66R mostraron deterioro de la memoria a los 6 meses en comparación con los controles, como lo revelaron las pruebas NOR y NOL. La administración de DBM fue suficiente para prevenir tal deterioro en nuestro modelo de enfermedad de ratón C9ORF72-FTD/ALS. Además, los ratones AAV-66R mostraron inclusiones de poli(GA) y poli(GR) en el hipocampo y la corteza, pero raramente en el cerebelo. Además, se encontró un aumento en la expresión de GFAP e Iba1, marcadores de astrogliosis y microgliosis respectivamente, en ratones AAV-66R. Sin embargo, DBM no disminuyó significativamente la expresión de estos marcadores. Con respecto a la expresión de blancos rio abajo de la fosforilación de eIF2α, como *Chop, Atf3, Trb3*, además de *Bip* y *Xbp1s,* no encontramos diferencias en el nivel de expresión medido por PCR en tiempo real. Finalmente, mediante análisis proteómico encontramos que los principales términos alterados por DBM en ratones FTD/ALS mediados por C9ORF72 fueron la organización del citoesqueleto y los procesos metabólicos.

En general, los resultados obtenidos en esta tesis doctoral sugieren un efecto protector luego de la administración farmacológica de DBM en la progresión de la patología destacando una posible nueva estrategia terapéutica en el tratamiento de C9FTD/ALS.

1. INTRODUCTION

1.1 Frontotemporal dementia (FTD) and amyotrophic lateral sclerosis (ALS).

FTD and ALS are two related neurodegenerative disorders that are characterized by motor and behavioral impairment, respectively. Importantly, FTD and ALS are clinically, pathologically and genetically overlapped, forming part of a spectrum of diseases (Burrell *et al.* 2016). FTD, also known as frontotemporal lobar degeneration (FTLD), is a heterogenic disorder involving a progressive neuronal atrophy of the frontal and/or anterior temporal lobes. Patients develop personality and behavioral changes, as well as gradual impairment of language skills. FTD is the second most common form of dementia after Alzheimer's disease (Van Langenhove *et al.* 2012). On the other hand, ALS is a neurodegenerative disorder that affects both upper and lower motor neurons of the brain and spinal cord (Hardiman *et al.* 2017). ALS is characterized by progressive muscle weakness culminating in the inability to coordinate movements and death due to respiratory failure, commonly within 3 years of symptoms onset (Rowland and Shneider 2001; Pasinelli and Brown 2006).

At the histopathological level, FTD and ALS display common molecular features, highlighting the accumulation of cytoplasmic TAR DNA-binding protein 43 (TDP-43) inclusions as a central pathological hallmark (Chen-Plotkin *et al.* 2010). TDP-43 is a nuclear protein that is mislocalizated in FTD and ALS, accumulating in the cytosol and ultimately impacting nuclear RNA processing and prompting the sequestration of RNA binding proteins and other interactors in the cytoplasm

(Renton *et al.* 2011; DeJesus-Hernandez *et al.* 2011). Mutations in microtubule-associated protein Tau (MAPT), granulin (GRN) and in the chromosome 9 open reading frame 72 gene (C9ORF72) have been widely associated with FTD and ALS, leading to abnormal protein aggregation and neurodegeneration.

Currently, it is known that the hexanucleotide repeat expansion GGGGCC (G_4C_2) in *C9ORF72* gene of the chromosome 9p21 is the most frequent genetic cause of both FTD and ALS (here referred to as C9FTD/ALS) (DeJesus-Hernandez *et al.* 2011; Renton *et al.* 2011). This landmark discovery has impacted the understanding of these disorders and confirmed a causal link in their etiologies, hence opening new areas in the field to search for new potential therapeutic target. Mutations in *C9ORF72* result on an equal probability of developing FTD or ALS (Ling *et al.* 2013). The G_4C_2 repeat expansion is located in a non-coding region of the *C9ORF72* gene and is present in around 5-20% of sporadic FTD and ALS patients, and in ~40% of familial cases of FTD and ALS (Majounie *et al.* 2012). It is well known that C9ALS/FTD patients can harbor hundreds to thousands of G4C2 repeats, however the minimum repeat number necessary to cause the disease has not been well defined yet. A recent meta-analysis report demonstrated that only 24 to 30 repeats are enough to cause ALS, increasing the number of cases that can be explained by this repeat expansion (Iacoangeli *et al.* 2019). The C9ORF72 gene consist in 11 exons with three alternatively transcript variants reported (DeJesus-Hernandez *et al.* 2011). These transcripts generate two isoforms of the protein: variant 1 encoding the short form (C9ORF72-S), a protein with 222 amino acids of

24 kDa, and variants 2 and 3 encoding the long form (C9ORF72-L), a 481-amino acid protein of 54 kDa (Renton *et al.* 2011; DeJesus-Hernandez *et al.* 2011).

Due to its intronic location, in normal conditions, the repeat expansion should be spliced out from the mature mRNA, however, it can be retained in a truncated transcript or as immature mRNA which can serve as templates for a non-canonical form of translation known as **r**epeat **a**ssociated **n**on-AUG (RAN) translation (Zu *et al.* 2013; Ash *et al.* 2013; Mori *et al.* 2013a).

Extensive research in the past 10 years has proposed three main hypothesis to explain how *C9ORF72* repeat expansion leads to C9ALS/FTD: one based on loss-of-function due to reduced C9ORF72 protein content (Waite *et al.* 2014; Xiao *et al.* 2015; Viodé *et al.* 2018), and the other two associated to gain-of-function mechanisms. The first is attributed to the generation of nuclear RNA foci and sequestration of RNA-binding proteins (DeJesus-Hernandez *et al.* 2011); the second, to the translation of different dipeptide repeats (DPR) from these RNAs by **r**epeat-**a**ssociated **n**on-ATG (RAN) translation in both sense and antisense directions, generating five different DPR: glycine-alanine (poly(GA)) and glycine-arginine (poly(GR)) from sense G_4C_2 repeats, proline-arginine (poly(PR)) and proline-alanine (poly(PA)) from antisense G_2C_4 repeats, and glycine-proline (poly(GP)) peptides from both sense and antisense transcripts (Zu *et al.* 2013; Ash *et al.* 2013; Mori *et al.* 2013a) **(Figure 1A).**

DPR form neuronal inclusions throughout the central nervous system (CNS) of C9FTD/ALS patients, and are considered as a histopathological hallmark of the disease (Mori *et al.* 2013b; Ash *et al.* 2013). Studies in flies and human derived cells,

suggest that poly(GA) as well as arginine-rich peptides, poly(GR) and poly(PR) may be the main drivers of neuronal toxicity (Mizielinska *et al.* 2014; Kramer *et al.* 2018; Freibaum and Taylor 2017; Zhang *et al.* 2014). These DPR present different physico-chemical characteristics, where the poly(GA) DPR are uncharged and have a high tendency to form aggregates; and poly(GR) and poly(PR) are both highly charged and polar. On the other hand, poly(GP) and poly(PA) are uncharged and apparently nontoxic (Freibaum and Taylor 2017).

Importantly, recent reports suggest that proteostasis dysfunction stand as a main cellular event triggered by *C9ORF72* genetic alterations (Kramer *et al.* 2018; Hetz and Saxena 2017; Ruegsegger and Saxena 2016; Prudencio *et al.* 2015; Zhang *et al.* 2014; Torres *et al.* 2021). Thus, in addition to generate abnormal protein aggregates with toxic properties, mutations in *C9ORF72* may also alter the equilibrium of the neuronal proteome resulting in synaptic and neuronal dysfunction due to disruption of the proteostasis machinery, which encompass all cellular processes involved with synthesis, folding, trafficking and degradation of proteins (Taylor *et al.* 2016; Dafinca *et al.* 2016; Shahheydari *et al.* 2017; Elliott *et al.* 2020).

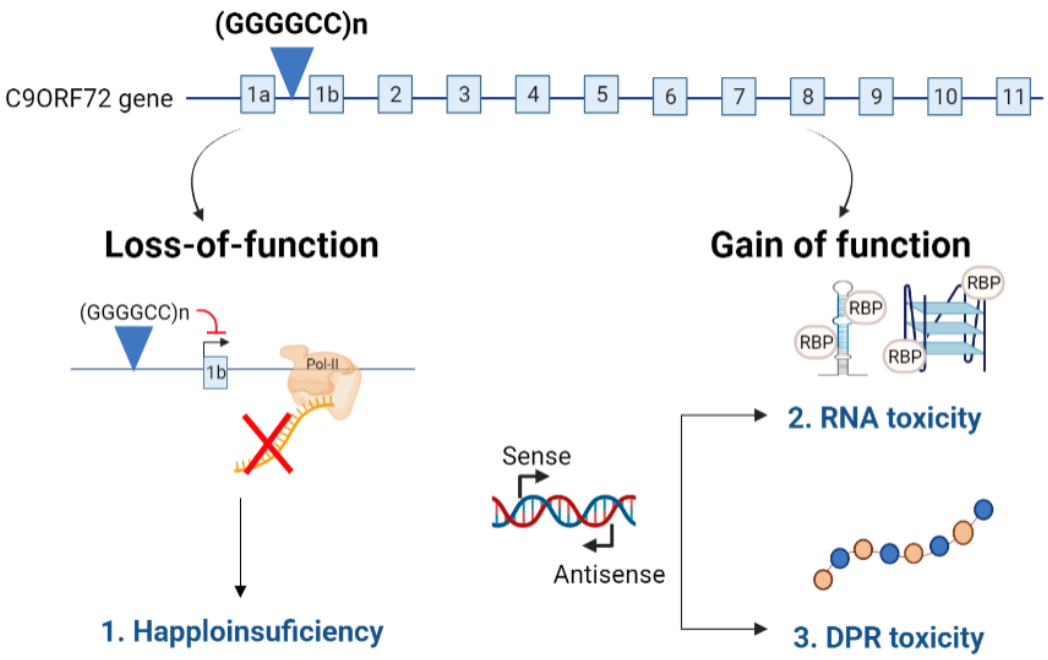

Figure 1. Mechanisms of C9ORF72 related toxicity. 1) Haploinsufficiency. The GGGGCC repeat expansion is located between exon 1a and 1b in the C9ORF72 gene. This mutation can lead the downregulation of C9ORF72 protein, causing haploinsufficiency. 2) RNA toxicity. Repeat expanded GGGGCC RNAs are retained in the nucleus where can form secondary structures as hairpins and G-quadruplexes that binds RBP (RNA binding proteins) to form insoluble nuclear foci. 3) DPR toxicity. These repeats expanded GGGGCC RNA can be translated by RAN translation generating five different DPR: poly-GA and poly-GR from sense strand, poly-PA, poly-PR from anti-sense strand and poly-GP from both strands.

1.2 Proteostasis disturbances in FTD and ALS

The development of genetic models of FTD/ALS has enabled dissection of different stages during disease course at the histological, cellular, and molecular level. Most of the field has relied in the use of mutant Tau transgenic mice as experimental FTD model and mutant SOD1 transgenic mice as experimental ALS model, with limited translational potential due to the low frequency of these mutations in patients (Wei *et al.* 2017). The recent development of new mouse models to study *C9ORF72* pathogenesis is expected to accelerate the understanding of the molecular mechanisms and the future development of experimental treatments (Chew *et al.* 2015). Although multiple pathways are proposed to drive FTD and ALS, protein homeostasis or proteostasis unbalance, arise as significant pathogenic process (Hetz and Saxena 2017). Relevant to this question, the endoplasmic reticulum (ER) is a major compartment involved in protein folding and quality control that is dramatically affected in FTD and ALS neurons and motoneurons, respectively.

Disturbance of ER proteostasis is counteracted by the activation of the **unfolded protein response (UPR)**, a signal transduction platform that mediates the engagement of adaptive programs to restore cell function (Walter and Ron 2011). Upon failure to mitigate ER stress, the UPR turns its signaling into an apoptotic phase to eliminate irreversibly damaged cells (Tabas and Ron 2011). Importantly, the occurrence of ER stress has been extensively reported in FTD and ALS patients, and in cellular models of C9ORF72-FTD/ALS (Medinas *et al.* 2017; Torres *et al.* 2021).

1.3 ER stress and UPR signaling

Multiple pathways have been proposed to drive ALS and FTD pathology, however proteostasis unbalance arises as significant altered process (Hetz and Saxena 2017; Ling *et al.* 2013). The major compartment involved in protein folding and quality control is the ER, and the function of the secretory pathway is severely affected in ALS and FTD (Kanekura *et al.* 2016; Gami-Patel *et al.* 2021; Prudencio *et al.* 2015; Kramer *et al.* 2018; Zhang *et al.* 2014).

At the ER nearly one third of the total proteome is synthetized and folded, which is increased in specialized secretory cells (Braakman and Bulleid 2011). Under physiological conditions, protein maturation is strictly mediated by ER chaperones and foldases, which bind and assist the correct folding of proteins preventing their aggregation. Nevertheless, different stress conditions alter the folding balance at the ER, resulting in rising levels of misfolded proteins, a condition referred to as “ER stress”. These insults include the expression mutant ER cargo that chronically misfold, altered ER calcium balance (essential cofactor of ER chaperones), redox unbalance (necessary to form disulfide bounds), disrupted chaperone function, among other perturbations. Equilibrated proteostasis requires the dynamic coordination of efficient folding of newly synthesized proteins and quality control and degradation mechanisms to reduce the load of unfolded/misfolded proteins and prevent abnormal protein aggregation (Walter and Ron 2011). Under ER stress, cells activate a dynamic signaling network known as the unfolded protein response (UPR) (Hetz *et al.* 2020). The UPR has an important function in stress adaptation and cell

survival; however, under chronic or irreversible ER stress a switch to pro-apoptotic signaling can lead to the elimination of damaged cells (Urra *et al.* 2013). Therefore, the UPR stands as a central controlled of cell fate under proteostasis stress. The UPR triggers initial adaptive responses through various mechanisms, including transcriptional and translational regulation that increase the folding capacity of the ER, among other effectors (Walter and Ron 2011).

The UPR is orchestrated by three type-I transmembrane ER proteins, including inositol-requiring protein 1α (IRE1α), protein kinase RNA-like ER kinase (PERK) and activating transcription-6 (ATF6) (Hetz and Papa 2018) **(Figure 2)**. Under resting conditions, these transducers are maintained inactive by their association with the ER chaperone BiP (also known as GRP78) at the ER lumen (Preissler and Ron 2019). When misfolded proteins accumulate, BiP dissociates from these sensors triggering the UPR to preferentially bind misfolded proteins. Alternatively, IRE1 and PERK may sense ER stress by a direct bind to misfolded proteins, resulting in their oligomerization and activation (Gardner *et al.* 2013). IRE1α catalyzes the unconventional splicing of mRNA encoding the transcription factor X-box binding protein-1 (XBP1), resulting in the production of a potent transcription factor known as XBP1s (for the spliced form) that transactivates the expression of a variety of proteostasis effectors (Park *et al.* 2021). PERK is a kinase that phosphorylates the translation initiation factor eIF2α, inhibiting global protein synthesis (Harding *et al.* 2000b). This event also triggers the alternative translation of the mRNA encoding the transcription factor ATF4. Subsequently, ATF4 translocate to the nucleus, which

increases the expression of CHOP and ATF3 and TRB3 (Ohoka *et al.* 2005; Liu *et al.* 2016b).

The preferential translation of ATF4 involves two upstream ORFs (uORFs): uORF1 and uORF2. uORF1 is a positive-acting element that facilitates ribosome scanning and re-initiation at the next coding region, uORF2, which is an inhibitory element that blocks *ATF4* expression in non-stressed cells. However, in stress conditions, efficiency of ribosomes is affected by the decrease in eIF2-GTP levels, increasing the time required for scanning ribosomes to restart translation, allowing the ribosomes to scan through the inhibitory uORF2 and reinitiate at the ATF4-coding region (Vattem and Wek 2004).

During stress conditions, phosphorylation of eIF2 and the accompanying reduction in the levels of eIF2-GTP increase the time required for the scanning ribosomes to become competent to reinitiate translation. This delayed reinitiation allows for ribosomes to scan through the inhibitory uORF2 and instead reinitiate at the ATF4-coding region.

Under ER stress, ATF6 is translocated to the Golgi apparatus and subsequently cleaved to release a cytosolic fragment containing an active transcription factor ATF6f (Haze *et al.* 1999). Together XBP1s, ATF4, and ATF6f engage transcriptional reprogramming inducing genes to improve the protein folding capacity, improve protein quality control and the degradation of misfolded proteins.

Over the past decade, genetic and pharmacological manipulation of ER stress have been used to understand the causal link between ER proteostasis and

neurodegeneration (Hetz *et al.* 2019; Maly and Papa 2014). These studies have exposed a multifaceted scenario wherein distinct signaling components of the UPR have specific, and sometimes even opposite effects on the disease pathophysiology depending on the disease type, the cell type affected and the stage of the disease (Hetz and Saxena 2017; Scheper and Hoozemans 2015; Smith and Mallucci 2016).

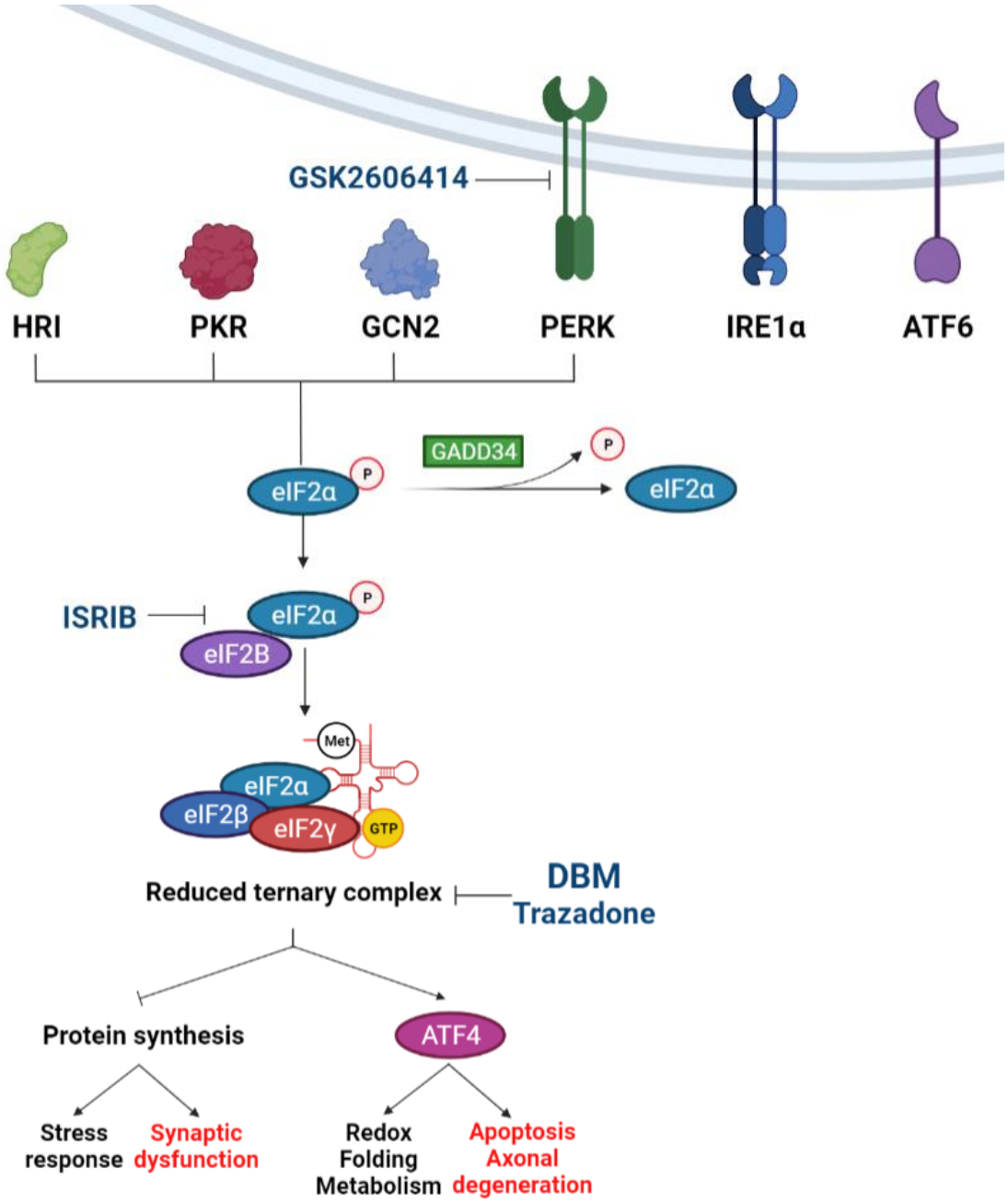

Figure 2. Unfolded protein response (UPR) and Integrated stress response (ISR) signaling and its contribution to proteostasis control and neurodegeneration.

1.4 ER stress and UPR signaling in C9FTD/ALS pathology

Maintaining cellular proteostasis becomes a greater challenge in diseases displaying mutant misfolded proteins which are chronically expressed throughout the life of an individual, such as ALS and FTD (Saxena and Caroni 2011). Accordantly, the occurrence of ER stress has been extensively reported in postmortem tissue derived from ALS patients and in most cellular and animal models of the disease (Hetz and Mollereau 2014; Saxena and Caroni 2011). ER stress has been proposed as the earliest molecular alteration detected during the asymptomatic phase of experimental ALS even before muscle denervation is observed (Saxena *et al.* 2009). Regarding C9ORF72 pathology, the accumulation of DPR induce the ER stress response as reported in several studies using cellular models and human tissue (Kramer *et al.* 2018; Dafinca *et al.* 2016; Zhang *et al.* 2014; Kanekura *et al.* 2016).

Recent reports using cell culture, primary cortical neurons and iPSC-derived human neurons suggested that C9ORF72 pathogenesis involves the occurrence of chronic and maladaptive ER stress as shown by sustained levels of PERK signaling (Zhang *et al.* 2014; Zhang *et al.* 2018b; Kramer *et al.* 2018; Wang *et al.* 2019). Moreover, gene expression studies of human brain tissue from patients affected by C9-ALS indicated deregulated UPR as a major pathological signature in cerebellum and frontal cortex (Prudencio *et al.* 2015). Additionally, C9-ALS iPSC-derived motoneurons treated with the ER stress agent tunicamycin showed a dose dependent increase in cell death compared to controls, suggesting altered ER proteostasis (Haeusler *et al.* 2014). Remarkably, an elegant study used an unbiased

genome wide CRISPR screening coupled to RNA sequencing to define modifiers of DPR toxicity. This screening revealed that ER-related proteins (such as ATF4) and secretory pathway components are highly altered by the accumulation of poly(PR_{50}) and where among the major cluster of regulators of DPR toxicity (Kramer *et al.* 2018).

Increasing evidence highlights the role of PERK-eIF2α in C9FTD/ALS pathogenesis in different models (further discussed in the next section) (Cheng *et al.* 2018; Green *et al.* 2017; Kanekura *et al.* 2016; Kramer *et al.* 2018; Sonobe *et al.* 2018; Westergard *et al.* 2019). Moreover, increased levels of caspase-3 and ER stress markers such as BIP, phosphorylated PERK and CHOP (a major ER stress proapoptotic factor), but not XBP1s and ATF6 (adaptive components), were detected in primary neurons overexpressing poly(GA_{50}) (Zhang *et al.* 2014), suggesting the induction of pro-apoptotic and degenerative programs. Importantly, recent results suggest that TDP-43 promotes stress granule formation and increased eIF2α phosphorylation, enhancing RAN translation and triggering the production of more DPR that contribute to neurodegeneration (Cheng *et al.* 2018). Overall, these findings highlight the role of PERK-eIF2α in C9FTD/ALS. **Although *C9ORF72* mutations are the main known cause of FTD and ALS, the possible therapeutic potential of targeting proteostasis with small molecules have not been explored in preclinical mouse models**, representing a major need to move forward novel therapeutic strategies into the clinic.

1.5 Integrated Stress Response in C9FTD/ALS pathology

As previously commented, PERK is one of the three UPR stress sensor that signals through protein translation inhibition and the expression of ATF4. Translational initiation involves the formation of a ternary complex, consisting of eIF2, initiator methionine transfer RNA and guanosine triphosphate (GTP), supplied by eIF2B, that loads the mRNA to be translated into the ribosome (Pakos-Zebrucka *et al.* 2016).

In addition to PERK, other three sensing kinases are capable to phosphorylate the subunit α of eIF2, a pathway known as the integrated stress response (ISR) (Costa-Mattioli and Walter 2020). Each of these kinases respond to different cellular stimuli: GCN2 senses amino acid starvation (Deval *et al.* 2009); PKR detects viral RNA under infection (Rojas *et al.* 2010) and HRI senses to heme deficiency, (Chen 2007). HRI is also a key effector of the mitochondrial UPR, controlling many genes involved in bioenergetics and mitochondrial fitness (Anderson and Haynes 2020). When eIF2α is phosphorylated, it binds to eIF2B, preventing it from loading GTP into the ternary complex. This event quickly reduces the load of proteins entering the ER, having an important pro-survival effect (Harding *et al.* 2000a) (Figure 2). However, a small subset of mRNAs can overcome this suppression through non-canonical translation initiation by using internal ribosome entry site (IRES) elements, upstream open reading frames (uORFs) or non-AUG initiation codons (Vattem and Wek 2004; Palam *et al.* 2011), as is the case of RAN translation.

Under normal physiology, eIF2α phosphorylation is considered neuroprotective, where the reduction of protein synthesis is accompanied by increased translation of selective mRNAs involved in cell survival. However, chronic stress and global protein synthesis inhibition can turn into a deleterious event leading to apoptosis and altered synaptic function (Pakos-Zebrucka *et al.* 2016; Costa-Mattioli and Walter 2020). The control of protein synthesis is a central process regulating neuronal physiology. In fact, studies in models of Prion disease, Parkinson´s disease and FTD have demonstrated that sustained phosphorylation of eIF2α due to PERK hyperactivation negatively affects the synthesis of synaptic proteins, impacting brain function and neuronal plasticity on a negative manner (Moreno *et al.* 2013; Moreno *et al.* 2012; Mercado *et al.* 2018). These biological activities are shared with other kinases of the ISR pathway, as reported in functional studies aimed at manipulating PKR and GCN2 levels in the context of synaptic plasticity and AD (Ma *et al.* 2013; Duran-Aniotz *et al.* 2014). Moreover, another report suggested that ATF4, induces axonal degeneration in AD models, propagating damaging signals on a cell-nonautonomous manner (Baleriola *et al.* 2014).

Importantly, cellular stresses that triggers ISR activation enhance RAN translation in cells and neurons (Cheng *et al.* 2018; Green *et al.* 2017; Westergard *et al.* 2019; Sonobe *et al.* 2018), suggesting a feed-forward loop between DPR production and the stress generated by the accumulation of these abnormal peptides **(Figure 3).** ISR activation has been widely associated to DPR accumulation in cells and flies models (Kramer *et al.* 2018; Westergard *et al.* 2019; Zhang *et al.* 2018a). In this context, a study reported that a small molecule that inhibits ISR, known as ISRIB

(Sidrauski *et al.* 2013) decreases the toxicity generated by poly(PR_{20}) (Kramer *et al.* 2018). Additionally, another report showed that ISR activation by sodium arsenite induced G_4C_2 repeat foci in *C9orf72* patient fibroblasts (Glineburg *et al.* 2021). Moreover, administration of ISRIB or the PERK inhibitor GSK2606414 to a fly model of C9ORF72 pathogenesis provided strong neuroprotection (Zhang *et al.* 2018a). Similar results were provided in iPSC-derived motoneurons from C9ORF72 positive ALS patients (Zhang *et al.* 2018a), suggesting that inhibition of the pathway at different levels might have beneficial effects. These results are in line with others findings indicating that the administration of PERK/eIF2α inhibitors reduce RAN translation and DPR accumulation (Cheng *et al.* 2018; Westergard *et al.* 2019). It was recently reported that RAN translation is not only mediated by phosphorylation of eIF2α through PERK activation, but also by PKR (Zu *et al.* 2020). Importantly, PKR inhibition dramatically decreases DPR accumulation *in vitro* and *in vivo*, and its inhibition improved behavior in a C9ORF72 ALS/FTD BAC transgenic mice (Zu *et al.* 2020).

Conversely, other study have suggested that inhibition of eIF2α phosphatases, where sustained eIF2α phosphorylation is induced, was protective in SOD1 mouse models (Jiang *et al.* 2014). However, another study showed that this inhibition accelerates the disease in a SOD1 mice (Vieira *et al.* 2015). The discrepancies in these reports could be possible attributable to factors like the timing of administration drug in the course of the disease, among others.

Overall, accumulating evidence indicates that strategies to reduce eIF2α phosphorylation or its downstream effects may have neuroprotective consequences

in the context of C9ALS/FTD pathogenesis. Therefore, restoration in protein synthesis could have the following neuroprotective effects: 1) improvement in synaptic function, 2) reduction of DPR production and 3) reduction of ER stress-mediated apoptosis. For the above-mentioned, it is important to define the therapeutic potential of the ISR in ALS/FTD.

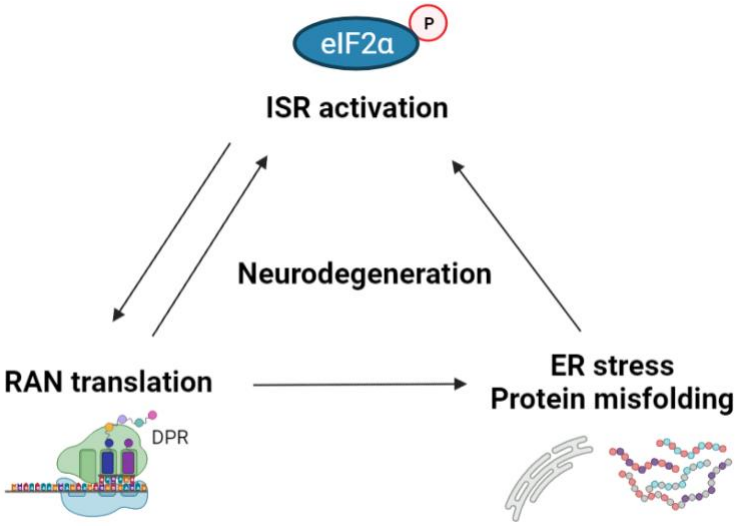

Figure 3. Feed-forward loop mechanism proposed by the literature to explain relationship between RAN translation and phosphorylation of eIF2α. DPR production can induce stress through ISR activation or ER stress. This stress caused by the repeat expansions can trigger a positive feed-forward loop that drives RAN translation while impairing global translation through eIF2α phosphorylation and subsequent production of additional DPR through ISR, thereby promoting neurodegeneration.

1.6 Pharmacological targeting of PERK/eIF2α pathway

Recent drug discovery efforts to target the PERK/eIF2α pathway have identified a subset of small molecules as possible candidates. The PERK inhibitor, GSK2606414, showed high bioavailability following oral administration, besides potency and high selectivity (Atkins *et al.* 2013; Axten *et al.* 2012) **(Figure 4).** Oral administration provided strong neuroprotection in prion-infected animals and models of FTD mediated by the expression of mutant Tau (Moreno *et al.* 2013; Radford *et al.* 2015). In a recent study from our laboratory we showed that oral treatment with GSK2606414 provided protection to nigral-dopaminergic neurons against a Parkinson's disease-inducing neurotoxin (Mercado *et al.* 2018). Despite its neuroprotective activity, GSK2606414 has serious side effects, provoking pancreatic toxicity (Moreno *et al.* 2013; Halliday *et al.* 2015). On the other hand, ISRIB, was identified as a highly selective drug to inhibit ATF4 expression (Sidrauski *et al.* 2013) **(Figure 4)** through the stabilization of eIF2B (Sekine *et al.* 2015; Sidrauski *et al.* 2015; Tsai *et al.* 2018; Zyryanova *et al.* 2017). ISRIB has low toxicity, in addition to cross the blood-brain barrier (BBB) (Sidrauski *et al.* 2013). This molecule blocks the downstream events following eIF2α phosphorylation, and was shown to improve synaptic plasticity in wild-type animals (Sidrauski *et al.* 2013), and protecting against experimental models of Prion infection (Halliday *et al.* 2015) and traumatic brain injury (Chou *et al.* 2017). Besides, as it was mentioned before, ISRIB was protective in cells and fly models of C9ORF72 (Zhang *et al.* 2018a; Kramer *et al.* 2018). ISRIB served as a fundamental tool to validate the role of ISR as a prominent target for disease intervention, however this molecule shows poor

solubility, hence limiting its translational potential. Nevertheless, accumulating evidence indicates that strategies to reduce eIF2α phosphorylation may have therapeutic applications in the context of neurodegenerative diseases.

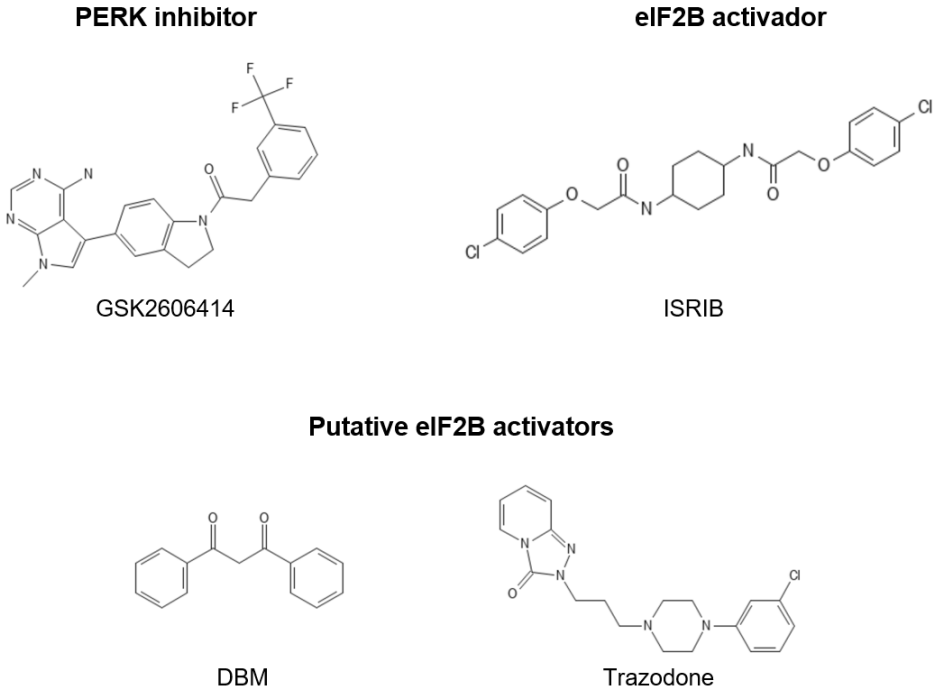

Figure 4. Small molecules to target PERK-eIF2α axis.

To solve the issue of the low solubility of ISRIB, a recent study identified small molecules with the potential to block eIF2α-P activity (Halliday *et al.* 2017). In those lines, our collaborator, Dr Giovanna Mallucci (University of Cambridge, UK) performed a phenotypic screen and discovered two compounds from a NINDS small molecule library that reversed translational attenuation triggered by eIF2α phosphorylation (**Figure 4**). The screening approach consisted of two consecutive steps: first, they tested the ability of 1040 compounds to prevent ER stress-induced developmental delay in *C. elegans*, leading to the identification of 20 compounds; second, using UPR-reporter cell lines, they validated five compounds that partially reduced CHOP expression under ER stress. Finally, **two compounds were selected for further preclinical studies based on their clinical potential: dibenzoylmethane (DBM)** and trazodone **(Figure 4)**. Importantly, the site of action of DBM was similar to ISRIB since it reduces ATF4 levels without affecting the phosphorylation of eIF2α. Those small molecules showed impressive therapeutic potential when applied to models of Tau-mediated FTD and Prion disease (Halliday *et al.* 2017) providing neuroprotection, reversing memory deficits, and delaying disease progression. Furthermore, **analysis of the bioavailability and pharmacokinetics of DBM indicated a remarkable BBB penetration and favorable stability** (Halliday *et al.* 2017).

The discovery of DBM as possible drug to target the ISR opens the possibility of a major new avenue to restore the functionality of the proteostasis network in FTD/ALS to potentiate synaptic function and neuronal survival. Thus, fine-tuning eIF2α phosphorylation for therapeutics requires further investigation in preclinical

models of FTD/ALS-C9ORF72 to understand in more detail possible side effects and determine the optimal administration regimen. This challenge represents the major subject of the current PhD thesis.

2. HYPOTHESIS

Oral administration of dibenzoylmethane (DBM), decreases dipeptide repeats (DPR) accumulation, prevents neuronal loss, and slows progression in a mouse model of C9ORF72-mediated FTD/ALS.

3. AIMS

3.1. General aim

To investigate the impact of DBM administration in the neurodegeneration associated to the accumulation of DPR in a mouse model of C9ORF72-FTD/ALS.

3.2. Specific aims

1) To investigate the effects of oral DBM treatment in a mouse model of C9ORF72-FTD/ALS at behavioral level.

2) To determine the consequences of DBM oral administration on histopathological and biochemical features in C9ORF72-FTD/ALS mice.

3) To determine proteomic changes mediated by DBM treatment in the hippocampus of C9ORF72-FTD/ALS mice.

4. Materials and methods

4.1 Mice

Experiments were carried out on *wild type* mice C57BL/ 6J strain. Animals were kept in cycles of 12:12 hours light / dark, at an ambient temperature of 22 ± 2 °C, with free access to food and water. Animal care and experiments were performed according to procedures approved by the Bioethics Committee of the Faculty of Medicine of the University of Chile (approved protocol CBA # 18214-MED-UCH).

4.2 Neonatal viral injections

Adeno-associated virus (AAV) packaged into serotype 9 type capsid, containing 2 or 66 repeats of G_4C_2 (AAV-2R and AAV-66R, respectively), were intracerebroventricular (ICV) injected in newborn C57BL/6J *wild type* mice to achieve efficient transduction in neurons of the central nervous system. Viral vectors for this study were provided by Dr. Leonard Petrucelli (Mayo Clinic, Jacksonville FL, USA).

Newborn mice were cryo-anesthetized on ice for a few minutes until no movements were observed. A 32-gauge needle (BD Biosciences) was inserted at 30-degreee angle, between lambda and the eye pup, and sunk to a depth of approximately two millimeters. Four microliters with 0.02% Fast Green (1E5 genomes/ul) of each virus were manually injected in the corresponding pups in the cerebral ventricle. Finally, pups were placed on a heat pad until they recovered movements and placed back

in their cages. Animals were weaned at 21 days of age and then subjected to cognitive and motor studies at 3 and 6 months of age. Finally, they were sacrificed at 8 months for biochemical and histopathological analyzes.

4.3 Pharmacological treatment

Food powdered was generated by grinding food pellets with a grinder and filtered to separate larger particles. Then, powdered chow was mixed with the drug into a Ziploc bag by hand, shaking, inverting, and rotating it for 5 minutes until obtained a homogenized solution. Finally, the mixed solution was placed in a powder feeder jar into the cage (Braintree Scientific, Inc.).

To determine target engagement of GSK2606414, wild type mice were fed with powdered food containing 100 mg/kg/d GSK2606414 or vehicle *ad libitum* for 7 days. GSK2606414 was provided by Dr. Jeffrey Axten. To determine target engagement of DBM (Sigma), wild type mice were fed with powdered chow containing 0.5% dibenzoylmethane (DBM) or vehicle *ad libitum* for 7 days.

To perform DBM (Sigma) treatment in the animals injected with the AAV-2R or AAV-66R., mice were fed with powdered chow containing 0.5% dibenzoylmethane (DBM) or vehicle *ad libitum* from month 2 till the end of the experiment.

4.4 Behavioral tests

In order to determine the progression of the C9ORF72 FTD/ALS disease, a battery of motor and behavioral tests was performed. This battery includes open field assay, novel object recognition test (NOR), novel object location test (NOL), rotarod test, hanging wire test and Barnes maze. All behavioral equipment was cleaned with 35% ethanol between each mouse. 14–16 mice were used per group as this gives adequate statistical power to detect changes in behavior.

4.4.1 Open Field Test

Open Field Test is used to measure both motor and cognitive deficits of the mouse. The apparatus consists in a 40x40 cm square box of polymethylmethacrylate (PMMA) with a video recorder on the top. Mice were placed in the center of the box and could explore freely the arena for fifteen minutes. Mice were recorded and movements were tracked and analyzed by AnyMaze program (Stoelting, Co.) This program divides the box into 16 equal quadrants, of which 4 form the center, 4 the corners and a total of 8 form the periphery. This test was performed to evaluate motor deficits and anxiety behaviors. The distance traveled in the center zone versus the total distance traveled were plotted.

4.4.2 Novel Object Recognition (NOR)

NOR task is used to evaluate the rodent's ability to recognize a novel object. NOR is performed in two consecutive days: on the first day, mice were allowed to freely explore two identical objects in an open field arena. Because of the innate mouse curiosity, mice will explore both objects equally. Interaction time with each object was determined. The test was performed for 5 minutes or until the interaction time of both objects reach 20 seconds. On the second day, 24 hours later, one of the identical objects is replaced for a novel object and interaction time with both objects is recorded. As same than day one, the task was performed for 5 minutes or until the interaction time of both objects reach 20 seconds. Normal mouse spent more time in the novel object because of innate mouse curiosity, however mice with memory problems will not be able to discriminate between the familiar and novel object. The percentage of time spent on the novel object is calculated using the following formula: (t new object/(t new object + t old object))*100%. Objects were randomly assigned to reduce object and place preference effects. Animals that did not interact with any object (0%) or those that interacted with only one object (100%), were excluded from the analysis.

4.4.3 Novel location recognition (NOL)

NOL test is a long-term spatial memory test, that is used to evaluate memory hippocampus dependent in rodents. A protocol similar to NOR was used. Unlike NOR, in the NOL test the location of one of the objects is changed on the second day of the test. The percentage of time spent on the changed object is calculated using the following formula: (t new location object/(t new location object + t old object))*100%. Animals that did not interact with any object (0%) or those that interacted with only one object (100%), were excluded from the analysis.

4.4.4 Hanging wire test

This test was performed to monitor muscle strength and coordination. The test is based in the mouse latency to fall from a metal wire stretched between two supports at a height of 35 cm. Each mouse was carried by the tail to the middle of the cable where it instinctively grabs it with the front legs. This test records the number of falls of the mouse for 2 minutes.

4.4.5 Rotarod test

Rotarod test was performed at three and six months of age. In this test the rodent is placed in a horizontally oriented rotating cylinder, suspended above the floor of the device, low enough not to injure the animal, but high enough to avoid

inducing fall. Rodents will naturally try to stay on the rotating cylinder and avoid falling to the ground (Jones & Roberts, 1968). This test is generally used to evaluate the motor capacity of the mouse, but applying a modified protocol (Chew *et al.* 2015), it is possible to study the motor and cognitive capacity of the mouse. This test was carried out for four consecutive days, where the first day the mouse is briefly trained to become familiar with the machine, this is done at a basal rate of 4 revolutions per minute (rpm) until the mouse is hold onto cylinder. Then the test is performed where the time the mouse is in the device is measured with an increasing speed from 4 to 40 rpm over a period of 5 minutes. Three attempts per mouse were made each day. Then the average of the three attempts of each day was graphed.

4.4.6 Barnes maze

Barnes maze is a circular maze with holes around its borders, designed to evaluate spatial learning and memory acquisition. It basically consists in teaching mice to find the hole corresponding to target location, which consists in a hidden dark box not visible from the platform. When mice find the target location and hide in the box, the test is completed. This protocol is repeated four times during 3 minutes for 5 consecutive days.

4.5 Tissue preparation

Mice were euthanized at 8 months old by inhalation of carbon dioxide (CO_2) and perfused transcardially with 0.9% NaCl solution. Mice brains were removed and split in two hemispheres: right for biochemical analysis and left for histopathological analysis.

For biochemical assays, different brain tissues were collected: frontal cortex, cortex, hippocampus, cerebellum, in addition to muscle (gastrocnemius and tibialis anterior), sciatic nerve, lumbar spinal cord and pancreas, which were stored at -80 °C. Additionally, blood glucose levels and brain weight were measured. A total of 63 mice were used in this experiment.

Left hemisphere was fixed at 4% PFA for histological analyzes to determine C9ORF72 FTD/ALS features: DPR inclusions, neuronal loss, and gliosis. Left hemisphere was dehydrated through a battery of alcohols (two hours in alcohol at 80, 90, 95, 95, 100 and 100% each one), xylene (six hours in xylene 100%) and the end, brains were put in paraffin (six hours) before being included in paraffin. Then 5 µm thick sections were serially cut into a microtome (microm HM 325, Thermo Fisher scientific) and 4 sections were mounted on a positively charged slide having 75 µm between each section. Finally, slides were dry at 37 °C overnight.

4.6 Immunohistochemistry

The slides containing the paraffin-embedded sections were deparaffinized and rehydrated in xylene (2x5 minute) and a battery of alcohols (100, 95, 90, 80, 70%) for 1 minute for each concentration and then washed in water (1 minute). The endogenous peroxidase was then blocked with a 0.3% H_2O_2 solution (Merck, Germany) in PBS solution. After that slides were washed in PBS (3 x 5 minutes) and antigen exposure was performed in a steam chamber (30 minutes) with citrate buffer (pH 6.0). After washing twice with PBS, sections were blocked using a blocking solution (5% BSA, 0.3% Triton in PBS) (45 minutes) or the M.O.M. (mouse-on-mouse) (BMK-2202, Vectastain) (1 hour) depending on primary antibody host. Finally, sections were incubated at room temperature in a humid chamber overnight, with the corresponding primary antibody.

Before to incubate with the secondary antibody, sections were washed thrice with PBS. The ABC Vectastain kit for mice (1:1000) (pk-6100, Vectastain) + blocking solution (1:66.67) was then used for secondary antibodies for one hour, followed by half an hour with solution A + B (1:50) in PBS. For rabbit ABC Vectastain kit (1: 200) (pk-4001, Vectastain) was incubated for half an hour, followed by another half hour with solution A + B (1: 100). The sections were then washed in PBS (3 x 5 minutes). Immunoreactivity was visualized with the 3,3′-diaminobenzidine (DAB) chromogen solution and stained with hematoxylin (Scyteck) when necessary. Finally, the samples were dehydrated in a battery of alcohols (70, 80, 95, 100%) for 1 minute for each concentration and xylene (2 x 5 minutes) and covered with Entellan (Merck,

Germany) and left to dry until the next day. The primary antibodies used were: anti-NeuN (1: 400) (# MAB377, Millipore); anti-Poly (GA) (1: 1500) (# TIP-C9-P01, CosmoBio); anti-Poly (GR) (1: 32000) (# TIP-C9-P01, CosmoBio); anti-GFAP (1: 200) (# ab7260, Abcam), anti-Iba1 (1: 500) (# 019-19741, Wako).

4.7 Gliosis

To quantify activation of microglia and astrocytes, immunostains were performed with antibodies for Iba1 and GFAP, respectively. Images were taken in the hippocampus with an optical microscope (Leica DM500) at a magnification of 10X. Two sections were taken per mouse to have a technical duplicate. The quantification was carried out in the hippocampus region with ImageJ program (NIH, Bethesda, United States) by determining the percentage of positive signal per each area.

4.8 DPR inclusions: poly(GA) and poly(GR)

In order to quantify DPR expression, inmunohistochemistry of poly(GA) and poly(GR) were performed. To this purpose, images of cortex (motor and somatosensorial) and hippocampus (CA1) were taken with optical microscope (Leica DM500) at a magnification of 20X. Two sections per mouse were used as a technical duplicate. Quantification was carried out manually, counting the positive cells for the signal of both poly dipeptides.

4.9 Neuronal quantification

Anti-NeuN immunohistochemistry was performed to quantify neurons. The entire motor and somatosensorial cortex were digitally acquired in an optical microscope (Leica DM500) at 10X magnification. Two sections were taken per mouse to have a technical duplicate. The quantifications were carried out using the ImageJ program (NIH, Bethesda, United States).

4.10 RNA extraction and RT-PCR

RNA was extracted from the cortex, cerebellum, and hippocampus. Tissues were homogenized in TEN buffer solution (10mM Tris-HCl, 1mM EDTA, 100mM NaCl, pH 8.0) with protease and phosphatase inhibitors (Sigma Aldrich). Then 50 µl of the homogenate was taken and an extraction was made with the TRIzol reagent (Life technologies) according to the supplier's instructions. The remaining volume was stored at -80 °C for backup. The yield of obtained RNA was obtained using a NanoDrop spectrophotometer (Biotek). Following this, 1 µg of RNA was used to obtain the cDNA by a reverse transcriptase polymerase chain reaction (RT-PCR) using a high-capacity reverse transcription kit (# 4368813, Applied Biosystems) according to manufacturer's instructions.

4.11 PCR

For each polymerase chain reaction (PCR), cDNA was incubated with Go Taq Master Mix (M7123, Promega, United States), according to the manufacturer's instructions. Reactions were carried out in thermocyclers (Biorad), to amplify regions present in the *Actin*, with the following thermal profile: 95 °C for 5 min; 27 cycles of amplification of 95 °C for 15 s, 58 °C for 15 s, 72 °C for 15 s; 1 final amplification cycle of 72 °C for 5 min.

To identify viral transduction of AAVs containing 2 and 66 repeats of the G4C2 hexanucleotide, primers were designed to amplify regions upstream of the sequences containing the repeats. The thermal profile for this PCR was: 1 denaturation cycle of 95 ° C for 5 min; 28 cycles of amplification of 95 ° C for 30 s, 60 ° C for 30 s, 72 ° C for 30 s; 1 final amplification cycle of 72 ° C for 10 min. PCR products were analyzed by 2% agarose gel electrophoresis with Sybr Safe (Invitrogen, United States) at 100 volts (V).

4.12 Real time PCR

Real time PCR reactions were performed using the EvaGreen reagent (Biodyne, United States) following the supplier's instructions. Real time PCRs were performed in the Stratagene Mx3000P system (Agilent Technologies). The thermal profile used for real-time PCR was: 1 denaturation cycle of 95 °C for 10 min; 40 cycles of amplification of 95 °C for 10 s, 58 °C for 15 s, 72 °C for 20 s; 1 final

amplification cycle of 95 °C for 15 s, 25 °C for 1 s, 70 °C for 15 s and 95 °C for 1 s. Relative amounts of mRNA were calculated from comparative threshold values of 40 cycles using Actin mRNA as internal expression control.

All the quantifications were plotted as mRNA relative levels. The values were calculated by method "ΔCt", determining the potency in base 2 of the delta between the housekeeping gene and gene of interest by the following formula: $\Delta Ct = 2^{(Ct\ (housekeeping\ gene) - Ct\ (gene\ of\ interest))}$.

Gene	Primer sequence (5' to 3')
Atf4	**F:** TCG ATG CTC TGT TTC GAA TG
	R: AAG CAG CAG AGT CAG GCT TC
Atf3	**F:**CAG ACC CCT GGA GAT GTC AGT
	R: TTC TTG TTT CGA CAC TTG GCA
Trb3	**F:** CCA GAG ATA CTC AGC TCC CG
	R: GAG GAG ACA GCG GAT CAG AC
Chop	**F:** GTC CCT AGC TTG GCT GAC AGA
	R: TGG AGA GCG AGG GCT TTG
Gadd34	**F:** GAG GGA CGC CCA CAA CTT C
	R: TTA CCA GAG ACA GGG GTA GGT
Bip	**F:** TCA TCG GAC GCA CTT GGA A
	R: CAA CCA CCT TGA ATG GCA AGA
Xbp1s	**F:** TGC TGA GTC GGC AGC AGG TG
	R: GAC TAG CAG ACT CTG GGG AAG
Actin	**F:** CTC AGG AGGAGC AAT GAT CTT GAT
	R: TAC CAC CAT GTA CCC AGG CA

Table 1. List of primer used in real time-PCR used. F: Forward; R: Reverse.

5. Statistical analyses

Statistical analyses were performed using Prism V7 software (GraphPad Software Inc., USA). Data were analyzed using one-way ANOVA and Tukey's post hoc test for multiple variables. All data in bar charts shows mean ± standard deviation (SD). Statistical differences were considered significant for values of $p<0.05$. The p-values are displayed as follows: *$p<0.05$, **$p<0.01$ and ***$p<0.001$.

6. RESULTS

6.1 Characterization of C9ORF72-mediated FTD/ALS mouse model.

Several mouse models of C9ORF72 have been reported, but the AAV model that consisted in the overexpression of 66 GGGGCC repeats (AAV-66R) in the CNS, recapitulates the disease at phenotypic and behavioral level at 6 months (Chew *et al.* 2015). To reproduce this model in the laboratory, we performed intracerebroventricular injections to deliver AAV encoding 2 or 66 tandem repeats (AAV-2R or AAV-66R, respectively) to the CNS of mice at neonatal state (0-2 days). Accordantly, using both rotarod and New Object Recognition (NOR) tests we could reproduce behavioral and motor phenotypes as previously reported by Chew *et al.* 2015 as we observed motor and cognitive impairment in animals injected with AAV-66R when compared to controls following 6 months of infection **(Figure 7A and B)**. At the same time window, we also found the accumulation of poly(GA) and poly(GR) peptides in neurons in hippocampus, cerebellum and frontal cortex **(Figure 7C).** Several studies suggest that C9ORF72 pathogenesis involves the occurrence of ER stress (Kramer *et al.* 2018; Wang *et al.* 2019; Zhang *et al.* 2014; Zhang *et al.* 2018a) although this has not been demonstrated in mouse models. To test this hypothesis, following six months of AAV delivery, animals were euthanized, and brains were dissected in frontal cortex, cerebellum, and hippocampus to evaluate UPR and ISR triggering. We evaluated mRNA expression of *Atf4, Atf3, Chop, Trb3* and *Xbp1s,* in frontal cortex by real time PCR. A significant increase in the mRNA expression levels of *Xpb1* was observed in AAV-66R mice compared to AAV-2R **(Figure 7D).**

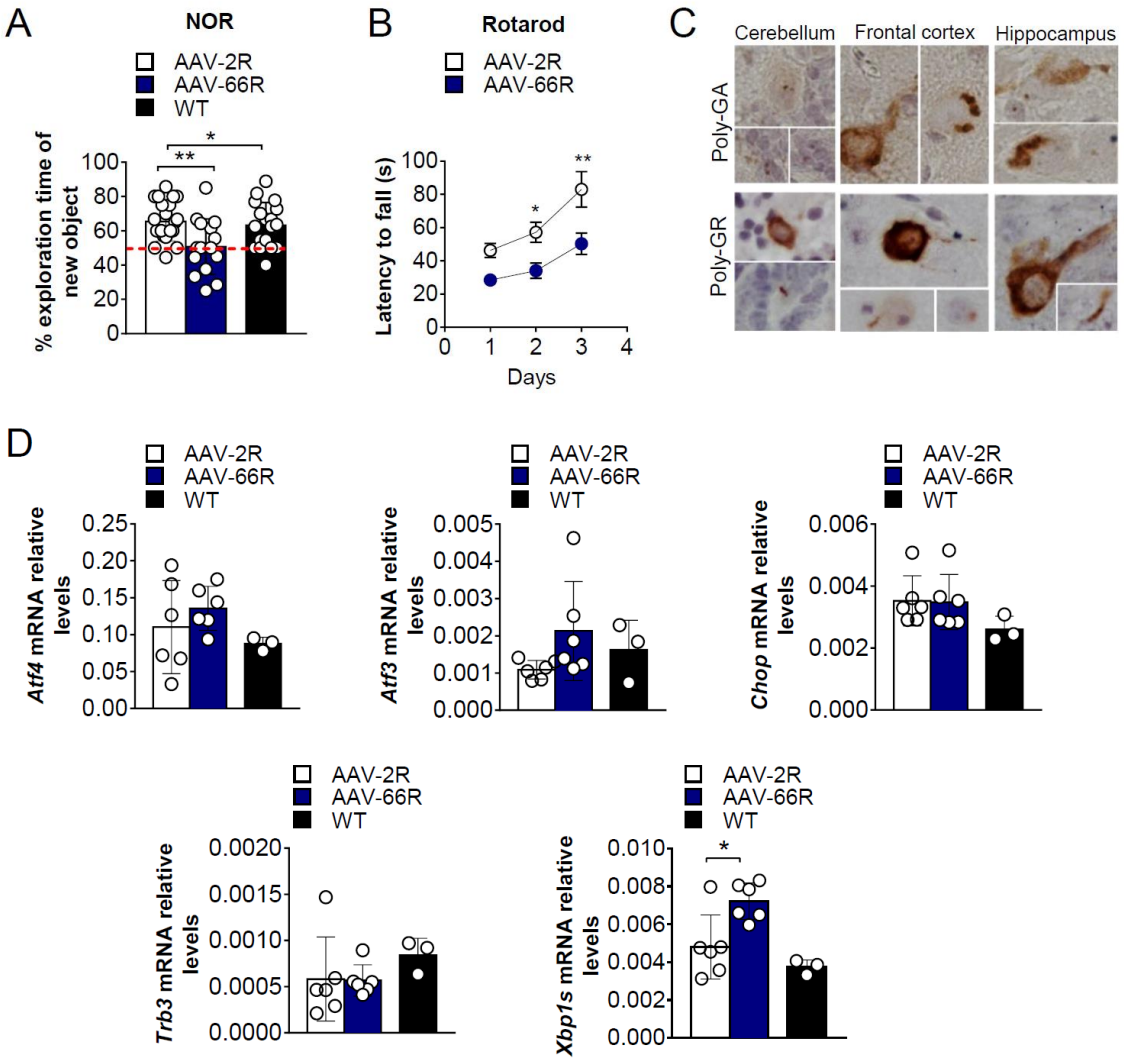

Figure 7. Characterization of C9orf72-mediated ALS/FTD. (A) New object recognition test (NOR) of mice injected with AAV-2R or AAV-66R at 6 months old. (B) Rotarod performance of WT mice injected with AAV-2R or AAV-66R at 6 months old. (C) Immunostaining of poly-GR and poly-GA inclusions from frontal cortex, hippocampus, and cerebellum of 6-month-old mice injected with AAV-66R at neonatal stage. (D) Determination of ER stress levels in the brain: RT-PCR for *Atf4, Atf3, Chop, Trb3* and *Xbp1s* from dissected frontal cortex of 6-month-old WT mice injected with AAV-2R or AAV-66R at neonatal stage. Each dot represents one animal. NT= non-treated. Data was normalized with *Actin* mRNA levels. Data are presented as mean ± S.D. *, $p < 0.05$. **; $p < 0.01$; ***, $p < 0.001$, one-way ANOVA followed by Tukey's multiple comparisons test.

These results suggest the incidence of UPR activation in C9ORF72 pathogenesis. Importantly, these results are the first demonstration of ER stress in a mouse model of C9ORF72.

6.2 Efficacy after oral delivery of small molecules to inhibit PERK/eIF2α signaling under experimental ER stress.

The activation PERK/eIF2α axis has been widely reported in different invertebrate C9ORF72 models (Zhang *et al.* 2014; Kramer *et al.* 2018; Wang *et al.* 2019; Prudencio *et al.* 2015; Westergard *et al.* 2019; Green *et al.* 2017), but not in mammalian models. Hence, we aimed to inhibit this signaling branch using small molecules in the viral-based model of C9ORF72 pathogenesis in mice. To this purpose, we first evaluated the efficacy of two drugs in wild type mice: GSK2606414, a PERK inhibitor, and DBM, an inhibitor of downstream signaling of eIF2α phosphorylation.

Searching for strategies to reduce the toxicity produced by the oral gavage administration of GSK2606414 (Radford *et al.* 2015; Halliday *et al.* 2015; Mercado *et al.* 2018), by the advice of Dr. Jeffrey Axten, we decided to administrate the drug mixed in food powdered *ad libitum.* This new route of administration is by far less stressful and invasive for animals compared to a twice-a-day oral gavage protocol, as classically used to deliver this compound in previous publications (Halliday *et al.* 2015; Radford *et al.* 2015; Mercado *et al.* 2018).

We first determined the concentration of the drug after oral delivery in blood and different tissues: frontal cortex, cerebellum, hippocampus, and spinal cord. To this aim, mice were treated with 100 mg/kg/day of GSK2606414 delivered in mixed powdered food for seven days. After this period, animals were euthanized, and their brains were dissected **(Figure 8A)**. The quantification of the drug in blood and CNS tissues was performed by protein precipitation followed by HPLC-MS/MS analysis with the collaboration of Dr. Jeffrey Axten at GlaxoSmithKline (GSK). Significant levels of GSK2606414 were found in all samples by the new administration regimen with mean concentrations of 4.83 µg/ml in blood and 1.34, 1.70, 1.89 and 1.66 µg/g in frontal cortex, spinal cord, cerebellum, and hippocampus, respectively **(Figure 8B)**. These values were different of those previously reported by our group in Mercado *et al.*, 2018, where mice were treated for three weeks by oral gavage with GSK2606414 (100 mg/kg/day). They reported higher values of the drug in serum and brain tissue, 4.15 µg/mL, and 5.20 µg/g, respectively.

Next, we measured the activity of this small molecule following experimental ER stress triggering *in vivo*. To accomplish this, wild type mice were pretreated with GSK2606414 for seven days and then exposed to tunicamycin (inhibitor of N-glycosylation), a classical activator of ER stress by intraperitoneal injection (5 mg/kg) **(Figure 8A)**. After 24 hours of tunicamycin treatment, animals were euthanized, and their brains were dissected. Mice were weighted every day of the experiment and at the end, blood glucose levels were measured. To determine the incidence of ER stress and the engage of the pathway by GSK2606414, we evaluate mRNA expression levels of downstream PERK targets: *Chop, Atf3, Trb3, Atf4 and also*

Xbp1s in frontal cortex by real time PCR (**Figure 8B and C**). Our results indicate that GSK2606414 administration decrease expression of UPR markers in the brain when compared to animals treated only with tunicamycin, suggesting that our regimen successfully attenuated ER stress triggering in brain tissue.

As previously reported in the gavage administration by Mercado *et al.*, 2018, oral administration of GSK2606414 by powdered food also led to decreased body weight compared to non-treated mice **(Figure 8F)**. This body weight drop was accompanied by a decrease in blood glucose levels **(Figure 8E)**. It is important to mention that mice that were fed with vehicle and treated with tunicamycin at day 7 lost 4.6% of body weight in one day and animals fed with GSK2606414 treated with tunicamycin lost 6.8% of body weight which could be attributed to a combined toxicity of both drugs. In addition, two of four mice of this group died minutes before scheduled time of euthanasia and the other two presented signs of morbidity, suggesting that the combination of the two drugs is lethal to mice.

Taken together, our results demonstrate that although GSK2606414 is active in the brain and blocks efficiently the PERK pathway in a pharmacological model of ER stress *in vivo*, GSK2606414 administration triggers serious side effects possibly due to pancreatic dysfunction.

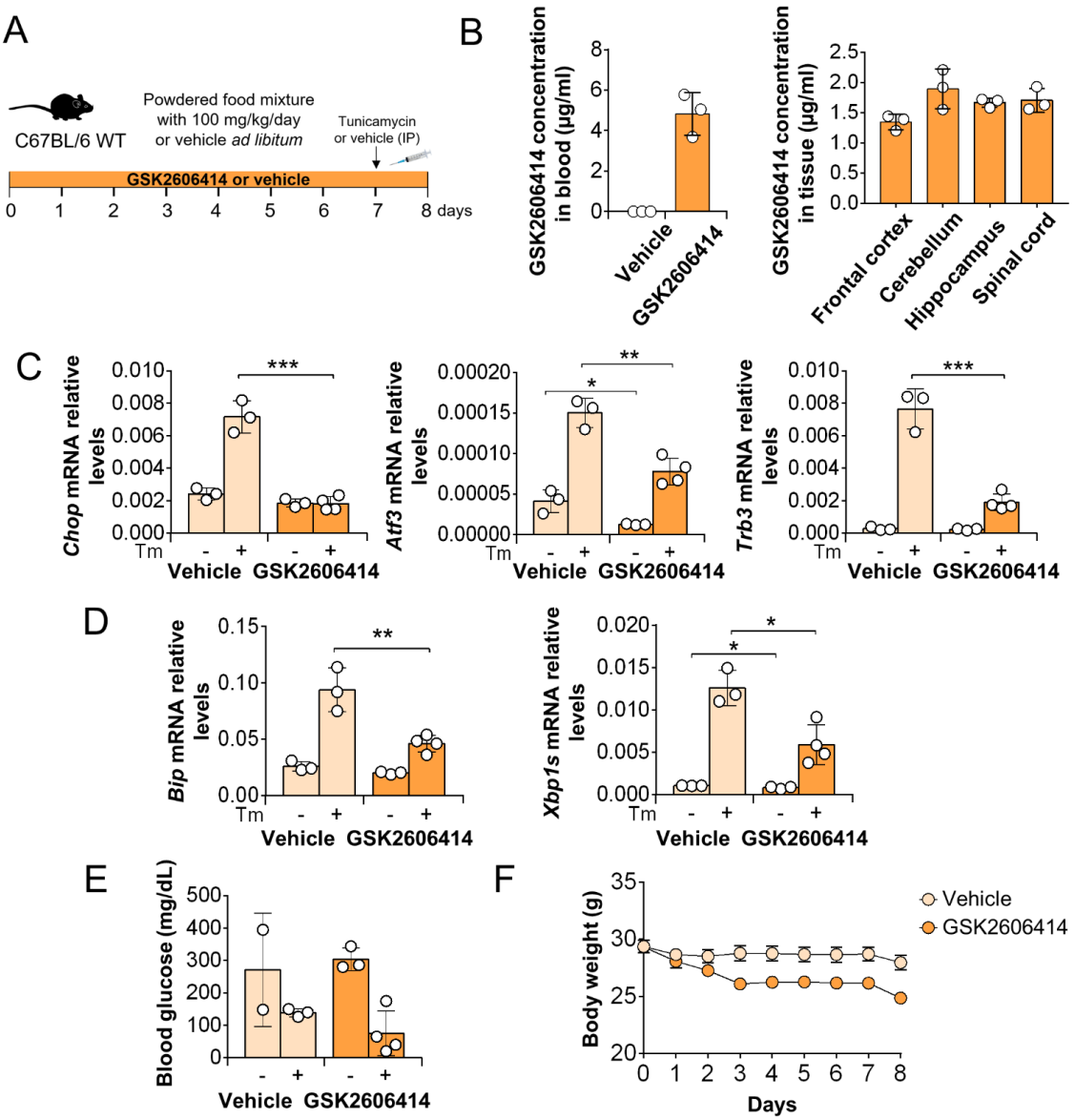

Figure 8. Food powdered administration effects of GSK2606414 in wild type mice under experimental ER stress. (A) Schematic representation of experimental design to test the efficacy of GSK2606414 administration on a pharmacological paradigm of ER stress. **(B)** Mice were treated with GSK2606414 (100 mg/kg/day) or vehicle for 7 days and the concentration of the drug in blood, frontal cortex, cerebellum, hippocampus, and spinal cord was determined by HPLC-MS/MS (n = 3). **(C)** Real time PCR analysis to monitor of *Chop*, *Atf3, Trb3* mRNA levels in frontal cortex of animals treated with GSK2606414 followed by injection of tunicamycin (Tm). **(D)** Real time PCR analysis to monitor *Bip* and *Xbp1s* mRNA levels in frontal cortex of animals treated with GSK2606414 followed by injection of tunicamycin (Tm). Data was normalized with *Actin* mRNA levels. **(E)** Glucose in blood was determinate and expressed as [mg/dL]. (F) Body weight was measured over time during treatment (N= 3-4). All data are presented as mean ± S.D. *, $p < 0.05$. **; $p < 0.01$; ***, $p < 0.001$, one-way ANOVA followed by Tukey's multiple comparisons test.

To overcome the toxicity of PERK inhibitors, we tested the efficacy of a different compound termed DBM, a drug that as was mentioned before, reverses p-eIF2α-mediated translational attenuation (Halliday *et al.* 2017). The experimental strategy to determine the DBM efficacy under experimental ER stress was the same used with PERK inhibitor GSK2606414. Mice were pre-treated for 1 week with DBM through the food (0.5% *ad libitum*) and then were exposed to tunicamycin **(Figure 9A)**. Following twenty-four hours, brains were dissected and mRNA expression levels of *Chop, Atf3, Trb3,* in addition to *Bip* and *Xbp1s* were measured by real time PCR **(Figure 9B)**. ATF4 target gene *Chop* was decreased in the frontal cortex of animals pretreated with DBM but not in those treated with the vehicle, while *Atf3* and *Bip* showed a trend of reduced expression (p value= 0.076 and 0.059, respectively). Unexpectedly, as we observed in GSK2606414 experiments, expression of *Xbp1s* was decreased both in frontal cortex **(Figure 9C)** and hippocampus **(Figure 9D)**.

Previous *in vitro* and fly models of C9ORF72 pathogenesis reported that blocking PERK/eIF2α signaling with small molecules like ISRIB or GSK2606414 had neuroprotective effects. Although these inhibitors have great efficacy in preclinical models of Tau-mediated degeneration, their translational potential is limited due to their low solubility or pancreatic toxicity, respectively. Hence, the use of small molecules with clinical potential is essential in the search for new possible treatments for such devastating diseases. In this context, DBM, which restores protein synthesis and prevents increased ATF4 translation, promoted impressive neuroprotector effects. DBM was able to rescue memory deficits in different models, with good pharmacokinetic properties and without side effects (Halliday *et al.* 2017).

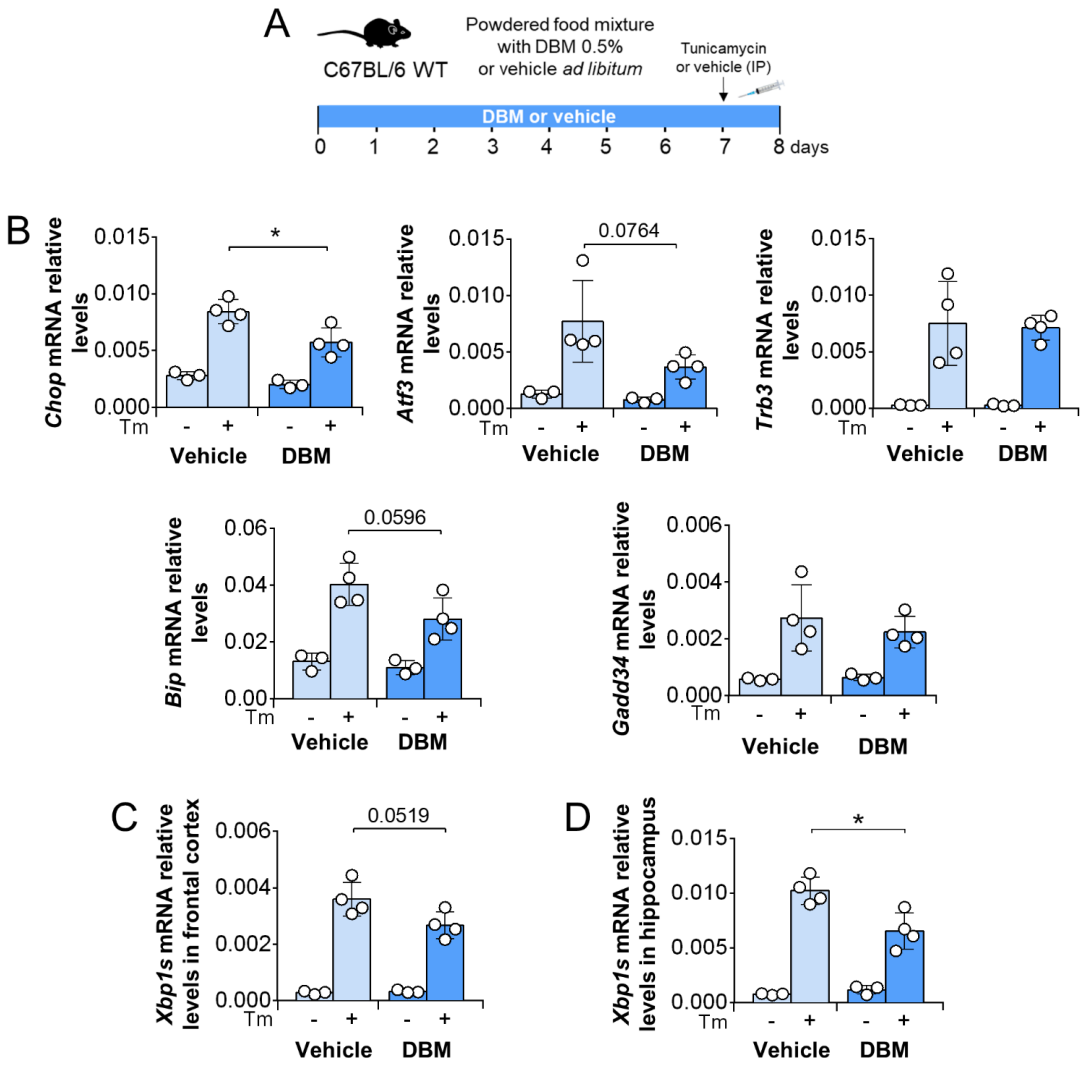

Figure 9. Oral administration of DBM decreases mRNA levels of *Chop* under experimental ER stress *in vivo*. (A) Schematic representation of experimental design to test the efficacy of DBM administration on a pharmacological paradigm of ER stress. **(B)** Real time PCR analysis to monitor *Chop*, *Atf3, Trb3, Bip* and *Gadd34* mRNA levels in frontal cortex of animals treated with DBM followed by injection of tunicamycin (Tm). **(C-D)** Real time PCR analysis to monitor mRNA of levels *Xbp1s* in frontal cortex in C, and in hippocampus in D of animals treated with DBM followed by injection of tunicamycin (Tm). All data was normalized with *Actin* mRNA levels. Data are presented as mean ± S.D. *, $p < 0.05$. **; $p < 0.01$; ***, $p < 0.001$, one-way ANOVA followed by Tukey's multiple comparisons test.

Finally, since we confirmed the efficacy of oral administration of DBM to inhibit the ISR on a model of ER stress in the brain, we selected this drug as a candidate for further studies to modulate the pathogenesis in AAV-C9ORF72-mediated FTD/ALS model.

6.3 Pharmacological treatment with DBM in C9ORF72-mediated FTD/ALS model.

To accomplish the first aim of this thesis, we followed the experimental strategy depicted in **Figure 6**. This strategy consisted in four experimental groups defined as AAV-2R/vehicle (n= 14), AAV-66R/vehicle (n=17), AAV-2R/DBM (n=17), and AAV-66R/DBM (n=15) **(Figure 5).** First, newborn pups were injected with AAV encoding AAV-2R or the expanded AAV-66R by intracerebroventricular injection. At two months of age, mice were orally treated with 0.5% of DBM mixture in powdered food *ad libitum* until the end of the experiment (eighth months later). At the third and sixth month of age, several behavioral tests were performed to evaluate disease progression. It is important to mention that three mice of our cohort were excluded from further analysis due to hydrocephaly, possible attributed to side effects of ICV injection.

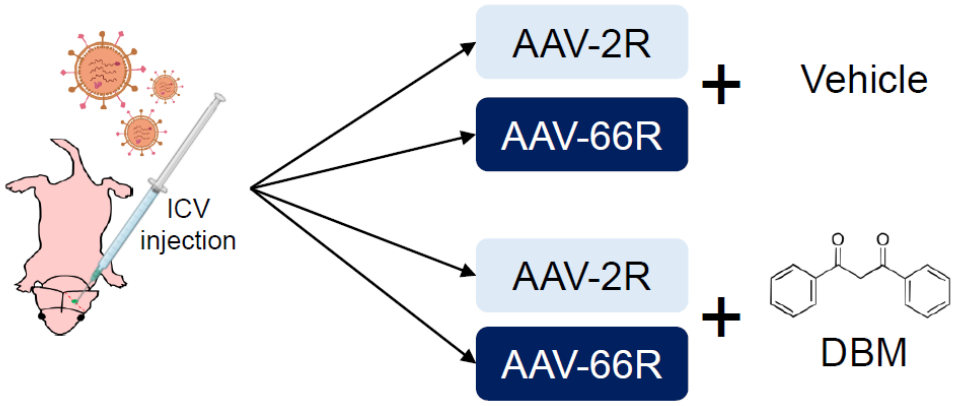

AAV	Treatment	Males	Females	Total
2R	Vehicle	7	7	14
66R	Vehicle	8	9	17
2R	DBM	7	10	17
66R	DBM	8	7	15
NT	Vehicle	6	5	11

Figure 5. Experimental groups and treatments performed in this study. NT: non-treated.

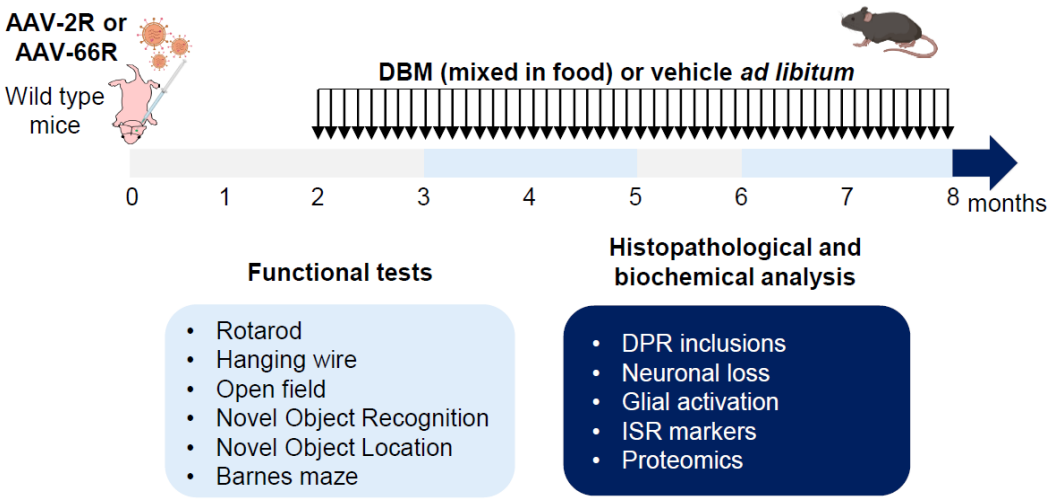

Figure 6. Experimental design of pharmacological treatment with DBM in C9ORF72 mice. Functional tests were performed at 3 and 6 months old and histopathological and biochemical analysis were performed after the euthanasia.

To first characterize behavioral alterations following DBM treatment in AAV-2R and AAV-66R mice, we subjected mice to a different motor and memory tests: Open field assay, NOR, NOL, Hanging wire test and Rotarod test at 3 and 6 months and Barnes maze only at 6 months of age **(Figure 6)**.

6.4 DBM administration prevents memory impairment on a mouse model of C9ORF72-mediated FTD/ALS.

NOR and NOL tests have been widely used in the study of the neurobiological mechanisms underlying memory formation (Vogel-Ciernia and Wood 2014). Those assays evaluate the capacity of animals to discriminate between familiar and novel objects or the displacement of objects in different quadrants. Both tasks rely on a rodent's innate preference for novelty. NOR test has been widely used in assessing non-spatial object memory in rodents. This memory is dependent of perirhinal cortex and hippocampus. On the other hand, NOL provides information about spatial memory acquisition and is associated to hippocampus-dependent memory formation.

To determine whether AAV-66R mice displayed memory impairment, NOL and NOR tests were performed at 3 and 6 months. No significant differences were found in both tests comparing AAV-2R/vehicle and AAV-66R/vehicle mice at 3 months **(Figure 10B and 11B)**, suggesting no further impairment in memory at this time window of disease progression. However, following 6 months of infection, AAV-66R mice showed disrupted cognitive performance when compared to AAV-2R in both tests **(Figure 10C and 11C)**. Interestingly, AAV-66R mice treated with DBM presented a strong protection showing behavior similar to controls, both in NOL and NOR tests at 6 months, these results indicate that DBM was able to block AAV-66R-mediated cognitive disruption. Representation of NOR and NOL test are showed in **Figure 10A and 11A**.

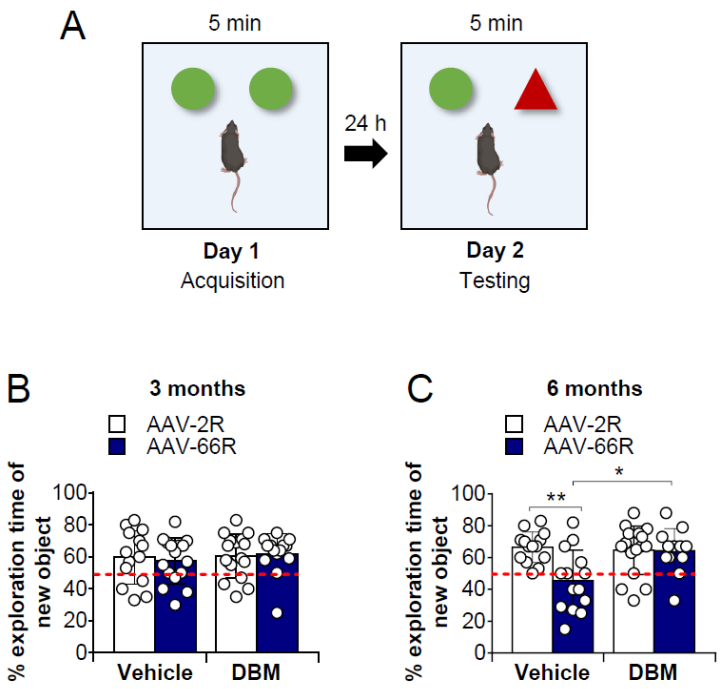

Figure 10. Memory performance evaluation at 3 and 6 months by novel object recognition (NOR) in C9ORF72-FTD/ALS mice. A) Representation of Novel object recognition (NOR) test. **B)** and **C)** NOR test performed at 3 and 6 months in mice injected with AAV-2R or AAV-66R, pharmacologically treated with DBM or vehicle to evaluate memory impairment. The percentage of exploration time of the new object on the second day of the test was graphed, where 50% of exploration is highlighted with a segmented line. Dots represents each animal (N=14-17). Data are presented as mean ± S.D. *, $p<0.05$. **; $p<0.01$; ***, $p<0.001$, one-way ANOVA followed by Tukey's multiple comparisons test.

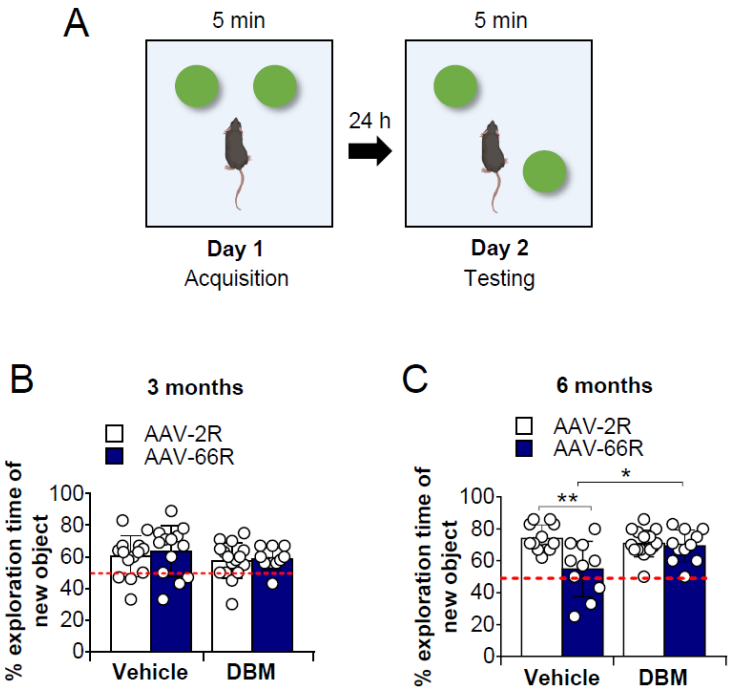

Figure 11. Spatial memory evaluation by novel object location (NOL) in C9ORF72-FTD/ALS mice. A) Representation of NOL test. **B)** and **C)** NOL test was performed at 3 and 6 months in mice injected with AAV-2R or AAV-66R, pharmacologically treated with DBM or vehicle to evaluate memory impairment. The percentage of exploration time of the new object on the second day of the test was graphed, where 50% of exploration is highlighted with a segmented line. Dots represents each animal (N=14-17). Data are presented as mean ± S.D. *, $p<0.05$. **; $p<0.01$; ***, $p<0.001$, one-way ANOVA followed by Tukey's multiple comparisons test.

Barnes maze is used to evaluate spatial learning and memory in rats and mice. It represents an alternative to the classical Morris Water maze, decreasing stress responses that can interfere with assessment of spatial learning as it is a dry maze (Harrison *et al.* 2009). Despite the impairment in hippocampus-dependent spatial memory acquisition found in AAV-66R/vehicle mice measured by NOL, no significant differences were found in Barnes Maze test **(Figure 12B and C)**. This negative result could be explained to the fact that this model is not aggressive enough to show differences in an intensive and repetitive test as Barnes maze, unlike that NOL, where the test is performed just for 5 minutes in the acquisition day and 5 minutes in the test day 24 hours later. A representation of Barnes maze test is depicted in **Figure 12A**.

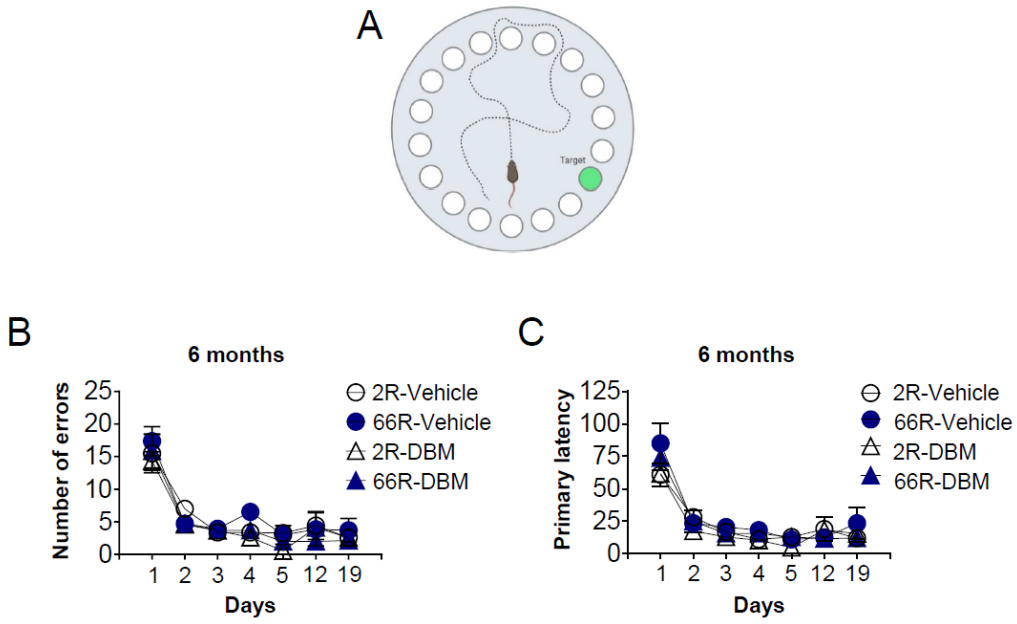

Figure 12. Spatial learning and memory evaluation by Barnes maze in C9ORF72-FTD/ALS mice. A) Representation of Barnes maze test. B) and C) NOL test was performed at 6 months in mice injected with AAV-2R or AAV-66R, pharmacologically treated with DBM or vehicle to evaluate memory impairment. The number of errors and primary latency was plotted. Data are presented as mean ± S.D. (N=14-17). *, $p<0.05$. **; $p<0.01$; ***, $p<0.001$, one-way ANOVA followed by Tukey's multiple comparisons test.

6.5 AAV-66R mice do not display motor deficits or anxiety-like behavior.

To determine whether AAV-66R mice displays motor impairment and anxiety-like behavior, as reported by Chew *et al.* 2015, we evaluated these features using the rotarod, hanging wire and open field tests following 3 and 6 months of infection. Rotarod test has been widely used to evaluate motor coordination and balance. The test consisted in placing the mouse in an accelerated rod and measuring the latency to fall for each animal **(Figure 13A)**. Using the rotarod test, we observed that AAV-66R/vehicle mice did not display motor impairment **(Figure 13B and C)** compared to controls neither at 3 nor 6 months, in contrast with data reported by Chew *et al.* 2015, where a decrease in the motor performance in AAV-66R mice compared to controls at 6 months was found. We observed equivalent results in Hanging wire test, as no significant differences were found following 3 or 6 months **(Figure 14B and C)**. This test consisted in hanging mice in a horizontal wire and recording the number of times they fall for 2 minutes **(Figure 14A)**. Thus, in our hands the AAV-66R recapitulates features of FTD rather than ALS.

To evaluate anxiety-like behavior and locomotor activity, the open field test was performed. This test consists in placing mice in an open square arena and recording their behavior **(Figure 15)**. When mice spend more time in the corners, it is considered to develop an anxiety-like behavior, and when the measured distance traveled is lower than controls, it is associated to motor deficits. By this test, no significant differences were found between groups at 3 and 6 months of age **(Figure 15B and C)**.

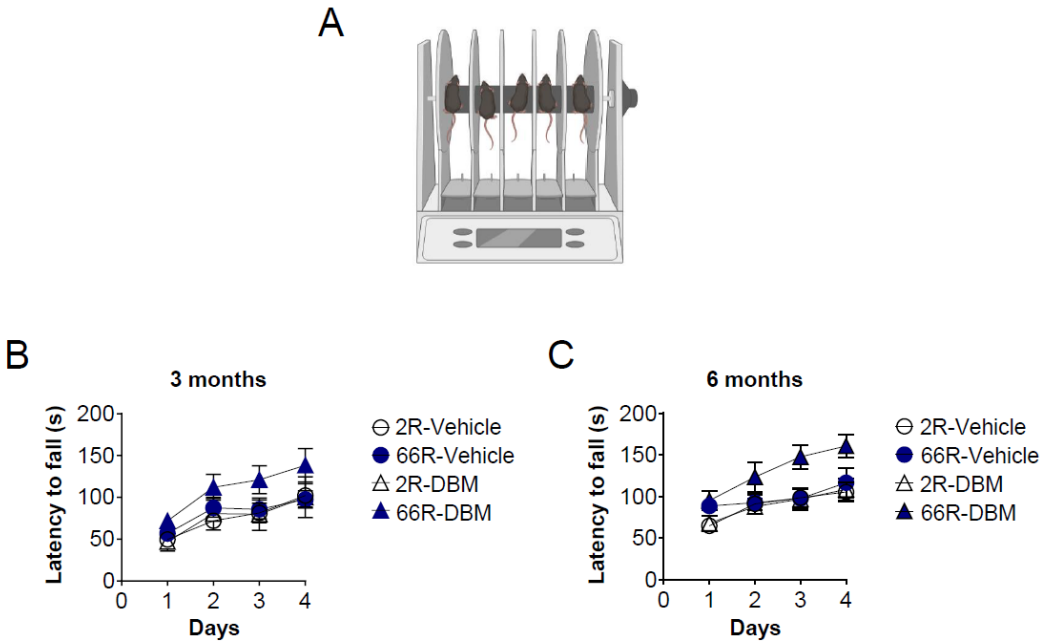

Figure 13. Motor skill learning evaluation by rotarod test in C9ORF72-FTD/ALS mice. A) Representation of rotarod apparatus. B) and C) Rotarod test was performed at 3 and 6 months in mice injected with AAV-2R or AAV-66R, pharmacologically treated with DBM or vehicle to evaluate memory impairment. The latency to fall was measured in seconds (s). The test was performed for 4 consecutive days, with three attempts per day, from 4 to 40 rpm in 5 minutes per attempt. (N=14-17). Data are presented as mean ± S.D. *, $p<0.05$. **; $p<0.01$; ***, $p<0.001$, one-way ANOVA followed by Tukey's multiple comparisons test.

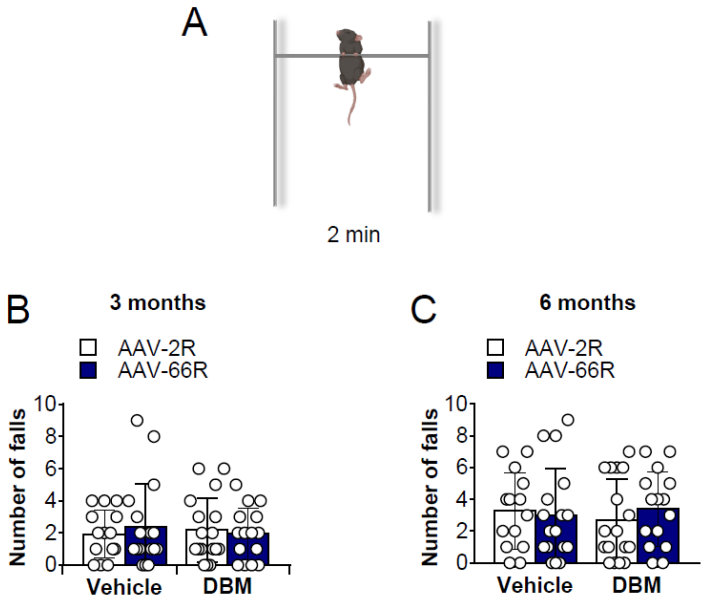

Figure 14. Motor function evaluation by Hanging wire test in C9ORF72-FTD/ALS mice. A) Representation of Hanging wire test. **B)** and **C)** Hanging wire test was performed at 3 and 6 months in mice injected with AAV-2R or AAV-66R, pharmacologically treated with DBM or vehicle. The number of falls in 2 minutes (min) was graphed. Dots represents each animal (N=14-17). Data are presented as mean ± S.D. One-way ANOVA followed by Tukey's multiple comparisons test.

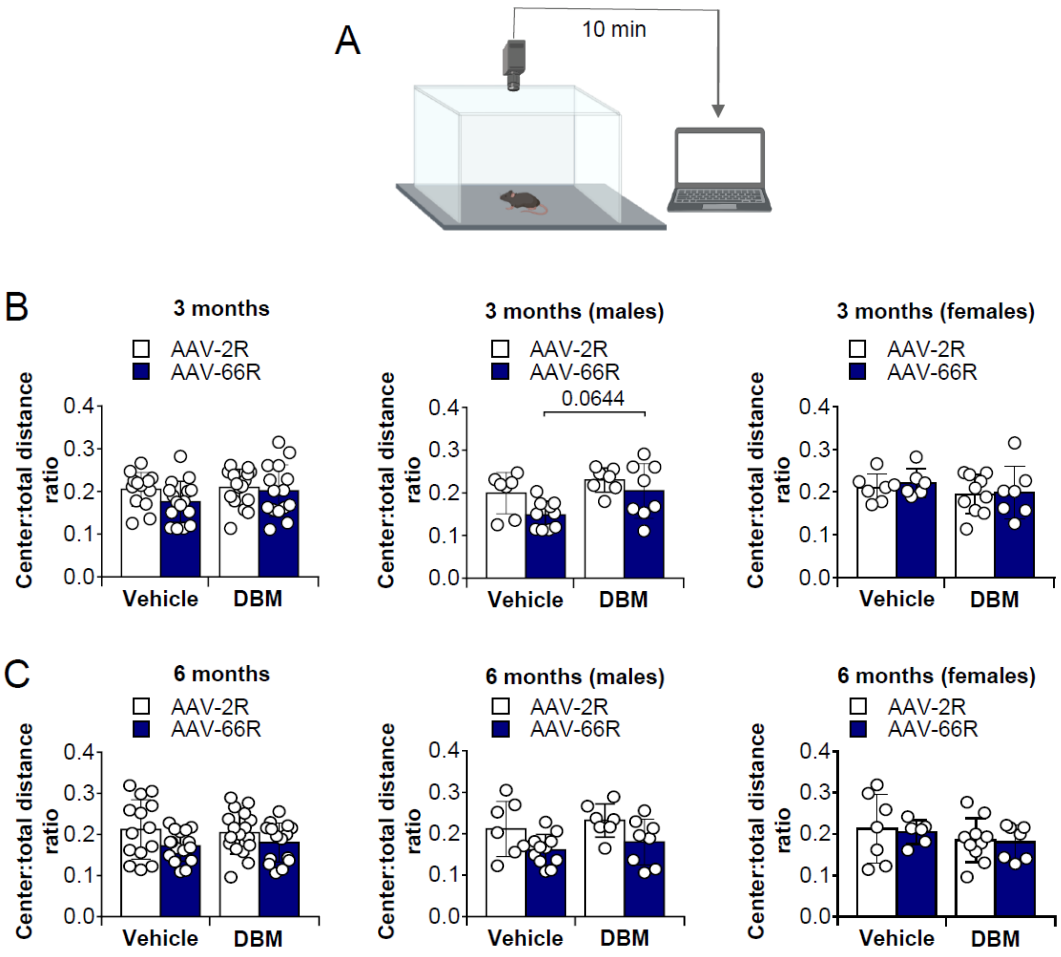

Figure 15. Exploratory and locomotor activity determination measured by open field test in C9ORF72-FTD/ALS mice. A) Representation of open field apparatus. **B)** and **C)** Open field test was performed at 3 and 6 months in mice injected with AAV-2R or AAV-66R, pharmacologically treated with DBM or vehicle to evaluate memory impairment. The ratio between center and total distance was plotted. Dots represents each animal (N=14-17). Data are presented as mean ± S.D. *, p<0.05. **; p<0.01; ***, p<0.001, one-way ANOVA followed by Tukey's multiple comparisons test.

6.6 AAV-66R/vehicle males showed body weight decrease at six months old.

In order to determine if AAV-66R expression or the pharmacological treatment induces body weight changes, mice were weighted periodically at 3, 6 and 8 months of age **(Figure 16)**. No significant changes were found at 3 months among the different groups **(Figure 16A)**, however at 6 months, AAV-66R/vehicle males showed a significant body weight decrease (11%) compared to AAV-2R/vehicle males **(Figure 16B)**. DBM administration prevented the reduction in body weight triggered by AAV-66R expression. These results are different of those reported by Chew *et al.* 2015, where they found the same percentage in body weight loss, but in females. Additionally, no differences between groups were found at 8 months **(Figure 16C)**. Overall, our studies indicate no high alterations in body weight in any of the groups analyzed, except for males at 6 months, suggesting that AAV or DBM administration did not have negative effects in body weight.

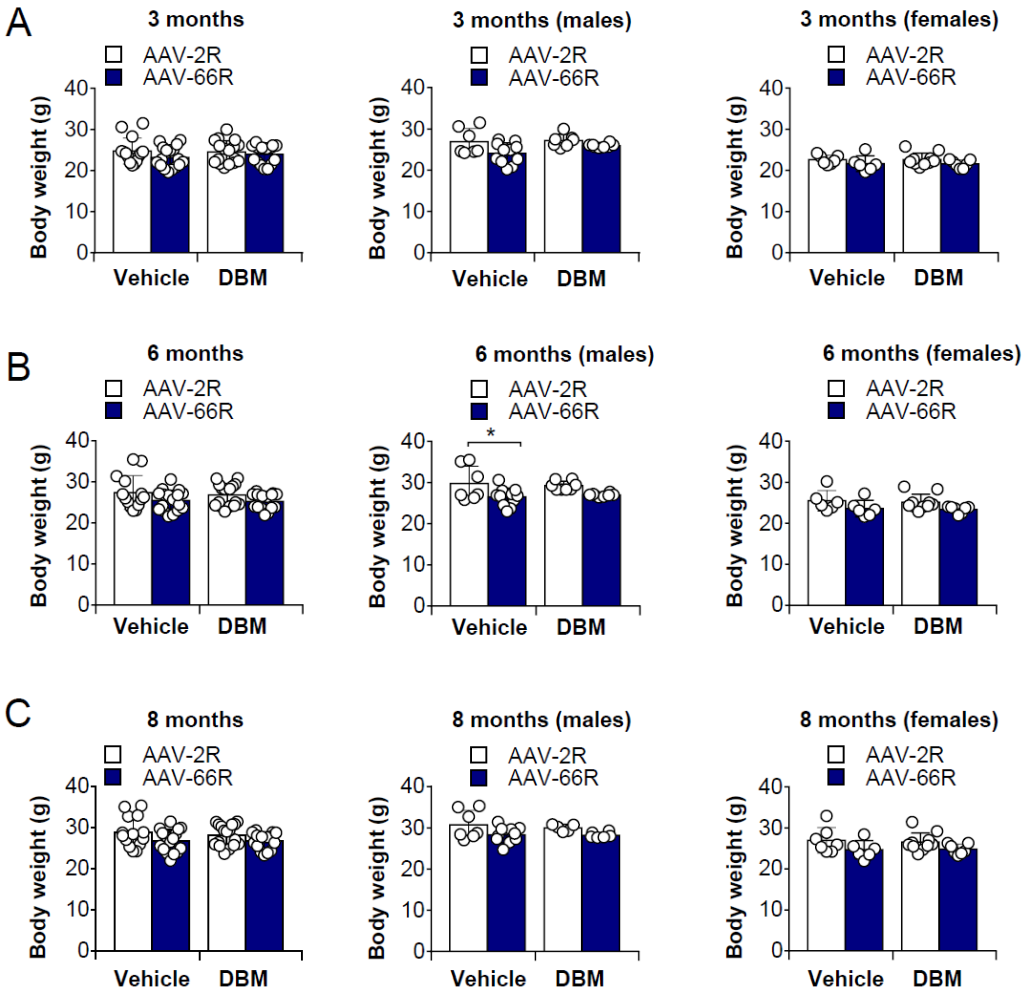

Figure 16. Body weight of C9orf72-FTD/ALS mice at 3-, 6- and 8-month-old. (A) At 3 months old, mice carrying 2 or 66 repeats (2R and 66R, respectively) treated with DBM or vehicle were weighted to evaluate possible differences caused by the repeat expansion or pharmacological treatment. (B) At 6 months of age, mice carrying 2 or 66 repeats (2R and 66R, respectively) treated with DBM or vehicle were weighted to evaluate possible differences caused by the repeat expansion or pharmacological treatment. (C) At 8 months of age, mice carrying 2 or 66 repeats (2R and 66R, respectively) treated with DBM or vehicle were weighted to evaluate possible differences caused by the repeat expansion or pharmacological treatment. (N=14-17). Data are presented as mean ± S.D. *, $p<0.05$, one-way ANOVA followed by Tukey's multiple comparisons test.

6.7 AAV-66R mice do not display significant brain weight decrease and blood glucose fluctuations at eight months old of age.

A trend of decreased brain weight was found in AAV-66R/vehicle females compared to controls (p= 0.0960) **(Figure 17A)**. These results were in line with those reported by Chew *et al.* 2015, where a significant decrease in total brain weight of AAV-66R female mice is reported, suggesting brain atrophy. Additionally, no significant differences were found in blood glucose levels among groups, suggesting that DBM does not trigger pancreatic side effects as observed in GSK2606414 treatment **(Figure 17B)**. However, this hypothesis must be confirmed by histological analysis of pancreas.

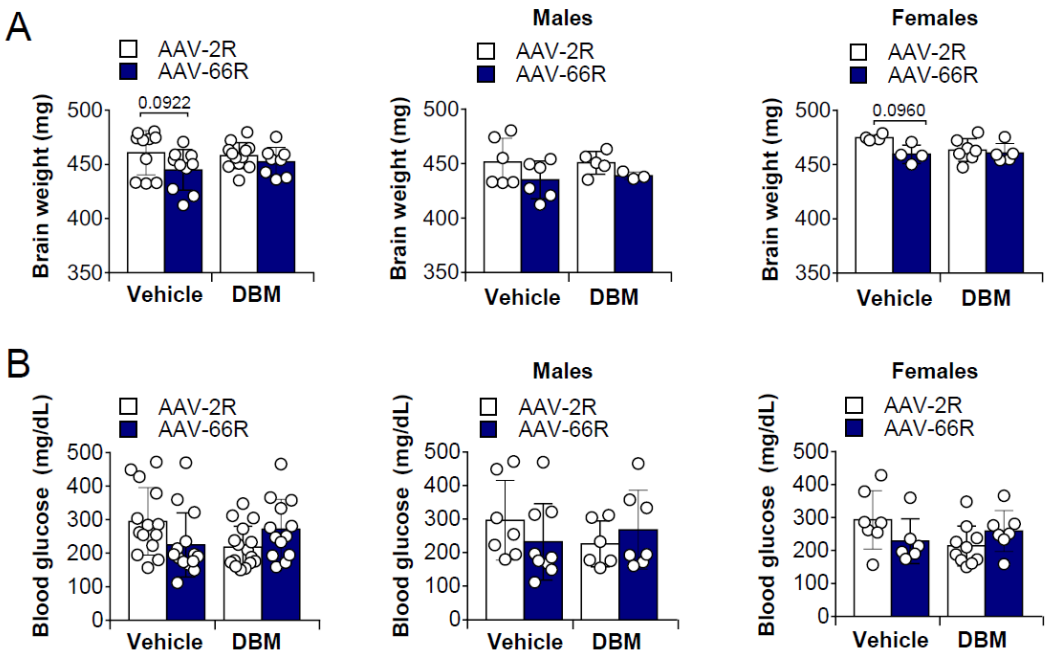

Figure 17. Mice expressing 66 repeats do not develop a significant decrease in brain weight and DBM does not cause fluctuations in blood glucose levels. (A) Brains of mice carrying AAV-2R and AAV-66R were weighted after euthanasia and expressed as milligrams (mg). (B) Glucose in blood levels of AAV-2R and AAV-66R mice were measured after euthanasia and expressed as milligrams per deciliter (mg/dL). Data are presented as mean ± S.D, one-way ANOVA followed by Tukey's multiple comparisons test.

6.8 ISR markers are not increased in the brain of C9ORF72-mediated FTD/ALS mice.

Phosphorylation of eIf2α is a convergent point of different intracellular stress signaling pathways, collectively known ISR (Pakos-Zebrucka *et al.* 2016). The activation of this pathway has been widely reported in fly and cellular models of C9ORF72 toxicity (Zhang *et al.* 2014; Kramer *et al.* 2018; Wang *et al.* 2019; Prudencio *et al.* 2015; Westergard *et al.* 2019; Green *et al.* 2017). In order to determine whether ISR is activated in our C9ORF72-FTD/ALS model, we measured mRNA expression levels of downstream targets of eIF2α phosphorylation by real time PCR.

Before measuring ISR activation in the brain, we confirmed AAV transduction levels of the virus in frontal cortex, hippocampus and cerebellum by conventional PCR**.** We found significant levels of viral transduction following ICV injection as it presented consistent levels in all brain regions measured **(Figure 18)**. Despite that PCR primers were designed for a common upstream region for both AAVs constructs and the same concentration of viruses was injected, AAV-66R expression was higher than AAV-2R in all samples analyzed, which may suggest a better viral transduction of AAV-66R **(Figure 18)**.

Based on transduction levels and behavior tests results, we selected 10 animals per group to perform the following qPCR analysis. We evaluated mRNA levels of *Chop, Atf3, Trb3, Bip* and *Xbp1s* in frontal cortex, hippocampus and cerebellum. As depicted in **Figure 19, 20 and 21,** no significant differences were found in the downstream targets of eIF2α phosphorylation.

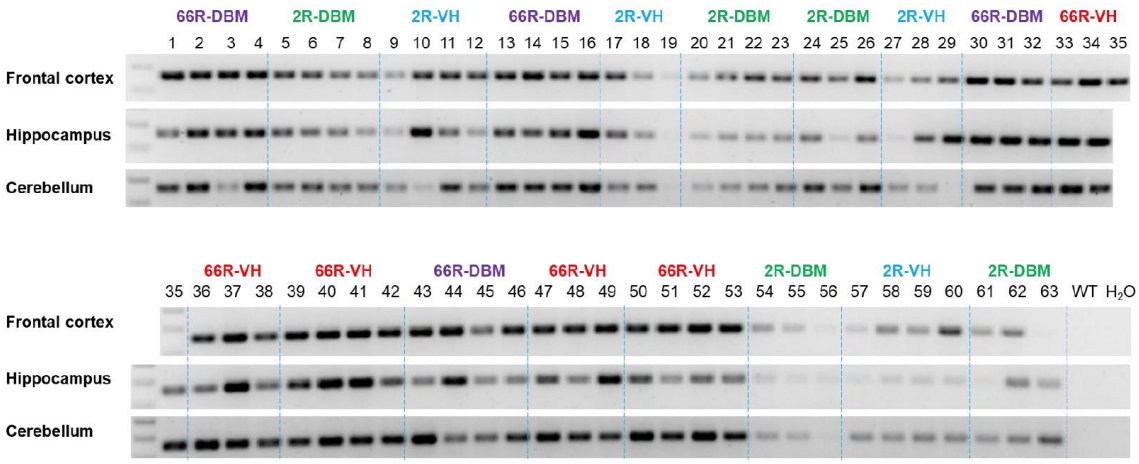

Figure 18. Viral detection of AAV-C9 in mice expressing AAV-2R and AAV-66R in different brain tissues. Transduction measurement of AAV-2R and AAV-66R viral particles by conventional PCR in frontal cortex, hippocampus, and cerebellum.

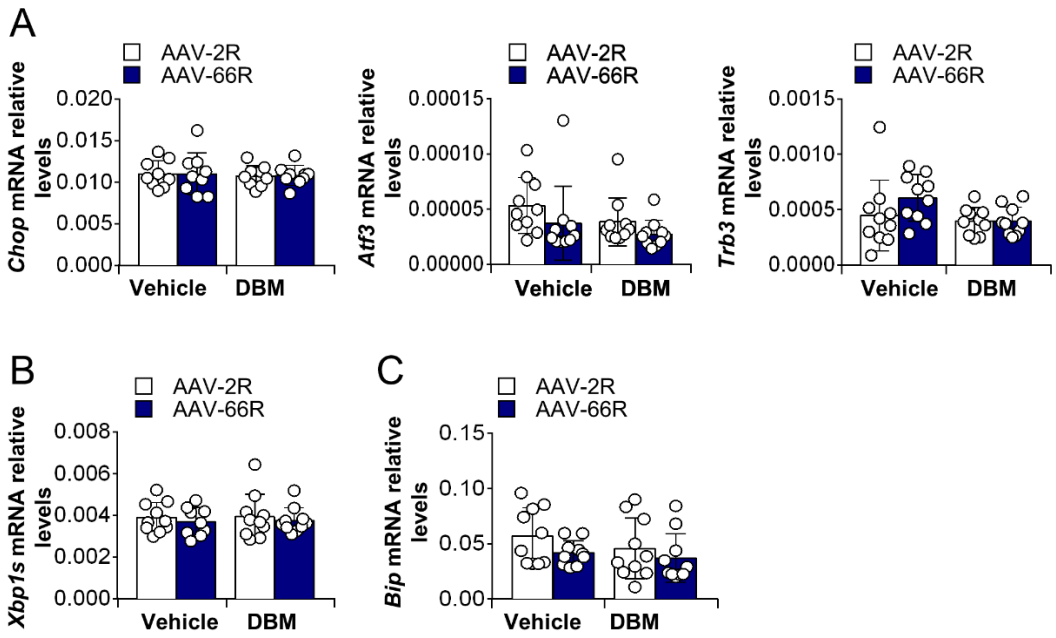

Figure 19. AAV-66R/vehicle mice and AAV-66R/DBM did not showed significant differences in the mRNA expression of ISR markers in frontal cortex. (A) Quantification by real time PCR of *Chop, Atf3 and Trb3* in C9orf72-mediated FTD/ALS mice treated with vehicle or DBM. **(B)** Quantification by real time PCR of *Xbp1s and* **(C)** *Bip* in C9orf72-mediated FTD/ALS mice treated with vehicle or DBM. Data are presented as mean ± S.D. *, $p < 0.05$. **; $p < 0.01$; ***; $p < 0.001$, one-way ANOVA followed by Tukey's multiple comparisons test.

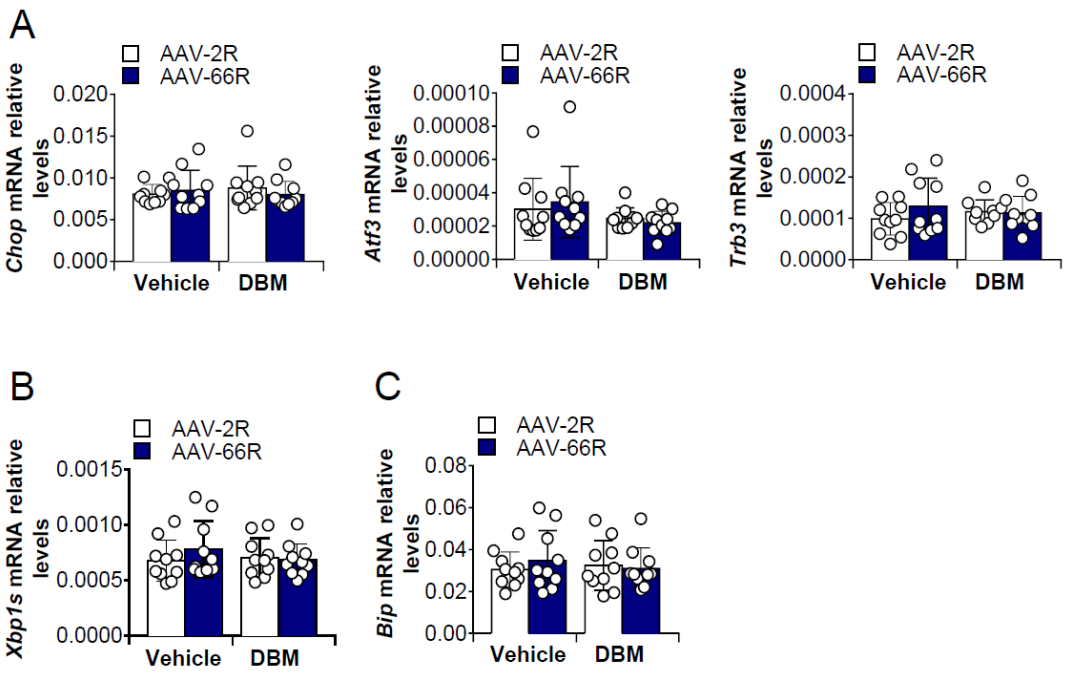

Figure 20. AAV-66R mice do not develop significant differences in the mRNA expression of ISR markers in hippocampus. (A) Quantification by real time PCR of *Chop, Atf3 and Trb3* in C9orf72-mediated FTD/ALS mice treated with vehicle or DBM. **(B)** Quantification by real time PCR of *Xbp1s* and **(C)** *Bip* in C9orf72-mediated FTD/ALS mice treated with vehicle or DBM. Data are presented as mean ± S.D. *, $p < 0.05$. **; $p<0.01$; ***, $p<0.001$, one-way ANOVA followed by Tukey's multiple comparisons test.

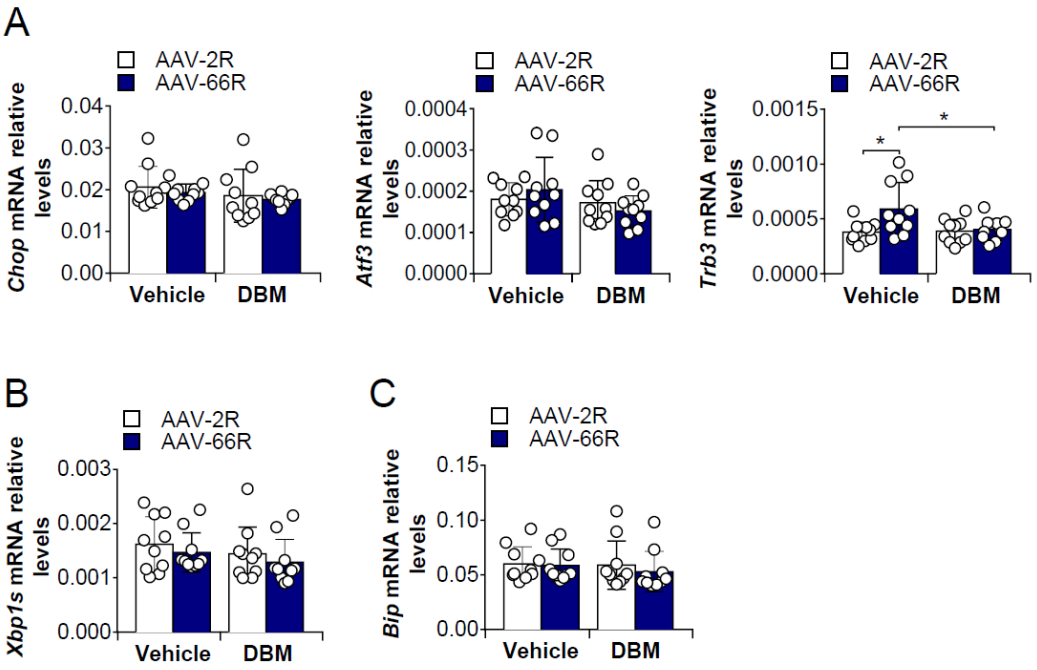

Figure 21. AAV-66R mice do not show significant differences in the mRNA expression of ISR markers in cerebellum. (A) Quantification by real time PCR of *Chop, Atf3 and Trb3* in C9orf72-mediated FTD/ALS mice treated with vehicle or DBM. **(B)** Quantification by real time PCR of *Xbp1s* and **(C)** *Bip* in C9orf72-mediated FTD/ALS mice treated with vehicle or DBM. Data are presented as mean ± S.D. *, $p < 0.05$. **; $p < 0.01$; ***, $p < 0.001$, one-way ANOVA followed by Tukey's multiple comparisons test.

Given the cognitive phenotype that we found in the AAV-C9ORF72 model and the protective effects observed after the treatment with DBM, we proposed as a third aim to elucidate possible molecular pathway that may explain such phenotypes. To accomplish this, the hippocampus of AAV-2R/vehicle, AAV-66R/vehicle, AAV-2R/DBM and AAV-66R/DBM mice, were mechanically homogenized and 50 µg of protein of each sample were sent to Dr. Birgit Schilling laboratory at The Buck Institute for Research on Aging, Novato, CA, by developing a research visit during January to February of 2020.

6.9 AAV-66R mice develop DPR pathology in hippocampus and cortex

To assess the presence of DPR inclusions due to AAV viral injection of G_4C_2 repeats, immunohistochemistry was performed to detect poly(GA) and poly(GR) DPR in hippocampus and cortex. The total number of positive cells with inclusions in both tissues was quantified for each animal, and additionally all the inclusions were classified according to their cellular distribution in: cytoplasmic, when covered all the cytoplasm with a strong signal; perinuclear, when have strong signal dots around the nucleus; and diffuse, when the inclusions covered all the cytoplasm with a weak signal **(Figure 22)**.

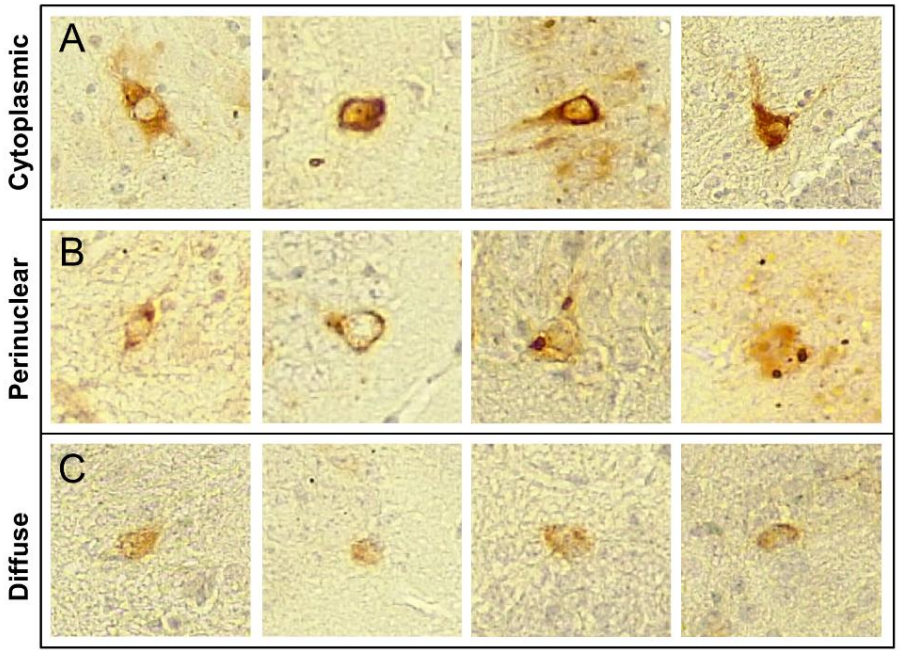

Figure 22. Representative images of inclusion classification. (A, B and C) Cytoplasmic, perinuclear and diffuse distribution of poly(GA) and poly(GR) inclusions in AAV-66R mice.

As depicted in **Figures 23 and 24**, representative images of poly(GA)-labelled cells for each experimental group at 20X magnification are showed. We found an important number of positive cells for poly(GA) both in hippocampus and cortex. However, in cerebellum, the number of positive cells was very low, for this reason we did not select this area for quantification.

For hippocampus, poly(GA)-positive cells were found mainly in CA1, which prompted us to select this zone for the quantification; in the case of brain cortex, poly(GA)-positive cells were found across the region as expected. We found poly(GA) inclusions in all AAV-66R mice but not in AAV-2R **(Figure 23 and 24)**. Interestingly, we found a trend of increased number of poly(GA)-positive cells in AAV-66R/DBM group when compared to AAV-66R/vehicle **(Figure 23 and 24)**. Regarding cerebral regions, the higher number of positive inclusions was observed in cortex, followed by hippocampus and finally, cerebellum, however no clear differences were observed in DBM treated animals.

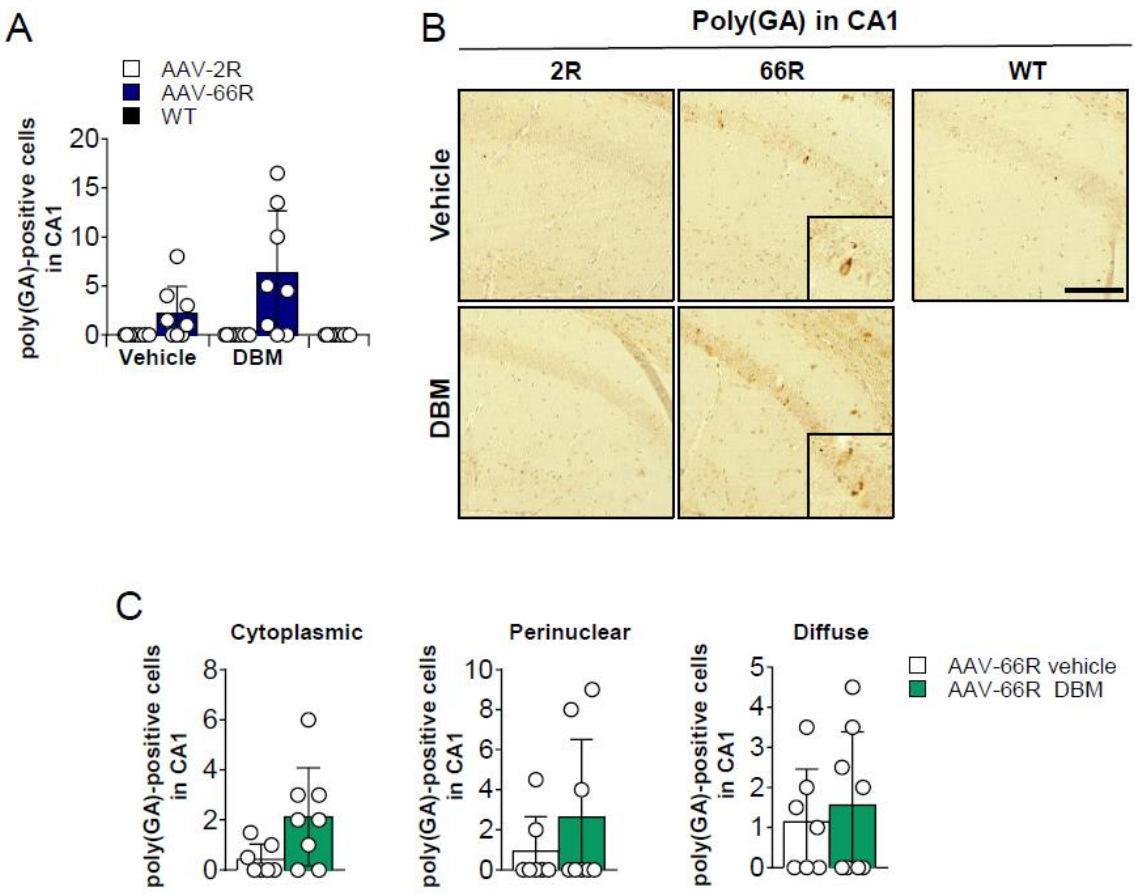

Figure 23. AAV-66R mice developed poly(GA) inclusions in CA1 of hippocampus. **(A)** Quantification of poly(GA)-positive cells in hippocampus and cortex of C9orf72-mediated FTD/ALS mice treated with vehicle or DBM. **(B)** Representative images of poly(GA)-labeled cells in the hippocampus and cortex. **(C)** Cellular distribution quantification of poly(GA)-inclusions in CA1. The number of postive cells in CA1 was plotted. Dots represents each animal (N=8 per group). Data are presented as mean ± S.D. Unpaired-t test, *, p<0.05. **; p<0.01; ***, p<0.001. Scale bar (B): 100 µm.

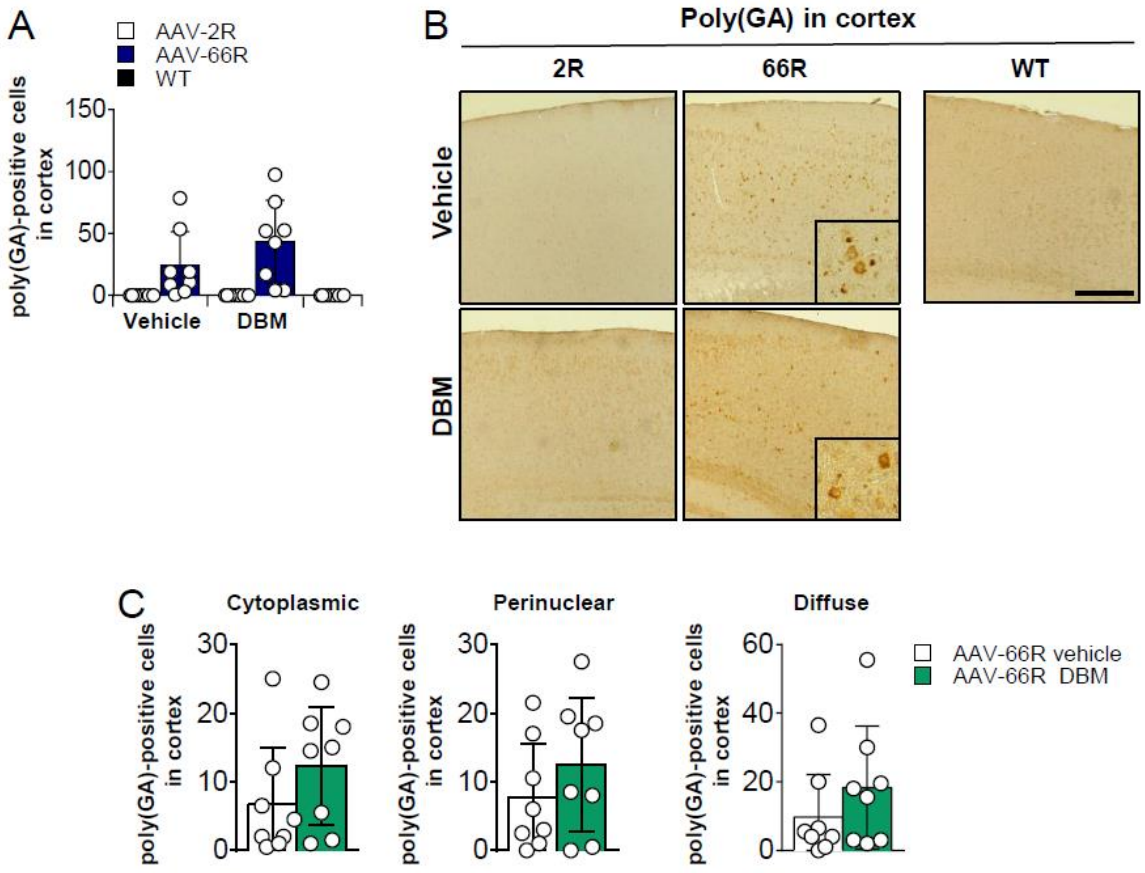

Figure 24. AAV-66R mice developed poly(GA) inclusions in cortex. (A) Quantification of poly(GA)-positive cells in cortex of C9orf72-mediated FTD/ALS mice treated with vehicle or DBM. **(B)** Representative images of poly(GA)-labeled cells in cortex. **(C)** Cellular distribution quantification of poly(GA)-inclusions in cortex. The number of postive cells in cortex was plotted. Dots represents each animal (N=8 per group). Data are presented as mean ± S.D. Unpaired-t test, *, $p<0.05$. **; $p<0.01$; ***, $p<0.001$. Scale bar (B): 300 µm.

Similar results were obtained related to poly(GR)-positive cells in C9ORF72-mediated FTD/ALS mice. As was expected, all AAV-66R mice presented poly(GR) inclusions in hippocampus and cortex, but not AAV-2R mice **Figures 25 and 26**.

No significant differences were found in the number of poly(GR)-positive cells when comparing AAV-66R/vehicle with AAV-66R/DBM groups. Both hippocampus and cortex showed a higher number of poly(GR)-positive cells compared to poly(GA)-labelled cells. **Figures 25 and 26** shows poly(GR) quantifications in hippocampus and cortex, respectively, in addition to representative images of each experimental group where inclusions of poly(GR) are highlighted. As observed in poly(GA)-positive cells, the higher number of poly(GR)-positive cells was found in cortex, followed by hippocampus and finally, cerebellum.

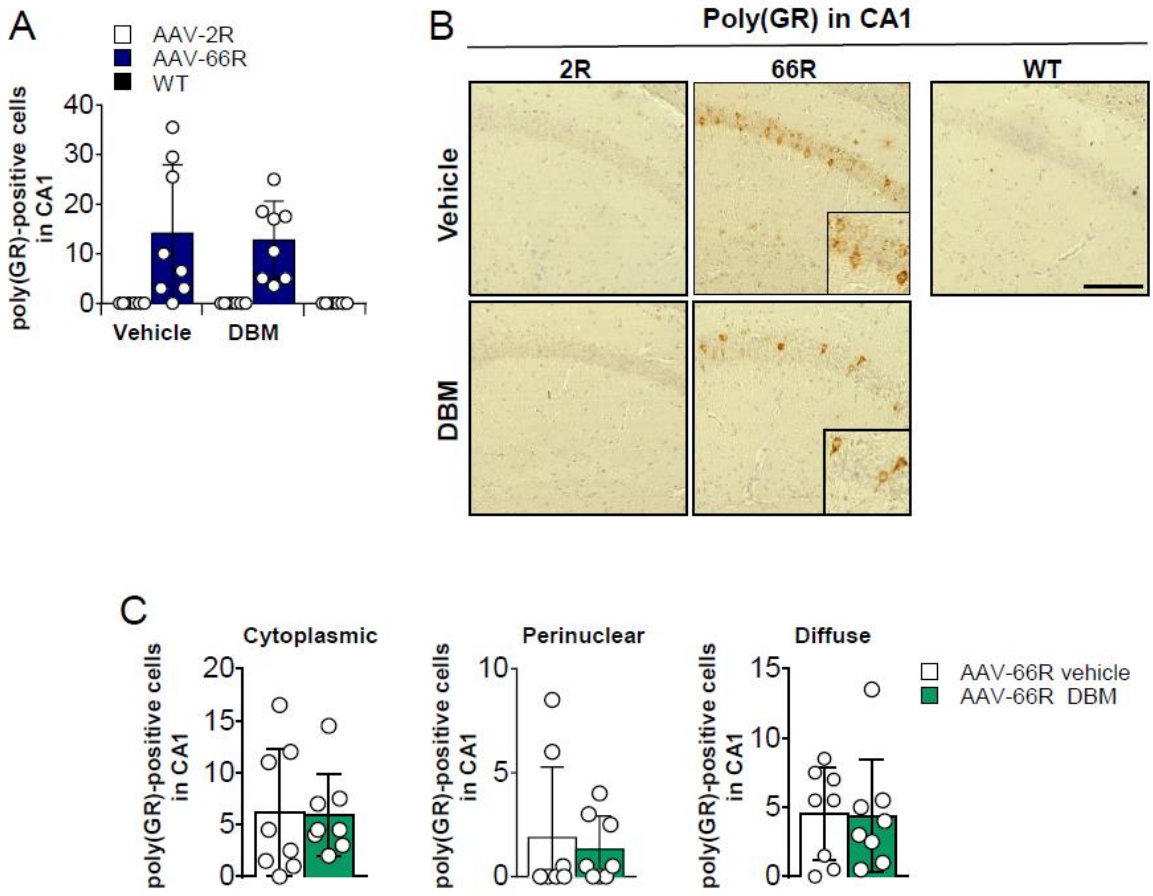

Figure 25. AAV-66R mice developed poly(GR) inclusions in hippocampus. (A) Quantification of poly(GR)-positive cells in hippocampus of C9orf72-mediated FTD/ALS mice treated with vehicle or DBM. **(B)** Representative images of poly(GR)-labeled cells in the hippocampus. **(C)** Cellular distribution quantification of poly(GR)-inclusions in CA1. The number of postive cells in CA1 was plotted. Dots represents each animal (N=8 per group). Data are presented as mean ± S.D. Unpaired-t test, *, $p<0.05$. **; $p<0.01$; ***, $p<0.001$. Scale bar (B): 100 µm.

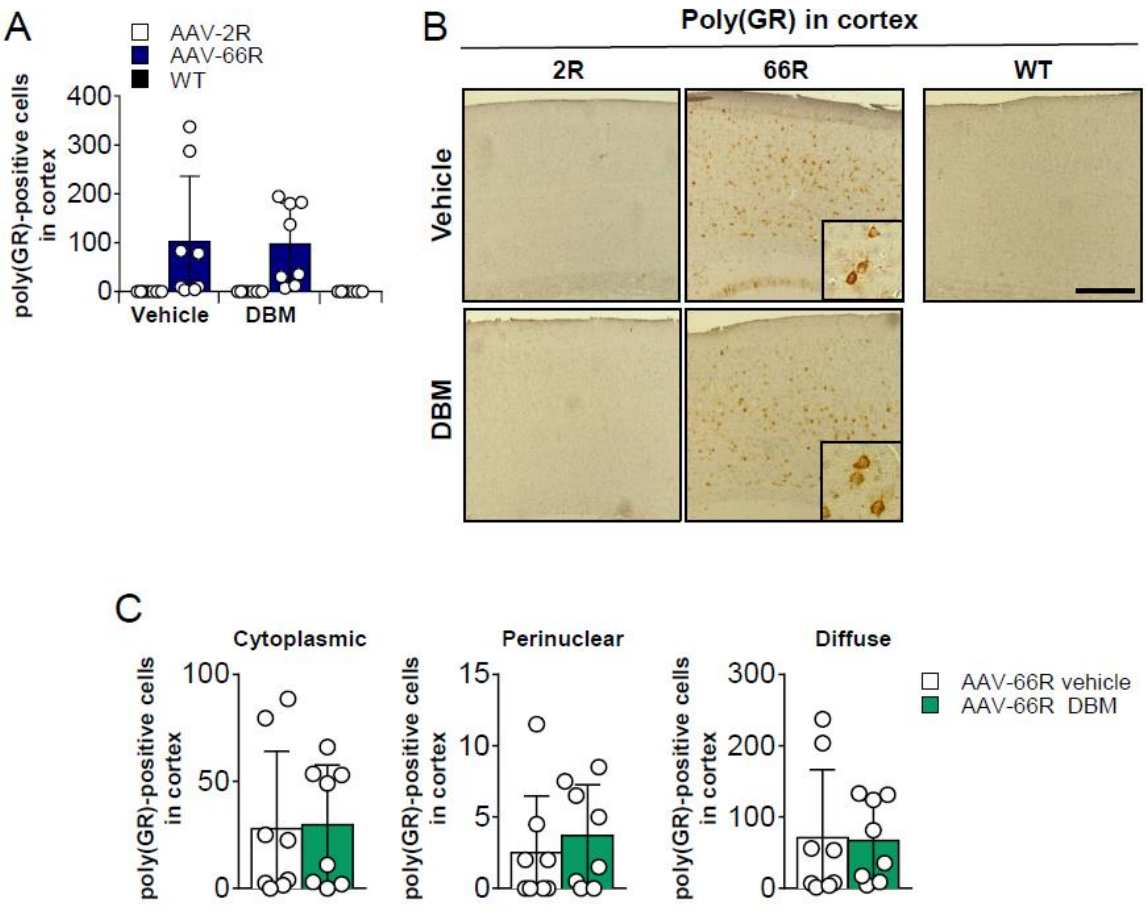

Figure 26. AAV-66R mice developed poly(GR) inclusions in cortex. (A) Quantification of poly(GR)-positive cells in cortex of C9orf72-mediated FTD/ALS mice treated with vehicle or DBM. **(B)** Representative images of poly(GR)-labeled cells in cortex. **(C)** Cellular distribution quantification of poly(GR)-inclusions in cortex. The number of postive cells in cortex was plotted. Dots represents each animal (N=8 per group). Data are presented as mean ± S.D. Unpaired-t test, *, $p<0.05$. **; $p<0.01$; ***, $p<0.001$. Scale bar (B): 300 µm.

6.10 AAV-66R mice develop astrogliosis and microgliosis.

It was previously reported that C9ORF72-mediated FTD/ALS model showed an increase in the expression of GFAP in mice that carried 66 repeats (Chew *et al.* 2015). We measured this parameter, in addition to determine microglial activation by the quantification of microglia marker Iba1. To this purpose, we performed immunohistochemistry to analyze the hippocampus of AAV-2R and AAV-66R mice. Additionally, we inferred if DBM treatment could impact gliosis in AAV-66R mice.

We found that reactive astrocyte marker GFAP was distributed through the hippocampus in all analyzed samples. We could detect an increased number of GFAP positive cells in AAV-66R/vehicle when compared to AAV-2R/vehicle **(Figure 27A)**. Unexpectedly, this increase was also found in the AAV-2R/DBM females but not in males, possible due to a sex-dependent effect of the drug **(Figure 28C)**. Additionally, DBM did not significatively changed the expression of GFAP in AAV-66R/DBM mice compared to AAV-66R/vehicle group **(Figure 27A)**.

Then, to determine microglial activation we detected Iba1 marker by immunohistochemistry in the hippocampus of the injected mice with AAV-2R or AAV-66R. We found that AAV-66R/vehicle mice expressed higher levels of Iba1 than control mice AAV-2R/vehicle, showing for the first time the incidence of microgliosis in this model **(Figure 27B)**.

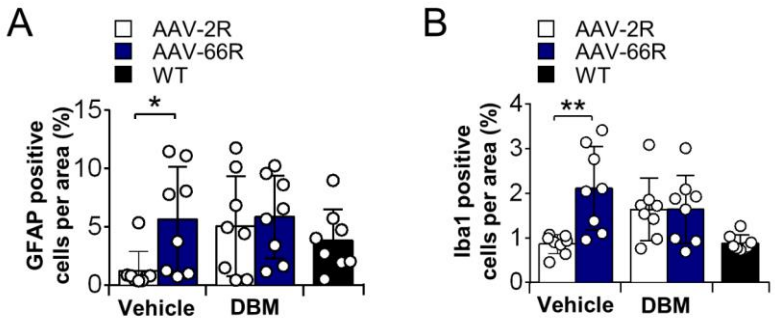

Figure 27. Glial activation measured by GFAP and Iba1 markers expression of C9ORF72-FTD/ALS mice. (A) Quantification of the astrocyte marker, GFAP, in hippocampus of C9ORF72-mediated FTD/ALS mice treated with vehicle or DBM. **(B)** Quantification of the microglia marker, Iba1, in hippocampus of C9ORF72-mediated FTD/ALS mice treated with vehicle or DBM. The percentage (%) of positive cells per area was plotted. Dots represents each animal (N=8 per group). Data are presented as mean ± S.D. Unpaired-t test, *, $p<0.05$. **; $p<0.01$; ***, $p<0.001$.

As we observed in GFAP determination, we found the same trend of unexpected increase of Iba1 in females of the control mice group AAV-2R/DBM **(Figure 29C)**. DBM treatment did not changed significatively Iba1 expression in AAV-66R/DBM mice compared to AAV-66R/vehicle mice **(Figure 27B)**.

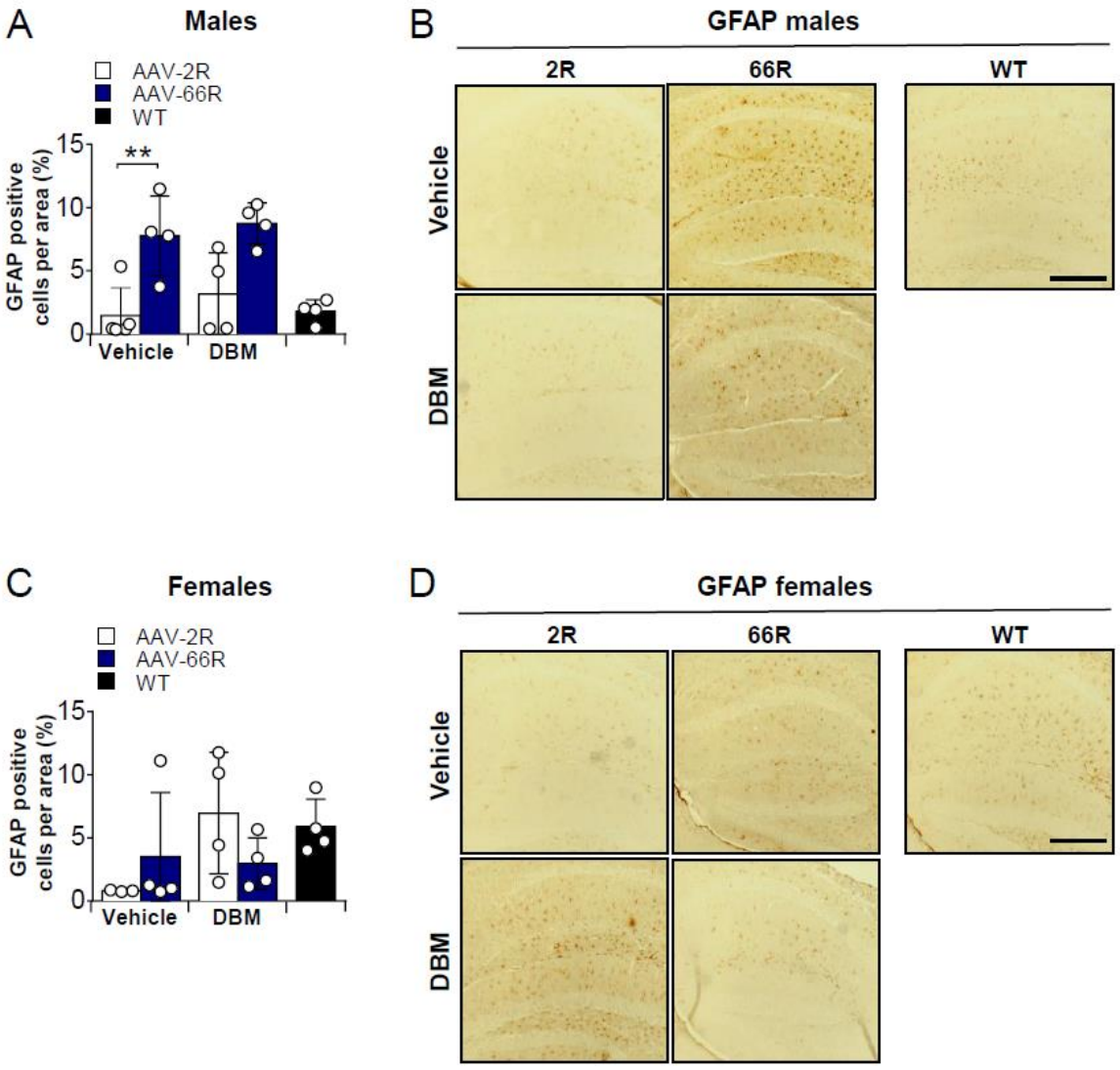

Figure 28. Differential GFAP expression between males and females in C9ORF72-FTD/ALS mice. (A) Quantification of GFAP in hippocampus of C9orf72-mediated FTD/ALS males treated with vehicle or DBM. (B) Representative images of each experimental group of males mice. (C) Quantification of GFAP in hippocampus of C9orf72-mediated FTD/ALS females treated with vehicle or DBM. (D) Representative images of each experimental group of females mice. The percentage (%) of positive cells per area was plotted. Dots represents each animal (N=8 per group). Data are presented as mean ± S.D. Unpaired-t test, *, $p<0.05$. **; $p<0.01$; ***, $p<0.001$. Scale bar (B and D): 300 µm.

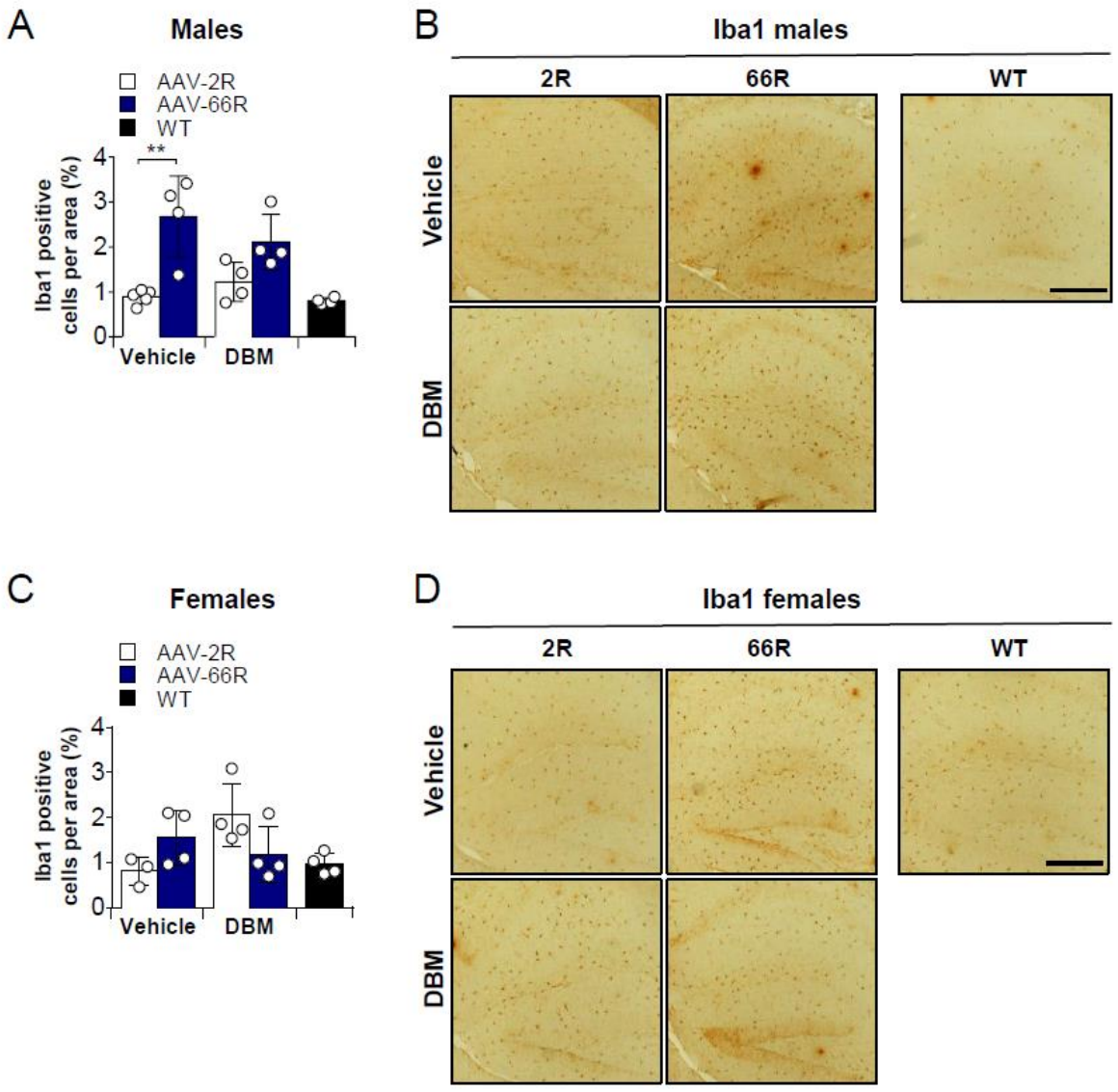

Figure 29. Differential Iba1 expression between males and females in C9orf72-FTD/ALS mice. (A) Quantification of Iba1 in hippocampus of C9orf72-mediated FTD/ALS males treated with vehicle or DBM. (B) Representative images of each experimental group of males mice. (C) Quantification of Iba1 in hippocampus of C9orf72-mediated FTD/ALS females treated with vehicle or DBM. (D) Representative images of each experimental group of females mice. The percentage (%) of positive cells per area was plotted. Dots represents each animal (N=8 per group). Data are presented as mean ± S.D. Unpaired-t test, *, $p<0.05$. **; $p<0.01$; ***, $p<0.001$. Scale bar (B and D): 300 µm.

6.11 AAV-66R mice do not develop neuron loss in cortex.

Previously, it was reported that AAV-66R injection caused neurodegeneration in cortex at 6 months old (Chew *et al.* 2015). Therefore, to determine if we observed the same tendency in our experiment, we performed an immunohistochemistry to detect the neuronal marker NeuN in mice injected with AAV-2R and AAV-66R. We quantified the percentage of NeuN-positive signal in cortex in each experimental group (n=8 per group) **(Figures 30A).** Representative images are shown for each condition **(Figures 30B)**.

We did not found differences in the percentage of NeuN-positive signal between AAV-2R/vehicle and AAV-66R/vehicle mice, indicating that neurodegeneration was not recapitulated in our experiment using this method. Additionally, no differences were found between AAV-2R/vehicle group and WT group, suggesting that neonatal injection and DBM treatment did not cause a significant neuronal loss in the evaluated region **(Figure 30).**

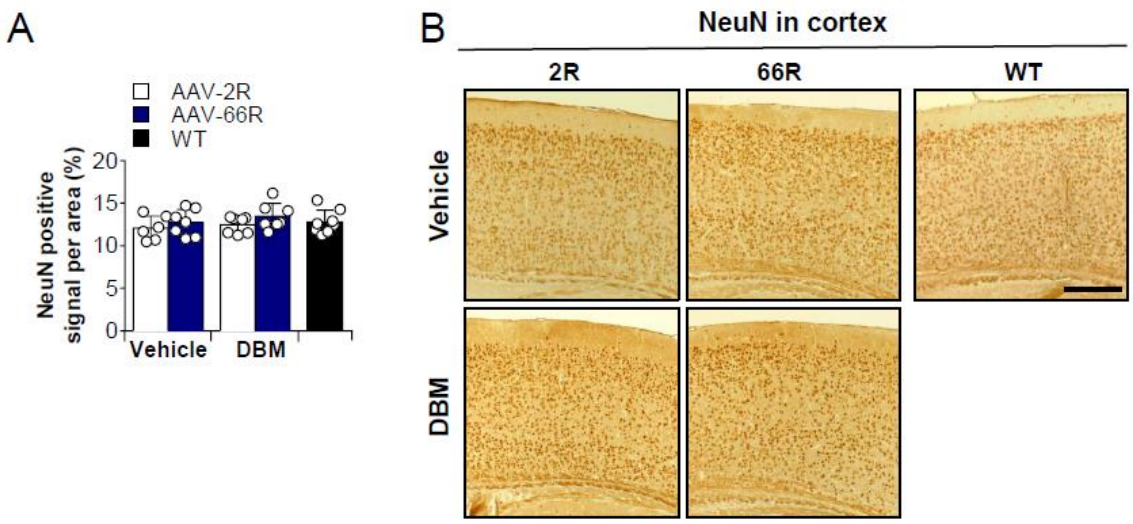

Figure 30. AAV-66R mice does not developed neuron los in cortex. (A) Quantification of NeuN-positive cells in cortex of C9ORF72-mediated FTD/ALS mice treated with vehicle or DBM. **(B)** Representative images of NeuN-labeled cells in cortex. The percentage of positive signal per area in cortex was plotted. Dots represents each animal (n=8 per group). Scale bar (B): 300 µm.

6.12 Proteomics analysis of hippocampal tissue reveals changes in components regulating cytoskeleton organization and metabolic processes induced by DBM administration in C9ORF72-mediated FTD/ALS mice.

In order to gain insight into the mechanistic behind our results, we performed proteomic profiling by LC-MS/MS of hippocampus of all experimental groups (n= 5, females per condition). We analyzed this region because it is directly related to the behavioral assessments performed in our study, in addition of presenting altered gliosis and DPR aggregation in our model.

First, we compared the whole proteome according to fold change values, contrasting AAV 66R-vehicle/AAV 2R-vehicle versus AAV 66R-DBM/AAV 66R-vehicle groups. Interestingly, we found a global reversion of the proteome with a negative Spearman correlation of 0.64, corresponding to 73% of whole identified proteins that expression levels were altered in opposite directions **(Figure 31A).**

Then, in order to identify which of these proteins significatively change its expression in opposite directions ($q<0.05$), a Venn diagram approach was used to display the overlap between these groups. We found an overlap of six proteins that changed in opposite directions: Alpha-internexin (INA), Tubulin Beta 4B (TUBB4B) and Vimentin (VIM), were upregulated in the model (AAV 66R-vehicle/AAV 2R-vehicle) but downregulated by DBM (AAV 66R-DBM/AAV 66R-vehicle); and Calcium Dependent Secretion Activator (CADPS), GDP Dissociation Inhibitor 1 (GDI1) and

Neurochondrin (NCDN) were downregulated in the model (AAV 66R-vehicle/2R-vehicle) but upregulated by DBM (AAV 66R-DBM/66R-vehicle).

Additionally, protein-protein interaction network analysis showed that despite the overlapped proteins do not interact directly, all altered proteins belong to the same interaction cluster **(Figure 31B)**.

Moreover, we performed a gene set enrichment analysis in order to highlight main biological process significatively affected ($q<0.05$) **(Figure 31B).** Notably, our analysis indicated that when upregulated proteins in the model (AAV 66R-vehicle/AAV 2R-vehicle) were compared with downregulated proteins by DBM (AAV 66R-DBM/AAV 66R-vehicle), the top enriched term in gene ontology database was “Cytoskeleton organization”, in which 13 of the 24 proteins that were upregulated in the model (AAV 66R-vehicle/AAV 2R-vehicle)” were associated to this term**.** This analysis suggests a possible role of this biological process in the pathogenesis related to the G_4C_2 repeat expansion. Remarkably, this analysis also showed that 6 of these 13 proteins were additionally associated to “Amyotrophic Lateral Sclerosis (ALS)” (top enriched term in KEGG pathway), suggesting that AAV-66R infection may recapitulate, at proteome level, alterations related to ALS pathogenesis **(Figure 31B).**

Moreover, when the downregulated proteins were compared in the model (AAV 66R-vehicle/AAV 2R-vehicle) with the upregulated by DBM (AAV 66R-DBM/AAV 66R-vehicle), the top enriched term in gene ontology database and KEGG pathway were “Pyruvate metabolic process” and “Glycolysis/Gluconeogenesis”, respectively. Interestingly, 5 of 25 proteins that were downregulated in the model

(AAV 66R-vehicle/AAV 2R-vehicle) were associated to both terms, suggesting a strong association of these proteins to metabolic processes affected by the G_4C_2 repeat expansion **(Figure 31B).**

Notably, Rab2a and Gdi1 (right panel of **Figure 31B**), proteins that are upregulated in AAV-66R mice by DBM, belong to Rab subfamily of small GTPases and dDENN domain which plays an important role in C9ORF72 pathogenesis, hence indicating that DBM could modify the expression of components of this particular protein family.

Overall, our results indicate that our model could recapitulate distinct proteomic alterations observed in ALS pathogenesis in addition of indicating putative biological pathways altered by this repeat expansion **(Figure 31).**

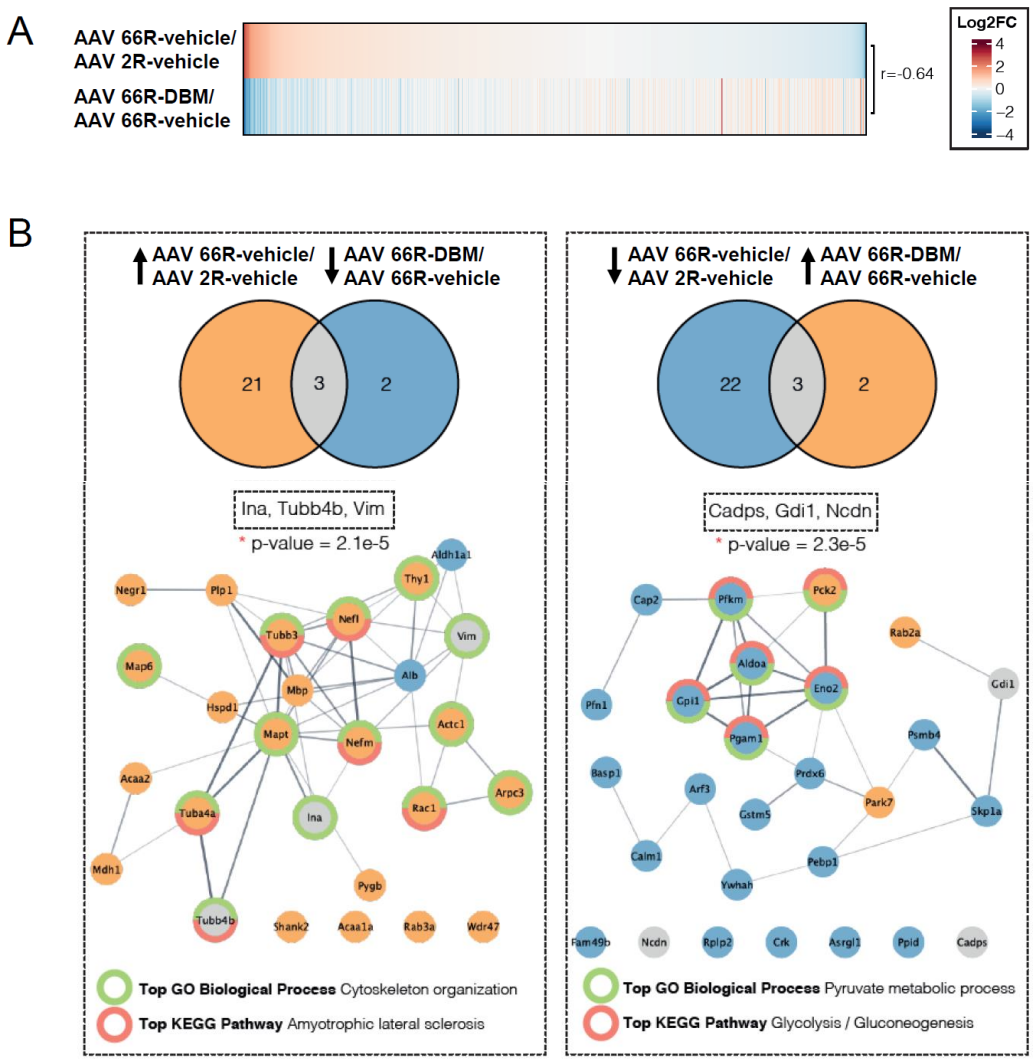

Figure 31. Differential protein expression in hippocampus of C9ORF72-mediated FTD/ALS mice identified by LC-MS/MS. (A) Heat map comparation of whole proteome changes. r= 0.64. **(B)** Venn diagram comparation and networking of main clusters of proteins that are upregulated in the model and downregulated with DBM and vice versa (q<0.05).

7. DISCUSSION

FTD and ALS are related neurodegenerative disorders that now are considered a disease spectrum (C9FTD/ALS). The most common genetic cause of both diseases is the expansion of a G_4C_2 hexanucleotide repeat in the first intron of chromosome 9 open reading frame 72. Three possible pathogenic mechanisms have been proposed to explain how the mutation causes neurodegeneration, where DPR production arises as the main driver of the disease (Mizielinska *et al.* 2014). DPR form neuronal inclusions throughout the central nervous system that may contribute to disease pathogenesis. A close relationship between the production of these DPR and the activation of the ISR has been reported (Westergard *et al.* 2019; Green *et al.* 2017; Cheng *et al.* 2018; Zhang *et al.* 2018a). In cellular models of C9ORF72, ISR activation promotes non-AUG (RAN) translation, generating more DPR and consequently more eIF2α phosphorylation, sustaining a positive feed-forward loop between DPR production and eIF2α phosphorylation (Green *et al.* 2017; Cheng *et al.* 2018; Westergard *et al.* 2019). The identification of small molecules to target ISR in different neurodegenerative diseases has emerged as requirement in the field (Sidrauski *et al.* 2015; Halliday *et al.* 2017; Halliday *et al.* 2015). However, the therapeutic potential of targeting ISR in a C9ORF72 mammal model has not been explored yet.

We successfully reproduced the AAV-C9ORF72 model in mice reported by Chew *et al.* 2015 in terms of DPR inclusions, gliosis and in some behavioral alterations **(Figure 7)**. We corroborate that the viral model generates poly(GA) and

poly(GR) inclusions through the brain of injected mice with the 66 repeats of the expansion. Because inclusions were also found in hippocampus, we investigated a potential impact in cognitive performance in those animals. Accordantly, mice carrying AAV-66R showed memory impairment at 6 months measured by NOR and NOL **(Figure 10 and 11)**. In line with these results, a mouse model of poly(PR)$_{50}$ showed memory deficits in addition of neuronal loss and brain atrophy (Zhang *et al.* 2019). However, mice expressing poly(GR)$_{80}$ did not show impaired working memory, as measured by T-maze test (Choi *et al.* 2019). The discordance between these results could be due to differences in the number of repeats of the expansion and the tests used. Additionally, we found increased *Xbp1s* expression in AAV-66R mice when compared to controls, suggesting ER stress triggering in the model **(Figure 7D)**. We found no significant differences in *Atf4, Atf3* and *Chop* mRNA expression levels, although these results do not necessarily correlate with the protein levels and we cannot exclude that ISR activation is engaged in the model.

Studies in cellular and fly models of C9ORF72 have reported the contribution of PERK-eIF2α activation in disease progression (Zhang *et al.* 2014; Zhang *et al.* 2018a; Kramer *et al.* 2018). Therefore, we evaluated if the use of small molecules to inhibit the pathway could alleviate the pathogenesis in mammals. To this purpose we first evaluated the efficacy of PERK inhibitor GSK2606414 **(Figure 8)**. Neuroprotector effects in different neurodegenerative models have been reported following GSK2606414 treatment (Moreno *et al.* 2013; Radford *et al.* 2015; Mercado *et al.* 2018; Kim *et al.* 2013) which correlated with reduced levels of p-PERK and p-eIF2α and restoration of protein synthesis in prion disease and FTD models (Moreno

et al. 2013; Radford *et al.* 2015). Such effects were attribute to increased protein synthesis of synaptic proteins, thus preventing synaptic failure and cognitive impairment (Moreno *et al.* 2013). Additionally, in a model of Parkinson disease, GSK2606414 treatment protected nigral-dopaminergic neurons against the neurotoxin 6-hydroxydopamine (6-OHDA). This protection sustained normal dopamine levels and synaptic proteins expression, improving motor performance (Mercado *et al.* 2018). Additionally, in a *Drosophila* model of ALS that overexpress TDP-43, GSK2606414 treatment decreased levels of eIF2α-P, in addition to mitigate TDP-43–induced climbing dysfunction and toxicity (Kim *et al.* 2013). Despite such significant neuroprotective results in multiple neurodegenerative diseases, GSK2606414 treatment was shown to evoke substantial side effects associated to pancreatic damage.

In order to find a possible form to decrease the toxicity, we delivered GSK2606414 by powdered food *ad libitum* instead of the previous oral gavage delivery. HPLC-MS/MS confirmed the presence of the drug in the brain in a similar concentration in all tissues **(Figure 8B)**. We found differences in the levels of GSK2606414 in blood and tissues compared to results reported by Mercado et al. 2018 (Mercado *et al.* 2018), where mice were treated for three weeks by oral gavage with GSK2606414 (100 mg/kg/day) twice a day. The differences found in the concentration of the drug may be related to differences in the administration regimens and drug metabolism. Despite differences in drug concentration in brain tissue, our results show a satisfactory exposure of the drug in all CNS, as such regimen could significantly engage the PERK pathway activation in the brain, as

shown by RT-PCR results. Indeed, *Chop* mRNA levels dropped ~100% in animals exposed to tunicamycin and GSK2606414, reaching the same values found in mice treated with DMSO (tunicamycin vehicle). Additionally, we observed that *Atf3* and *Trb3* were also significantly reduced **(Figure 8C)**. These reduction was higher than the one reported by our group (Mercado *et al.* 2018), where the differences were not significant, indicating that oral administration by food powdered ad libitum is more effective and efficient than oral gavage in the inhibition of the pathway following tunicamycin treatment. Moreover, the administration of tunicamycin reported by Mercado was locally delivered based on stereotaxic injection in the substantia nigra pars compacta (SNpc) which likely contributed to the differences found in our study. Unexpectedly, levels of *Xbp1s, the target of a different UPR sensor,* were also decreased **(Figure 8D)**. Mercado et al. 2018, only reported *Xbp1* expression by conventional PCR splicing assay, which does not provide quantitative changes when compared to real-time quantitative PCR (Mercado *et al.* 2018). We observed this event with both under GSK2606414 and DBM treatment, inhibitors that act in the same pathway but at different levels **(Figures 8D, 9C and D)**. This result suggests a possible crosstalk between the two arms of the UPR, IRE1 and PERK, where one arm could be regulating the other. Conversely, it has been demonstrated that PERK pathway disruption by GSK2606414 and ISRIB enhances IRE1 phosphorylation and XBP1s in response to ER stress in cellular models (Chang *et al.* 2018). Additionally, it was recently reported that PERK modulation by GSK2606414 and ISRIB, resulted in a higher expression of XBP1s in primary neurons but not in HEK293 cells (Bugallo *et al.* 2020). The discrepancies could be attributable to differences in the models used and the window that is analyzed.

Despite the impressive results obtained in the pharmacological modulation of PERK pathway, oral administration of GSK2606414 by powdered food led to decreased body weight compared to non-treated mice **(Figure 8F)**, the same reported by Mercado et al. (Mercado *et al.* 2018). This body weight drop was accompanied by a decrease in blood glucose levels **(Figure 8E)**. These results are in agreement with previous reports, where prion-infected mice showed weight loss, accompanied by a reduction of ~50% in pancreatic weight and increased blood glucose levels after GSK2606414 treatment (Halliday *et al.* 2015). This toxicity was also reported in models of FTD and PD (Radford *et al.* 2015; Mercado *et al.* 2018). The same phenomena is observed with the genetic deletion of PERK, where $PERK^{-/-}$ mice showed early severe postnatal decline in endocrine and exocrine pancreatic function leading to hyperglycemia and reduced insulin levels in serum (Harding *et al.* 2001). These consequences occur because the pancreas is a highly secretory organ where UPR activation is essential to its normal physiology. Full restoration of protein synthesis, ~100% *in vivo* (Moreno *et al.* 2013) and ~90% *in vitro* (Halliday *et al.* 2015), is detrimental because certain degree of phosphorylated eIF2α is essential to deal with misfolded proteins. Therefore, the fine-tuning of PERK inhibition by GSK2606414 dosage in powdered food presents an exciting protocol to find the balance between the safe dosage and therapeutic outcomes in the brain.

Moreover, the specificity GSK2606414 has been questioned. Rojas-Rivera et al. (Rojas-Rivera *et al.* 2017) reported that GSK2606414 and its second generation drug GSK2656157 inhibits receptor-interacting serine/threonine-protein kinase 1 (RIPK1), a protein that plays a crucial role in apoptosis and necroptosis, at

concentrations that did not affect PERK activity. However, these finding were only obtained in cell culture and Mercado et al. (Mercado *et al.* 2018) did not found kinase activation of RIPK1 or RIPK3 in the brain of mice treated with GSK2606414.

It is important to mention that we demonstrate for the first time that administration of GSK2606414 by powdered food *ad libitum* is an efficient route of drug delivery, in addition of being less invasive and less stressful for animals, compared to the previous protocol based on oral gavage. The differences in PERK inhibition compared to those reported by Mercado et al. 2018 (Mercado *et al.* 2018) are likely mediated by the substantial difference in drug administration and regimen. Hence, it is suggested that *ad libitum* availability of the compound conferred sustained inhibition of the pathway, as compared to acute delivery of GSK2606414 every twelve hours by oral gavage (Mercado *et al.* 2018). Overall, these results demonstrate that GSK2606414 efficiently inhibit the PERK pathway in the brain in an experimental ER stress model *in vivo*, although it triggered side effects possibly due to pancreatic toxicity **(Figure 8)**.

Another small molecule, the ISR inhibitor ISRIB, reverses the effects of eIF2α phosphorylation by binding to eIF2B (Tsai *et al.* 2018; Zyryanova *et al.* 2018; Sidrauski *et al.* 2015). This molecule have demonstrated impressive neuroprotector effects in models of prion disease and importantly, without causing pancreatic toxicity (Halliday *et al.* 2015). Additionally, ISRIB improved synaptic plasticity in wild type mice (Sidrauski *et al.* 2013) and reversed cognitive deficits after traumatic brain injury (Chou *et al.* 2017). However, ISRIB presents solubility problems, making it unsuitable for its use in humans (Halliday *et al.* 2015). Given the toxic side effects

found by the food powdered administration of GSK2606414, in accordance with those previously reported (Moreno *et al.* 2013; Halliday *et al.* 2015; Mercado *et al.* 2018; Radford *et al.* 2015), we evaluated the efficacy of another small molecule with translational potential and neuroprotector effects, in addition to presenting a good pharmacokinetics properties and no side effects reported (Halliday *et al.* 2017), the small molecule DBM. DBM mimics the effects of ISRIB, and it is a natural product found in licorice root. Our results demonstrated that the drug engaged the pathway in a model of experimental ER stress *in vivo* in wild type mice, decreasing significatively the mRNA levels of *Chop* in frontal cortex **(Figure 9B)**. This result corroborated that the drug is active in the brain and efficiently modulate ISR signaling, as previously reported (Halliday *et al.* 2017).

Initially, the aim of this project was to dissect the pathway evaluating the effects of GSK2606414 and ISRIB in the viral-based C9ORF72 model. However, because of the extensive of the pharmacological treatment (6 months) and the toxicity found in GSK2606414 regimen *ad libitum*, in addition to the low translational potential of ISRIB due to its insolubility, we decided to change the selected drug and use DBM in the study.

In the current study, we investigated the consequences of inhibiting the eIF2α effects with the small molecule DBM in the C9ORF72 model. DBM has reported to reverse translational attenuation and decrease ATF4 *in vitro* and *in vivo*, without affecting eIF2α phosphorylation (Halliday *et al.* 2017). In addition, DBM prevented neuron loss in the hippocampus, improving memory performance and increased lifespan in models of prion disease and tauopathy model of FTD. Importantly, these

effects were without produce damage to the pancreas (Halliday *et al.* 2017). We found that AAV-66R/vehicle mice presented memory impairment at 6 months compared to controls, as revealed by NOR and NOL tests **(Figures 10 and 11)**. Interestingly, DBM preserved memory performance in AAV-66R mice similar to unaffected controls at 6 months. Given that DBM mimics the effects of ISRIB (i.e. partially restoring global protein synthesis levels and decreasing expression of ATF4 (Halliday *et al.* 2017), we postulate that such improvement in memory performance could be attributed to this molecular mechanism. Protein synthesis restoration is essential to maintain neural connections (Sidrauski *et al.* 2013), including synaptic scaffold components which are crucial for normal neuronal functioning (Moreno *et al.* 2012).

Additionally, AAV-66R mice developed inclusions of poly(GA) and poly(GR) in hippocampus and frontal cortex, but rarely in cerebellum **(Figures 23, 24, 25 and 26).** Unlike that was reported by Chew *et al.* 2015, where authors only showed a semi-quantitative analysis indicating the number of inclusions as high, moderate, low and rare, we determined the number of positive cells per area in addition to the characterization of inclusion distribution per cell. We found a different distribution patron comparing poly(GA) and poly(GR) immunopositive cells, where in poly(GA) the cellular distribution was predominantly perinuclear and in poly(GR) the cellular distribution was mainly cytoplasmic and diffuse. We found a higher number of poly(GR)-positive cells than poly(GA), different that was previously reported where the predominant DPR was poly(GA) (Chew *et al.* 2015). However it is possible that our poly(GA) quantification would be underestimated because puncta inclusions

where observed in most of the cases, and it was difficult to discern whether correspond to cellular inclusions or cellular debris. For this reason, puncta inclusions where not included in the quantification.

Neuroinflammation is an important hallmark of ALS and FTD (Lall and Baloh 2017), where cell morphology and increased markers of gliosis from astrocytes, microglia and oligodendrocytes, main glial cells in the CNS, are altered (Glass *et al.* 2010). Activated microglia and astrocytes have been reported in patients with C9-ALS and FTD by immunohistochemistry (Lant *et al.* 2014; Brettschneider *et al.* 2012) and in C9orf72 BAC transgenic mice (Liu *et al.* 2016a).

In this context, we found that AAV-66R/vehicle mice showed an increase in GFAP and Iba1, cellular markers of astrocytes and microglia, respectively, in hippocampus **(Figure 27)** but not in cortex. These results are different than those previously reported (Chew *et al.* 2015), where astrogliosis was found in cortex, but there was no information about GFAP or Iba1 expression in hippocampus or other brain tissue. Importantly, this is the first time that microgliosis is reported in this AAV-C9ORF72 viral model. Moreover, AAV-66R/vehicle mice showed astrogliosis, which is in line with was reported previously (Chew *et al.* 2015) **(Figure 27A)**. Interestingly, AAV-66R also developed microgliosis given by an increase in Iba1 immunopositive detection compared to control AAV-2R/vehicle which has not been previously reported. We additionally found a differential increase in GFAP and Iba1 markers between males and females **(Figures 28 and 29)**. In this context, different studies have showed differences between males and females related to quantity and phenotype of microglia and astrocytes (Santos-Galindo *et al.* 2011; Guneykaya *et*

al. 2018; McCarthy *et al.* 2015; Acaz-Fonseca *et al.* 2015). Regarding to these differences, a study reported that males presented a higher density in astrocytes and microglia positive cells in the proximity of the wound than females, in a mouse model of cortical brain injury, indicating differences in neuroinflammatory responses (Acaz-Fonseca *et al.* 2015).

Whole proteomic analysis of female animals revealed that our AAV-based model could recapitulate some proteomic alterations found both in ALS patients and animal models **(Figure 31).** Two main hits altered in AAV-66R infected mice treated with DBM were members of Rab subfamily of small GTPases and dDENN domain: Rab2a and Gdi1**(Figure 31B, right panel)**. Rab2a, when bound to GTP, recruit and/or activate a variety of effector molecules controlling cellular trafficking events, including autophagy (Webster *et al.* 2016), being involved with the regulation of autophagosome formation and impacting the autophagic flux in mammalian cells (Ding *et al.* 2019). Notably, autophagy is a main node of the proteostasis network altered in C9ORF72 pathology, being suggested as a central mechanism of pathogenesis in ALS/FTD (Nassif *et al.* 2017; Torres *et al.* 2021). The other hit, Gdi1 regulates the GDP-GTP exchange reaction of members of the Rab family, thus regulating vesicular trafficking (Garrett *et al.* 1994). Interestingly, Gdi1 knock out animals, present cognitive impairment with impaired biogenesis and recycling of synaptic vesicles in the hippocampus (Bianchi *et al.* 2009) and its mutations are associated to X-linked mental retardation in humans (D'Adamo *et al.* 1998). Additionally, intermediate filaments vimentin (Vim) and alpha-internexin (Ina) were also impacted following DBM treatment in AAV-66R infected mice **(Figure 31B)**. Of

interest, toxic PR poly-dipeptide encoded by the repeat sequences expanded in the C9orf72 were reported to bind mainly to intermediate filaments, thus disassembling Vim (Lin *et al.* 2016). Remarkably, Vim was shown to be protective during protein misfolding stress as it protects differentiated cells by binding protein aggregates and granules formed by RNA-binding intrinsically disordered proteins and directing their asymmetric partitioning (Pattabiraman *et al.* 2020). Additionally, it has been recently reported that degradation of vimentin bundles at perinucleus and dissociation of β-tubulin network is induced by poly(PR) treatment (Shiota *et al.* 2020).

Overall, our proteomic analysis suggests at least two mechanistic bases to explain our behavior phenotypes following DBM treatment in C9ORF72 pathology: one based in the regulation of autophagy by the Rab family and other based on the regulation of intermediate cytoskeleton components, like Vimentin. These cytoskeleton effects are consistent with synaptic plasticity, where formation of dendritic spines is crucial for the synapse dynamics.

Moreover, in our proteomic analysis we do not found reversion effects in apoptosis, chaperones, or ISR markers, components that would impact DPR aggregation by DBM administration, which is agreement with was found by biochemical and histological analysis. Therefore, according to the proteomic results we speculate that protective effects in cognitive tests are probable related to effects at the level of synaptic plasticity. In this context, proteins like “Calcium Dependent Secretion Activator” (CADPS) and “Neurochondrin” (NCDN) are associated to synaptic function. Interestingly, both proteins were downregulated in the model (AAV

66R-vehicle/ AAV 2R-vehicle) but upregulated by DBM treatment (AAV 66R-DBM/AAV 66R-vehicle).

Regulation of the protein synthesis by phosphorylation of eIF2α has been widely studied in memory consolidation (Trinh *et al.* 2012; Costa-Mattioli *et al.* 2005; Chou *et al.* 2017; Costa-Mattioli *et al.* 2007). Specifically, chronic activation of PERK signaling, and subsequent eIF2α-P increases cognitive decline due to reduced synthesis in synaptic proteins in models of prion disease (Moreno *et al.* 2013; Moreno *et al.* 2012). In this context, either genetic or pharmacological ISR inhibition have been reported to improve memory in mice (Sidrauski *et al.* 2013; Costa-Mattioli *et al.* 2007). A knock-in mouse model of eIF2α+/S51A, where a substitution (serine to alanine at the S51 phosphorylation site) prevents the phosphorylation of the mutated form of eIF2α, showed enhanced synaptic plasticity and memory compared to *wild type* littermates (Costa-Mattioli *et al.* 2007). Additionally, suppression of GCN2 or PKR, prevented synaptic impairment and facilitate long-term memory formation (Costa-Mattioli *et al.* 2005; Zhu *et al.* 2011). On the other hand, preventing the reduction of eIF2α phosphorylation by salubrinal, an inhibitor of eIF2α-P dephosphorylation, exacerbated toxicity and reduced survival in prion-diseased mice (Moreno *et al.* 2012). Therefore, in the context of neurodegenerative diseases, several reports have supported the concept that ISR activation is detrimental for memory consolidation and synaptic plasticity process and the reversal of the ISR activation effects by genetic or pharmacological intervention has favorable effects in neuronal function and memory. We did not found differences at mRNA levels of ISR components as measured by RT-PCR in the C9ORF72 model neither in DBM

treated mice in total extracts and histological analysis to detect ISR signaling in individual cells is required **(Figure 19, 20 and 21)**. This can be attributed to dilution problems of this technique by using total brain extracts. Finally, in contrast with the results reported by Chew *et al.* 2015, we did not found motor problems in AAV-66R mice, as measured by rotarod at 6 months **(Figure 13)**. This data correlates with the results that we found using Hanging wire test **(Figure 14)** and open field assay **(Figure 15)**, indicating that AAV-66R mice do not showed motor impairment in those tests. The differences between our results and those reported by Chew *et al.* 2015 could be attributed to altered AAV spreading following ICV injection.

In summary, we have demonstrated that oral administration of GSK2606414 by powdered food was highly efficient in inhibiting the PERK pathway in a model of experimental ER stress *in vivo*. This inhibition was higher than the previous reported by oral gavage. However, despite the promising results found, GSK2606414 treatment presented toxic effects possible due to pancreatic injury. For this reason, we discard the use of this drug in a long-term treatment in mice. On the other hand, DBM demonstrated to inhibit the ISR in the brain on a model of ER stress *in vivo*. Given that DBM does not present side effects reported, we selected this drug as a candidate to treat AAV-C9ORF72-mediated FTD/ALS mice. After 4 months of pharmacological treatment, we found that DBM was able to preserve cognitive function in C9ORF72 model, sustaining that such regimen approach could present promising translational results in the clinic. Finally, regarding to proteomics analysis, we found that the main terms altered by DBM in C9ORF72-mediated FTD/ALS mice were cytoskeleton organization and metabolic processes.

8. CONCLUSIONS

This thesis has revealed the preventive effects of DBM administration in a C9ORF72-mediated FTD/ALS mice model. The most relevant findings obtained lead us to conclude the following:

- AAV-66R/vehicle mice showed memory impairment at 6 months compared to controls as measured by NOR and NOL tests without any further motor impairment as measured by rotarod, hanging wire and open field tests.
- Food powdered DBM administration could fully prevent cognitive impairment observed in AAV-66R mice.
- Expression of poly(GA) and poly(GR) DPR were found in AAV-66R mice both in hippocampus and cerebral cortex but DBM treatment did not significantly altered the number of positive cells for inclusions.
- Increased number of GFAP and Iba1 positive cells was found in the hippocampus of AAV-66R/vehicle mice compared to controls, indicative of gliosis in the C9ORF72-mediated FTD/ALS mice model. Of note, DBM did not significatively altered the proportion of GFAP nor Iba-1 positive cells in AAV-66R mice.
- Proteomic analysis of hippocampal tissue revealed that the main biological pathways altered in AAV-66R mice were related to ALS. Furthermore, analysis of AAV-66R mice treated with DBM highlighted cytoskeleton organization and metabolic processes as most enriched biological terms. Those findings suggest possible mechanistic insights into DBM protective effect in cognitive disruption mediated by 66R pathology.

9. PERSPECTIVES

As future perspectives for the data presented in this doctorate thesis, we aim to:

- **Validate the most significantly alterations highlighted in our proteomic screening**. A direct validation by western blotting of proteins involved with cytoskeleton will grant more certainty into possible mechanistic behind our results that could potentially be evaluated in cellular models.
- **Evaluation of ISR components by western blotting and/or immunohistochemistry following DBM oral treatment.** Our study still lacks important validation regarding the effect of the drug into ISR signaling. Besides, immunohistochemistry could further clarify a differential contribution of DBM treatment in distinct cellular types in the brain following C9ORF72 pathology. Such analysis would be better assessed by single cell RNA seq studies.
- **Determine the concentration of DBM that reaches the brain following our regimen of treatment in powdered food.** Although we have performed such analysis for GSK2606414, we shall evaluate the bioavailability for DBM as well.

PUBLICATIONS

Torres P., Cabral-Miranda F., Gonzalez-Teuber V. and Hetz C. (2021). Proteostasis deregulation as a driver of C9ORF72 pathogenesis. *Journal of Neurochemistry,* 00, 1-17. https://doi.org/10.1111/jnc.15529. Review.

CONFERENCES

Torres P., Valenzuela V., Astorga J. and Hetz C. Dibenzoylmethane restores memory impairment in C9FTD/ALS. XXXIII Annual Meeting of Chilean Society for Cell Biology (SBCCH), November 25-29, 2019, Puerto Varas.

Astorga J., Becerra D., van Dijken I., **Torres P.**, Sardi P., Valenzuela V. and Hetz C. A gene therapy-based strategy to modulate the unfolded protein response and target alterations in C9ALS/FTD. XXXIII Annual Meeting of Chilean Society for Cell Biology (SBCCH), November 25-29, 2019, Puerto Varas.

INTERNSHIP

Visiting student, Verdin Lab: Buck Institute of Research on Aging.
January 2020-February 2020. Two-months internship to learn about the technique: cellular thermal shift assay (CETSA) to determine the protein target of a DBM.

10. REFERENCES

Acaz-Fonseca E., Duran J. C., Carrero P., Garcia-Segura L. M., Arevalo M. A. (2015) Sex differences in glia reactivity after cortical brain injury. *Glia* **63**, 1966–1981.

Anderson N., Haynes C. (2020) Folding the Mitochondrial UPR into the Integrated Stress Response. *Trends Cell Biol.* **30**, 428–439.

Ash P. E. A., Bieniek K. F., Gendron T. F., Caulfield T., Lin W. L., DeJesus-Hernandez M., Blitterswijk M. M. Van, et al. (2013) Unconventional Translation of C9ORF72 GGGGCC Expansion Generates Insoluble Polypeptides Specific to c9FTD/ALS. *Neuron* **77**, 639–646.

Atkins C., Liu Q., Minthorn E., Zhang S. Y., Figueroa D. J., Moss K., Stanley T. B., et al. (2013) Characterization of a novel PERK kinase inhibitor with antitumor and antiangiogenic activity. *Cancer Res.* **73**, 1993–2002.

Axten J. M., Medina J. R., Feng Y., Shu A., Romeril S. P., Grant S. W., Li W. H. H., et al. (2012) Discovery of 7-methyl-5-(1-{[3-(trifluoromethyl)phenyl]acetyl}-2,3-dihydro- 1H-indol-5-yl)-7H-pyrrolo[2,3-d]pyrimidin-4-amine (GSK2606414), a potent and selective first-in-class inhibitor of protein kinase R (PKR)-like endoplasmic reticulum kinase (PERK). *J. Med. Chem.* **55**, 7193–7207.

Baleriola J., Walker C. A., Jean Y. Y., Crary J. F., Troy C. M., Nagy P. L., Hengst U. (2014) Axonally synthesized ATF4 transmits a neurodegenerative signal across brain regions. *Cell* **158**, 1159–1172.

Bianchi V., Farisello P., Baldelli P., Meskenaite V., Milanese M., Vecellio M., Mühlemann S., et al. (2009) Cognitive impairment in Gdi1-deficient mice is associated with altered synaptic vesicle pools and short-term synaptic plasticity, and can be corrected by appropriate learning training. *Hum. Mol. Genet.* **18**, 105–117.

Braakman I., Bulleid N. J. (2011) Protein Folding and Modification in the Mammalian Endoplasmic Reticulum. *Annu. Rev. Biochem.* **80**, 71–99.

Brettschneider J., Toledo J., Deerlin V. Van, Elman L., McCluskey L., Lee V., Trojanowski J. (2012) Microglial activation correlates with disease progression and upper motor neuron clinical symptoms in amyotrophic lateral sclerosis. *PLoS One* **7**.

Bugallo R., Marlin E., Baltanás A., Toledo E., Ferrero R., Vinueza-Gavilanes R., Larrea L., Arrasate M., Aragón T. (2020) Fine tuning of the unfolded protein response by ISRIB improves neuronal survival in a model of amyotrophic lateral sclerosis. *Cell Death Dis.* **11**, 1–16.

Burrell J. R., Halliday G. M., Kril J. J., Ittner L. M., Götz J., Kiernan M. C., Hodges J. R. (2016) *The frontotemporal dementia-motor neuron disease continuum*. Lancet Publishing Group.

Chang T. K., Lawrence D. A., Lu M., Tan J., Harnoss J. M., Marsters S. A., Liu P., Sandoval W., Martin S. E., Ashkenazi A. (2018) Coordination between Two Branches of the Unfolded Protein Response Determines Apoptotic Cell Fate. *Mol. Cell* **71**, 629-636.e5.

Chen-Plotkin A. S., Lee V. M.-Y., Trojanowski J. Q. (2010) TAR DNA-binding protein 43 in neurodegenerative disease. *Nat. Rev. Neurol. 2010 64* **6**, 211–220.

Chen J.-J. (2007) Regulation of protein synthesis by the heme-regulated eIF2α kinase: relevance to anemias. *Blood* **109**, 2693–2699.

Cheng W., Wang S., Mestre A. A., Fu C., Makarem A., Xian F., Hayes L. R., et al. (2018) C9ORF72 GGGGCC repeat-associated non-AUG translation is upregulated by stress through eIF2α phosphorylation. *Nat. Commun.* **9**.

Chew J., Gendron T. F., Prudencio M., Sasaguri H., Zhang Y.-J., Castanedes-Casey M., Lee C. W., et al. (2015) C9ORF72 repeat expansions in mice cause TDP-43 pathology, neuronal loss, and behavioral deficits. *Science* **348**, 1151–1154.

Choi S. Y., Lopez-Gonzalez R., Krishnan G., Phillips H. L., Li A. N., Seeley W. W., Yao W. D., Almeida S., Gao F. B. (2019) C9ORF72-ALS/FTD-associated poly(GR) binds Atp5a1 and compromises mitochondrial function in vivo. *Nat. Neurosci.* **22**, 851–862.

Chou A., Krukowski K., Jopson T., Zhu P. J., Costa-Mattioli M., Walter P., Rosi S. (2017) Inhibition of the integrated stress response reverses cognitive deficits after traumatic brain injury. *Proc. Natl. Acad. Sci. U. S. A.* **114**, E6420–E6426.

Costa-Mattioli M., Gobert D., Harding H., Herdy B., Azzi M., Bruno M., Bidinosti M., et al. (2005) Translational control of hippocampal synaptic plasticity and memory by the eIF2α kinase GCN2. *Nature* **436**, 1166–1170.

Costa-Mattioli M., Gobert D., Stern E., Gamache K., Colina R., Cuello C., Sossin W., et al. (2007) eIF2α Phosphorylation Bidirectionally Regulates the Switch from Short- to Long-Term Synaptic Plasticity and Memory. *Cell* **129**, 195–206.

Costa-Mattioli M., Walter P. (2020) The integrated stress response: From mechanism to disease. *Science (80-.).* **368**.

D'Adamo P., Menegon A., Nigro C. Lo, Grasso M., Gulisano M., Tamanini F., Bienvenu T., et al. (1998) Mutations in GDI1 are responsible for X-linked non-specific mental retardation. *Nat. Genet. 1998 192* **19**, 134–139.

Dafinca R., Scaber J., Ababneh N., Lalic T., Weir G., Christian H., Vowles J., et al. (2016) C9orf72 Hexanucleotide Expansions Are Associated with Altered Endoplasmic Reticulum Calcium Homeostasis and Stress Granule Formation in Induced Pluripotent Stem Cell-Derived Neurons from Patients with Amyotrophic Lateral Sclerosis and Frontotemporal Demen. *Stem Cells* **34**, 2063–2078.

DeJesus-Hernandez M., Mackenzie I. R., Boeve B. F., Boxer A. L., Baker M., Rutherford N. J., Nicholson A. M., et al. (2011) Expanded GGGGCC Hexanucleotide Repeat in Noncoding Region of C9ORF72 Causes Chromosome 9p-Linked FTD and ALS. *Neuron* **72**, 245–256.

Deval C., Chaveroux C., Maurin A.-C., Cherasse Y., Parry L., Carraro V., Milenkovic D., et al. (2009) Amino acid limitation regulates the expression of genes involved in several specific biological processes through GCN2-dependent and GCN2-independent pathways. *FEBS J.* **276**, 707–718.

Ding X., Jiang X., Tian R., Zhao P., Li L., Wang X., Chen S., et al. (2019) RAB2 regulates the formation of autophagosome and autolysosome in mammalian cells. *Autophagy* **15**, 1774–1786.

Duran-Aniotz C., Martínez G., Hetz C. (2014) *Memory loss in Alzheimer's disease: Are the alterations in the UPR network involved in the cognitive impairment?* Frontiers Media SA.

Elliott E., Bailey O., Waldron F. M., Hardingham G. E., Chandran S., Gregory J. M. (2020) Therapeutic Targeting of Proteostasis in Amyotrophic Lateral Sclerosis—a Systematic Review and Meta-Analysis of Preclinical Research. *Front. Neurosci.* **14**, 1–16.

Freibaum B. D., Taylor J. P. (2017) *The role of dipeptide repeats in C9ORF72-related ALS-FTD*. Frontiers Media S.A.

Gami-Patel P., Dijken I. van, Meeter L. H., Melhem S., Morrema T. H. J., Scheper W., Swieten J. C. van, Rozemuller A. J. M., Dijkstra A. A., Hoozemans J. J. M. (2021) Unfolded protein response activation in C9orf72 frontotemporal dementia is associated with dipeptide pathology and granulovacuolar degeneration in granule cells. *Brain Pathol.* **31**, 163–173.

Gardner B. M., Pincus D., Gotthardt K., Gallagher C. M., Walter P. (2013) Endoplasmic Reticulum Stress Sensing in the Unfolded Protein Response. *Cold Spring Harb. Perspect. Biol.* **5**, a013169.

Garrett M. D., Zahner J. E., Cheney C. M., Novick P. J. (1994) GDI1 encodes a GDP dissociation inhibitor that plays an essential role in the yeast secretory pathway. *EMBO J.* **13**, 1718–1728.

Glass C. K., Saijo K., Winner B., Marchetto M. C., Gage F. H. (2010) Mechanisms Underlying Inflammation in Neurodegeneration. *Cell* **140**, 918–934.

Glineburg M. R., Zhang Y., Krans A., Tank E. M., Barmada S. J., Todd P. K. (2021) Enhanced detection of expanded repeat mRNA foci with hybridization chain reaction. *Acta Neuropathol. Commun. 2021 91* **9**, 1–16.

Green K. M., Glineburg M. R., Kearse M. G., Flores B. N., Linsalata A. E., Fedak S. J., Goldstrohm A. C., Barmada S. J., Todd P. K. (2017) RAN translation at C9orf72-associated repeat expansions is selectively enhanced by the integrated stress response. *Nat. Commun.* **8**.

Guneykaya D., Ivanov A., Hernandez D. P., Haage V., Wojtas B., Meyer N., Maricos M., et al. (2018) Transcriptional and Translational Differences of Microglia from Male and Female Brains. *Cell Rep.* **24**, 2773-2783.e6.

Haeusler A. R., Donnelly C. J., Periz G., Simko E. A. J., Shaw P. G., Kim M.-S., Maragakis N. J., et al. (2014) C9orf72 nucleotide repeat structures initiate molecular cascades of disease. *Nature* **507**, 195.

Halliday M., Radford H., Sekine Y., Moreno J., Verity N., Quesne J. Le, Ortori C. A., et al. (2015) Partial restoration of protein synthesis rates by the small molecule ISRIB

prevents neurodegeneration without pancreatic toxicity. *Cell Death Dis.* **6**.

Halliday M., Radford H., Zents K. A. M., Molloy C., Moreno J. A., Verity N. C., Smith E., et al. (2017) Repurposed drugs targeting eIF2α-P-mediated translational repression prevent neurodegeneration in mice. *Brain* **140**, 1768–1783.

Hardiman O., Al-Chalabi A., Chio A., Corr E. M., Logroscino G., Robberecht W., Shaw P. J., Simmons Z., Berg L. H. Van Den (2017) *Amyotrophic lateral sclerosis*. Nature Publishing Group.

Harding H. P., Novoa I., Zhang Y., Zeng H., Wek R., Schapira M., Ron D. (2000a) Regulated Translation Initiation Controls Stress-Induced Gene Expression in Mammalian Cells. *Mol. Cell* **6**, 1099–1108.

Harding H. P., Zeng H., Zhang Y., Jungries R., Chung P., Plesken H., Sabatini D. D., Ron D. (2001) *Diabetes Mellitus and Exocrine Pancreatic Dysfunction in Perk/ Mice Reveals a Role for Translational Control in Secretory Cell Survival*.

Harding H. P., Zhang Y., Bertolotti A., Zeng H., Ron D. (2000b) Perk is essential for translational regulation and cell survival during the unfolded protein response. *Mol. Cell* **5**, 897–904.

Harrison F. E., Hosseini A. H., McDonald M. P. (2009) Endogenous anxiety and stress responses in water maze and Barnes maze spatial memory tasks. *Behav. Brain Res.* **198**, 247.

Haze K., Yoshida H., Yanagi H., Yura T., Mori K. (1999) Mammalian Transcription Factor ATF6 Is Synthesized as a Transmembrane Protein and Activated by Proteolysis in Response to Endoplasmic Reticulum Stress. *Mol. Biol. Cell* **10**, 3787.

Hetz C., Axten J., Patterson J. (2019) Pharmacological targeting of the unfolded protein response for disease intervention. *Nat. Chem. Biol.* **15**, 764–775.

Hetz C., Mollereau B. (2014) Disturbance of endoplasmic reticulum proteostasis in neurodegenerative diseases. *Nat. Rev. Neurosci.* **15**, 233.

Hetz C., Papa F. R. (2018) The Unfolded Protein Response and Cell Fate Control. *Mol. Cell* **69**, 169–181.

Hetz C., Saxena S. (2017) ER stress and the unfolded protein response in

neurodegeneration. *Nat. Rev. Neurol.* **13**, 477–491.

Hetz C., Zhang K., Kaufman R. (2020) Mechanisms, regulation and functions of the unfolded protein response. *Nat. Rev. Mol. Cell Biol.* **21**, 421–438.

Iacoangeli A., Khleifat A. Al, Jones A. R., Sproviero W., Shatunov A., Opie-Martin S., Morrison K. E., et al. (2019) C9orf72 intermediate expansions of 24–30 repeats are associated with ALS. *Acta Neuropathol. Commun. 2019 71* **7**, 1–7.

Jiang H. Q., Ren M., Jiang H. Z., Wang J., Zhang J., Yin X., Wang S. Y., Qi Y., Wang X. D., Feng H. L. (2014) Guanabenz delays the onset of disease symptoms, extends lifespan, improves motor performance and attenuates motor neuron loss in the SOD1 G93A mouse model of amyotrophic lateral sclerosis. *Neuroscience* **277**, 132–138.

Kanekura K., Yagi T., Cammack A. J., Mahadevan J., Kuroda M., Harms M. B., Miller T. M., Urano F. (2016) Poly-dipeptides encoded by the C9ORF72 repeats block global protein translation. *Hum. Mol. Genet.* **25**, 1803–1813.

Kim H.-J., Raphael A. R., LaDow E. S., McGurk L., Weber R. A., Trojanowski J. Q., Lee V. M.-Y., Finkbeiner S., Gitler A. D., Bonini N. M. (2013) Therapeutic modulation of eIF2α phosphorylation rescues TDP-43 toxicity in amyotrophic lateral sclerosis disease models. *Nat. Genet.* **46**, 152–160.

Kramer N. J., Haney M. S., Morgens D. W., Jovičić A., Couthouis J., Li A., Ousey J., et al. (2018) CRISPR–Cas9 screens in human cells and primary neurons identify modifiers of C9ORF72 dipeptide-repeat-protein toxicity. *Nat. Genet.*, 1.

Lall D., Baloh R. (2017) Microglia and C9orf72 in neuroinflammation and ALS and frontotemporal dementia. *J. Clin. Invest.* **127**, 3250–3258.

Langenhove T. Van, Zee J. Van Der, Broeckhoven C. Van (2012) The molecular basis of the frontotemporal lobar degeneration-amyotrophic lateral sclerosis spectrum. *Ann. Med.* **44**, 817–828.

Lant S., Robinson A., Thompson J., Rollinson S., Pickering-Brown S., Snowden J., Davidson Y., Gerhard A., Mann D. (2014) Patterns of microglial cell activation in frontotemporal lobar degeneration. *Neuropathol. Appl. Neurobiol.* **40**, 686–696.

Lin Y., Mori E., Kato M., Xiang S., Wu L., Kwon I., McKnight S. L. (2016) Toxic PR Poly-Dipeptides Encoded by the C9orf72 Repeat Expansion Target LC Domain Polymers.

Cell **167**, 789-802.e12.

Ling S. C., Polymenidou M., Cleveland D. W. (2013) Converging mechanisms in als and FTD: Disrupted RNA and protein homeostasis. *Neuron* **79**, 416–438.

Liu Y., Pattamatta A., Zu T., Reid T., Bardhi O., Borchelt D. R., Yachnis A. T., Ranum L. P. W. (2016a) C9orf72 BAC Mouse Model with Motor Deficits and Neurodegenerative Features of ALS/FTD. *Neuron* **90**, 521–534.

Liu Z., Shi Q., Song X., Wang Y., Wang Y., Song E., Song Y. (2016b) Activating Transcription Factor 4 (ATF4)-ATF3-C/EBP Homologous Protein (CHOP) Cascade Shows an Essential Role in the ER Stress-Induced Sensitization of Tetrachlorobenzoquinone-Challenged PC12 Cells to ROS-Mediated Apoptosis via Death Receptor 5 (DR5) Signaling. *Chem. Res. Toxicol.* **29**, 1510–1518.

Ma T., Trinh M. A., Wexler A. J., Bourbon C., Gatti E., Pierre P., Cavener D. R., Klann E. (2013) Suppression of eIF2α kinases alleviates Alzheimer's disease-related plasticity and memory deficits. *Nat. Neurosci.* **16**, 1299–1305.

Majounie E., Renton A. E., Mok K., Dopper E. G. P., Waite A., Rollinson S., Chiò A., et al. (2012) Frequency of the C9orf72 hexanucleotide repeat expansion in patients with amyotrophic lateral sclerosis and frontotemporal dementia: a cross-sectional study. *Lancet Neurol.* **11**, 323–330.

Maly D. J., Papa F. R. (2014) Druggable sensors of the unfolded protein response. *Nat. Chem. Biol.* **10**, 892–901.

McCarthy M. M., Pickett L. A., VanRyzin J. W., Kight K. E. (2015) Surprising origins of sex differences in the brain. *Horm. Behav.* **76**, 3–10.

Medinas D. B., Valenzuela V., Hetz C. (2017) Proteostasis disturbance in amyotrophic lateral sclerosis. *Hum. Mol. Genet.* **26**, R91–R104.

Mercado G., Castillo V., Soto P., López N., Axten J. M., Sardi S. P., Hoozemans J. J. M., Hetz C. (2018) Targeting PERK signaling with the small molecule GSK2606414 prevents neurodegeneration in a model of Parkinson's disease. *Neurobiol. Dis.* **112**, 136–148.

Mizielinska S., Grönke S., Niccoli T., Ridler C. E., Clayton E. L., Devoy A., Moens T., et al. (2014) C9orf72 repeat expansions cause neurodegeneration in Drosophila through

arginine-rich proteins. *Science (80-.).* **345**, 1192–1194.

Moreno J. A., Radford H., Peretti D., Steinert J. R., Verity N., Martin M. G., Halliday M., et al. (2012) Sustained translational repression by eIF2α-P mediates prion neurodegeneration. *Nature* **485**, 507–511.

Moreno J. a, Halliday M., Molloy C., Radford H., Verity N., Axten J. M., Ortori C. A., et al. (2013) Oral Treatment Targeting the Unfolded Protein Response PreventsNeurodegeneration and Clinical Disease in Prion-Infected Mice . *Sci. Transl. Med.* **138**, 206ra138.

Mori K., Arzberger T., Grässer F., Gijselinck I., May S., Rentzsch K., Weng S., et al. (2013a) Bidirectional transcripts of the expanded C9orf72 hexanucleotide repeat are translated into aggregating dipeptide repeat proteins. *Acta Neuropathol.* **126**, 881–893.

Mori K., Weng S.-M., Arzberger T., May S., Rentzsch K., Kremmer E., Schmid B., et al. (2013b) The C9orf72 GGGGCC Repeat Is Translated into Aggregating Dipeptide-Repeat Proteins in FTLD/ALS. *Science (80-.).* **339**, 1335–1338.

Nassif M., Woehlbier U., Manque P. A. (2017) The Enigmatic Role of C9ORF72 in Autophagy. *Front. Neurosci.* **0**, 442.

Ohoka N., Yoshii S., Hattori T., Onozaki K., Hayashi H. (2005) TRB3, a novel ER stress-inducible gene, is induced via ATF4–CHOP pathway and is involved in cell death. *EMBO J.* **24**, 1243–1255.

Pakos-Zebrucka K., Koryga I., Mnich K., Ljujic M., Samali A., Gorman A. M. (2016) The integrated stress response. *EMBO Rep.* **17**, 1374–1395.

Palam L., Baird T., Wek R. (2011) Phosphorylation of eIF2 facilitates ribosomal bypass of an inhibitory upstream ORF to enhance CHOP translation. *J. Biol. Chem.* **286**, 10939–10949.

Park S. M., Kang T. Il, So J. S. (2021) Roles of XBP1s in Transcriptional Regulation of Target Genes. *Biomedicines* **9**.

Pasinelli P., Brown R. H. (2006) Molecular biology of amyotrophic lateral sclerosis: insights from genetics. *Nat Rev Neurosci* **7**, 710–723.

Pattabiraman S., Azad G. K., Amen T., Brielle S., Park J. E., Sze S. K., Meshorer E., Kaganovich D. (2020) Vimentin protects differentiating stem cells from stress. *Sci. Reports 2020 101* **10**, 1–15.

Preissler S., Ron D. (2019) Early Events in the Endoplasmic Reticulum Unfolded Protein Response. *Cold Spring Harb. Perspect. Biol.* **11**.

Prudencio M., Belzil V. V., Batra R., Ross C. A., Gendron T. F., Pregent L. J., Murray M. E., et al. (2015) Distinct brain transcriptome profiles in C9orf72-associated and sporadic ALS. *Nat. Neurosci.* **18**, 1175–1182.

Radford H., Moreno J. A., Verity N., Halliday M., Mallucci G. R. (2015) PERK inhibition prevents tau-mediated neurodegeneration in a mouse model of frontotemporal dementia. *Acta Neuropathol.* **130**, 633–642.

Renton A. E., Majounie E., Waite A., Simón-Sánchez J., Rollinson S., Gibbs J. R., Schymick J. C., et al. (2011) A Hexanucleotide Repeat Expansion in C9ORF72 Is the Cause of Chromosome 9p21-Linked ALS-FTD. *Neuron* **72**, 257–268.

Rojas-Rivera D., Delvaeye T., Roelandt R., Nerinckx W., Augustyns K., Vandenabeele P., Bertrand M. J. M. (2017) When PERK inhibitors turn out to be new potent RIPK1 inhibitors: Critical issues on the specificity and use of GSK2606414 and GSK2656157. *Cell Death Differ.* **24**, 1100–1110.

Rojas M., Arias C. F., López S. (2010) Protein Kinase R Is Responsible for the Phosphorylation of eIF2α in Rotavirus Infection. *J. Virol.* **84**, 10457–10466.

Rowland L. P., Shneider N. A. (2001) Amyotrophic Lateral Sclerosis. *N. Engl. J. Med.* **344**, 1688–1700.

Ruegsegger C., Saxena S. (2016) Proteostasis impairment in ALS. *Brain Res.* **1648**, 571–579.

Santos-Galindo M., Acaz-Fonseca E., Bellini M. J., Garcia-Segura L. M. (2011) Sex differences in the inflammatory response of primary astrocytes to lipopolysaccharide. *Biol. Sex Differ.* **2**, 1–11.

Saxena S., Cabuy E., Caroni P. (2009) A role for motoneuron subtype–selective ER stress in disease manifestations of FALS mice. *Nat. Neurosci.* **12**, 627.

Saxena S., Caroni P. (2011) Selective Neuronal Vulnerability in Neurodegenerative Diseases: from Stressor Thresholds to Degeneration. *Neuron* **71**, 35–48.

Scheper W., Hoozemans J. J. M. (2015) The unfolded protein response in neurodegenerative diseases: a neuropathological perspective. *Acta Neuropathol.* **130**, 315–331.

Sekine Y., Zyryanova A., Crespillo-Casado A., Fischer P. M., Harding H. P., Ron D. (2015) Mutations in a translation initiation factor identify the target of a memory-enhancing compound. *Science (80-.).* **348**, 1027 LP – 1030.

Shahheydari H., Ragagnin A., Walker A. K., Toth R. P., Vidal M., Jagaraj C. J., Perri E. R., Konopka A., Sultana J. M., Atkin J. D. (2017) Protein Quality Control and the Amyotrophic Lateral Sclerosis/Frontotemporal Dementia Continuum. *Front. Mol. Neurosci.* **0**, 119.

Shiota T., Nagata R., Kikuchi S., Nanaura H., Matsubayashi M., Nakanishi M., Kobashigawa S., et al. (2020) C9orf72- derived proline:arginine poly-dipeptides disturb cytoskeletal architecture. *bioRxiv*, 2020.10.14.338566.

Sidrauski C., Acosta-Alvear D., Khoutorsky A., Vedantham P., Hearn B. R., Li H., Gamache K., et al. (2013) Pharmacological brake-release of mRNA translation enhances cognitive memory. *Elife* **2**, e00498.

Sidrauski C., McGeachy A. M., Ingolia N. T., Walter P. (2015) The small molecule ISRIB reverses the effects of eIF2α phosphorylation on translation and stress granule assembly. *Elife* **4**, e05033.

Smith H. L., Mallucci G. R. (2016) The unfolded protein response: mechanisms and therapy of neurodegeneration. *Brain* **139**, 2113–2121.

Sonobe Y., Ghadge G., Masaki K., Sendoel A., Fuchs E., Roos R. P. (2018) Translation of dipeptide repeat proteins from the C9ORF72 expanded repeat is associated with cellular stress. *Neurobiol. Dis.* **116**, 155–165.

Tabas I., Ron D. (2011) Integrating the mechanisms of apoptosis induced by endoplasmic reticulum stress. *Nat. Cell Biol.* **13**, 184.

Taylor J. P., Brown Jr R. H., Cleveland D. W. (2016) Decoding ALS: from genes to mechanism. *Nature* **539**, 197.

Torres P., Cabral-Miranda F., Gonzalez-Teuber V., Hetz C. (2021) Proteostasis deregulation as a driver of C9ORF72 pathogenesis. *J. Neurochem.*

Trinh M. A., Kaphzan H., Wek R. C., Pierre P., Cavener D. R., Klann E. (2012) Brain-Specific Disruption of the eIF2α Kinase PERK Decreases ATF4 Expression and Impairs Behavioral Flexibility. *Cell Rep.* **1**, 676–688.

Tsai J. C., Miller-Vedam L. E., Anand A. A., Jaishankar P., Nguyen H. C., Renslo A. R., Frost A., Walter P. (2018) Structure of the nucleotide exchange factor eIF2B reveals mechanism of memory-enhancing molecule. *Science (80-.).* **359**.

Urra H., Dufey E., Lisbona F., Rojas-Rivera D., Hetz C. (2013) When ER stress reaches a dead end. *Biochim. Biophys. Acta - Mol. Cell Res.* **1833**, 3507–3517.

Vattem K., Wek R. (2004) Reinitiation involving upstream ORFs regulates ATF4 mRNA translation in mammalian cells. *Proc. Natl. Acad. Sci. U. S. A.* **101**, 11269–11274.

Vieira F. G., Ping Q., Moreno A. J., Kidd J. D., Thompson K., Jiang B., Lincecum J. M., et al. (2015) Guanabenz Treatment Accelerates Disease in a Mutant SOD1 Mouse Model of ALS. *PLoS One* **10**, e0135570.

Viodé A., Fournier C., Camuzat A., Fenaille F., Bank N. B., Latouche M., Elahi F., et al. (2018) New Antibody-Free Mass Spectrometry-Based Quantification Reveals That C9ORF72 Long Protein Isoform Is Reduced in the Frontal Cortex of Hexanucleotide-Repeat Expansion Carriers. *Front. Neurosci.* **0**, 589.

Vogel-Ciernia A., Wood M. A. (2014) Examining object location and object recognition memory in mice. *Curr. Protoc. Neurosci.* **2014**, 8.31.1-8.31.17.

Waite A. J., Bäumer D., East S., Neal J., Morris H. R., Ansorge O., Blake D. J. (2014) Reduced C9orf72 protein levels in frontal cortex of amyotrophic lateral sclerosis and frontotemporal degeneration brain with the C9ORF72 hexanucleotide repeat expansion. *Neurobiol. Aging* **35**, 1779.e5-1779.e13.

Walter P., Ron D. (2011) The Unfolded Protein Response: From Stress Pathway to Homeostatic Regulation. *Science (80-.).* **334**, 1081–1086.

Wang R., Xu X., Hao Z., Zhang S., Wu D., Sun H., Mu C., Ren H., Wang G. (2019) Poly-PR in C9ORF72-Related Amyotrophic Lateral Sclerosis/Frontotemporal Dementia Causes Neurotoxicity by Clathrin-Dependent Endocytosis. *Neurosci. Bull.*

Webster C. P., Smith E. F., Bauer C. S., Moller A., Hautbergue G. M., Ferraiuolo L., Myszczynska M. A., et al. (2016) The C9orf72 protein interacts with Rab1a and the ULK1 complex to regulate initiation of autophagy. *EMBO J.* **35**, 1656–1676.

Wei Q., Zhou Q., Chen Y., Ou R., Cao B., Xu Y., Yang J., Shang H. F. (2017) Analysis of SOD1 mutations in a Chinese population with amyotrophic lateral sclerosis: a case-control study and literature review. *Sci. Reports 2017 71* **7**, 1–6.

Westergard T., McAvoy K., Russell K., Wen X., Pang Y., Morris B., Pasinelli P., Trotti D., Haeusler A. (2019) Repeat-associated non-AUG translation in C9orf72-ALS/FTD is driven by neuronal excitation and stress. *EMBO Mol. Med.* **11**.

Xiao S., MacNair L., McGoldrick P., McKeever P. M., McLean J. R., Zhang M., Keith J., Zinman L., Rogaeva E., Robertson J. (2015) Isoform-specific antibodies reveal distinct subcellular localizations of C9orf72 in amyotrophic lateral sclerosis. *Ann. Neurol.* **78**, 568–583.

Zhang K., Daigle J. G., Cunningham K. M., Coyne A. N., Ruan K., Grima J. C., Bowen K. E., et al. (2018a) Stress Granule Assembly Disrupts Nucleocytoplasmic Transport. *Cell* **173**, 958-971.e17.

Zhang Y.-J., Jansen-West K., Xu Y.-F., Gendron T. F., Bieniek K. F., Lin W.-L., Sasaguri H., et al. (2014) Aggregation-prone c9FTD/ALS poly(GA) RAN-translated proteins cause neurotoxicity by inducing ER stress. *Acta Neuropathol.* **128**, 505–524.

Zhang Y. J., Gendron T. F., Ebbert M. T. W., O'Raw A. D., Yue M., Jansen-West K., Zhang X., et al. (2018b) *Poly(GR) impairs protein translation and stress granule dynamics in C9orf72-associated frontotemporal dementia and amyotrophic lateral sclerosis*. Nature Publishing Group.

Zhang Y. J., Guo L., Gonzales P. K., Gendron T. F., Wu Y., Jansen-West K., O'Raw A. D., et al. (2019) Heterochromatin anomalies and double-stranded RNA accumulation underlie C9orf72 poly(PR) toxicity. *Science (80-.).* **363**.

Zhu P. J., Huang W., Kalikulov D., Yoo J. W., Placzek A. N., Stoica L., Zhou H., et al. (2011) Suppression of PKR promotes network excitability and enhanced cognition by interferon-γ-mediated disinhibition. *Cell* **147**, 1384–1396.

Zu T., Guo S., Bardhi O., Ryskamp D. A., Li J., Tusi S. K., Engelbrecht A., et al. (2020)

Metformin inhibits RAN translation through PKR pathway and mitigates disease in C9orf72 ALS/FTD mice. *Proc. Natl. Acad. Sci.* **117**, 18591–18599.

Zu T., Liu Y., Bañez-Coronel M., Reid T., Pletnikova O., Lewis J., Miller T. M., et al. (2013) RAN proteins and RNA foci from antisense transcripts in C9ORF72 ALS and frontotemporal dementia. *Proc. Natl. Acad. Sci.* **110**, E4968–E4977.

Zyryanova A. F., Weis F. F., Faille A., Alard A. A., Crespillo-casado A., Harding H. P., Allen F., et al. (2017) Binding of the integrated stress response inhibitor, ISRIB, reveals a regulatory site in the nucleotide exchange factor, eIF2B. *bioRxiv* **1536**, 224824.

Zyryanova A. F., Weis F., Faille A., Abo Alard A., Crespillo-Casado A., Sekine Y., Harding H. P., et al. (2018) Binding of ISRIB reveals a regulatory site in the nucleotide exchange factor eIF2B. *Science (80-.).* **359**, 1533–1536.